PEOPLE'S DEMOCRATIC REPUBLIC OF ALGERIA

MINISTRY OF HIGHER EDUCATION

AND SCIENTIFIC RESEARCH

SAAD DAHLAB UNIVERSITY OF BLIDA

Institute of Aeronautics and Space Studies

Department of Aeronautical Construction

MASTER'S THESIS FOR THE AWARD OF THE MASTER'S DEGREE

Specialization: Aeronautics

Option: Aircraft Propulsion

Topic: Innovative Elliptical Dual Bell Nozzle Design Proposal : Comparison with Conventional Dual Bell Nozzle Design

Supervised by:

Mr KBAB Hakim : Supervisor.

Mr TCHERAK Anis : Co supervisor.

Conducted by:

HAMLAOUI Anissa.

TOURI Aid Badis.

Blida, July 2024.

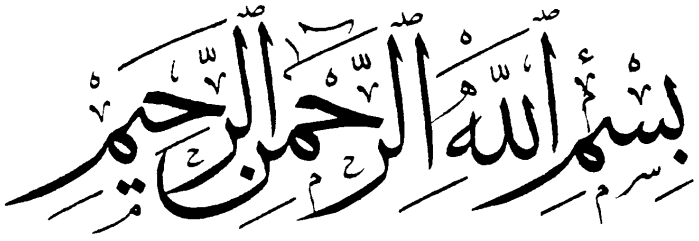
بسم الله الرحمن الرحيم

ACKNOWLEDGMENT

First and foremost, we thank Allah, the Almighty, who granted us the strength, patience, and determination to complete this modest thesis work.

Secondly, we express our gratitude to our supervisor**, Mr. KBAB Hakim**, for his exceptional guidance throughout this project. His availability, insightful advice, and expertise have been invaluable, enabling us to progress and overcome challenges encountered along the way.

Similarly, we extend our thanks to our Co-supervisor, **Mr. TCHAREK Anis**, for his valuable assistance, encouragement, and constructive criticism, which played a crucial role in the culmination of this work. His rigor and deep subject knowledge enriched our analysis and refined our thinking.

Thanks to their continuous support and invaluable guidance, we were able to successfully and enrichingly complete this project. Our sincere appreciation also goes to the **members of the jury** for their interest in our research, accepting to evaluate our work and enrich it with their suggestions.

We also thank **all the teachers and faculty members of the Institute of Aeronautics and Space Studies at the University of Saad Dahleb** for sharing their knowledge and expertise throughout our education. Their teachings and encouragement enabled us to acquire the necessary knowledge and skills to accomplish this project.

Lastly, we extend our heartfelt thanks to our **families and friends** for their moral support and constant encouragement. Their presence alongside us has been an invaluable source of motivation and strength.

To everyone who has contributed, directly or indirectly, to the completion of this project, we express our deepest gratitude. Thank you all.

DEDICATIONS

I dedicate this work first and foremost to my dear late **parents**. Wherever you are, I hope you would be proud of me. Your love and values continue to guide me every day.

To my dearest sister **Aida**, who has always believed in me and stood by my side. Your trust and support have been invaluable throughout this journey.

To my very **dear neighbors**, who hold a special place in my heart. Your constant help and support have been of great value to me.

To my partner **HAMLAOUI Anissa**, for your valuable collaboration, presence, and unwavering support throughout this academic adventure. Your contribution and friendship have been precious.

To all my **friends**, for their sincere friendship, unwavering support, and constant encouragement. Your presence has greatly helped me to persevere.

Finally, to all the people who believed in me and supported me in one way or another. This project is the result of your trust and encouragement.

Thank you all.

TOURI Aid Badis.

DEDICATIONS

I dedicate this thesis to my mother, **FELLAHI Hassiba**, who left us too soon. May this work be a tribute to her unconditional love and all the sacrifices she made for our happiness.

To my father, **HAMLAOUI Abdelkader**, whose unwavering support has been the source of my perseverance and success. His constant encouragement and sacrifices to help me achieve my ambitions have been invaluable.

To my aunt **FELLAHI Salima**, whose wise counsel and constant affection have been essential pillars throughout my journey.

To my grandmother **mémé,** whose generosity and tenderness have always been a source of comfort and inspiration.

To my sisters, **Yasmine**, **Aziza**, **Mordjane**, and my brother, **Redha**, whose encouragement and love have always inspired me. Their presence by my side has given me the strength to overcome difficulties and persevere.

To my partner, **TOURI Aid Badis**, with whom I have shared so many challenges, successes, and unforgettable moments. His collaboration and support have been indispensable to the completion of this project.

To my **family and friends** for their support and encouragement.

HAMLAOUI Anissa.

RESUME

Les tuyères de fusée sont essentielles à la propulsion spatiale, car elles convertissent l'énergie des gaz de combustion en poussée vers l'avant. Parmi les différentes conceptions, les tuyères à double cloche se distinguent comme une solution prometteuse pour améliorer les moteurs de fusée du premier étage, offrant deux modes de fonctionnement adaptés à différentes altitudes pour réduire les pertes par désadaptation. Traditionnellement, ces tuyères ont une section cylindrique et ont été étudiées à travers de nombreuses expérimentations et simulations.

D'autre part, les tuyères à double contour représentent une avancée significative dans la propulsion spatiale, offrant une conception dynamique adaptative pour optimiser les performances des moteurs de fusée à différentes altitudes. Grâce à leur capacité à ajuster leur forme pour une expansion optimale des gaz d'échappement à différentes altitudes, ils permettent une efficacité accrue tout au long du vol. Cette adaptabilité peut se traduire par une augmentation de la charge utile ou une amélioration globale de l'efficacité énergétique du système de propulsion, ouvrant ainsi des perspectives prometteuses pour l'avenir de l'exploration et des transports spatiaux.

En proposant une approche innovante avec une tuyère à double cloche à section de sortie elliptique, notre travail vise à élargir les possibilités de conception et à améliorer les performances des tuyères de fusée. Une étude numérique basée sur la dynamique des fluides computationnelle (CFD) sera entreprise pour évaluer les paramètres thermodynamiques et les performances de cette buse, fournissant ainsi un aperçu des avantages potentiels de cette conception innovante. Une analyse comparative sera ensuite menée avec une buse à double cloche conventionnelle, offrant ainsi un aperçu des avantages potentiels de cette conception innovante.

Abstract

Rocket nozzles are vital for space propulsion, converting the energy of combustion gases into forward thrust. Among various designs, double-bell nozzles stand out as a promising solution for enhancing first-stage rocket engines, offering two operating modes suited for different altitudes to reduce mismatch losses. Traditionally, these nozzles have a cylindrical section and have been studied through numerous experiments and simulations.

On the other hand, double-contoured nozzles represent a significant advancement in space propulsion, providing adaptive dynamic design to optimize the performance of rocket engines at different altitudes. With their ability to adjust shape for optimal expansion of exhaust gases at various altitudes, they enable increased efficiency throughout the flight. This adaptability can translate into payload increase or overall energy efficiency improvement of the propulsion system, thus opening promising prospects for the future of space exploration and transportation.

By proposing an innovative approach with an elliptical outlet section dual bell nozzle, our work aims to broaden design possibilities and enhance rocket nozzle performance. A computational fluid dynamics (CFD) based numerical study will be undertaken to assess thermodynamic parameters and performance of this nozzle, providing insights into potential advantages of this innovative design. A comparative analysis will then be conducted with a conventional double-bell nozzle, thus offering insights into potential benefits of this innovative design.

TABLE OF CONTENT

LISTS OF FIGURES

LISTS OF TABLES

NOMENCLATURE

Coordinate system :

x	axial coordinate
y	Radial coordinate

Latin letters :

A	area	[m²]
At	throat area	[m²]
A_e	Nozzle exit area	[m²]
C	Compression Factor	
C_d	The discharge coefficient	
C_{dk}	Effect of the nozzle throat geometry on the sonic line	
$C_{d\delta}$	Effect of the boundary layer	
C^*	Characteristic velocity	[m/s]
		[J/kg/K]
C_p	Heat capacity at constant pressure	[J/kg/K]
Cf	The thrust coefficient	
C^+	Upward characteristic lines	
C^-	Downward characteristic lines	
F	The thrust	[N]
I_s	Specific impulse	[s]
I	Total impulse	
$\dot{m}$	Mass flow rate	[kg/s]
L	Length	[cm]
L $\alpha_{,cone}$	The length of the conical profile	
M	Mach number	
P_t	Total pression	[Pa]
Pch	Pressure in the combustion chamber	[Pa]
Pe	the static pressure at the exit	
P_a	the ambient pressure	[Pa]
		[Pa]
pw	wall pressure	

pi	incipient separation pressure	[Pa]
pp	pressure plateau	[Pa]
pw,vac	wall pressure from its evolution in a vacuum	[Pa]
rtd	the downstream curvature radius	[m]
Rtd	throat radius of curvature	[m]
rt	the nozzle radius	[m]
S_c	Nozzle exit area	[m²]
Tch	Temperature in the combustion chamber	[K]
Ve	The exit velocity	[m/s]
V_{eff}	The effective velocity	[m/s]

Greek letters :

ρ	density	[kg/m^3]
ε	section ratio or expension ratio of the nozzle	
γ	Ratio of specific heats at pressure and constant volume	
σ_{ij}	Viscous stress tensor	
δ_{ij}	Kronecker tensor	
θN	slope in the throat region	
η_{geo}	the geometric efficiency	
θ	Angle	[rad]

Abréviations :

RANS	Reynolds Averaged Navier-Stokes
CFD	Computational Fluid Dynamics
SST	Shear Stress Tensor
TOC	Thrust-Optimized Contour
TIC	Truncated Ideal Contour
TOP	Thrust-Optimized Parabolic
CTIC	Compressed Truncated Ideal Contour
CPC	Constant Pressure Contour
ITC	the Ideal Truncated Contour
TICCP	Thrust-Optimized Parabolic Contour Convergent Divergent Nozzle
TICNP	Thrust-Optimized Conical Nozzle Plug

TICPP	Thrust-Optimized Parabolic Plug Nozzle
FSS	Free Shock Separation
RSS	Restricted Shock Separation
TDK	Two-Dimensional Kinetics
DBN	Dual-Bell Nozzle
CD	Converging-Diverging nozzle
V2	Vulcan 2
MOC	Method of Characteristics
CD	Converging-Diverging
E-D	expansion-deflection
MNG	Multi Nozzle Grid
MDO	Multi-Disciplinary Optimization
NPR	Nozzle Pressure Ratio
AE	Aerospike Engine
DB	Dual bell
NPRtr	the transition pressure ratio
DFN	La dynamique des fluides numérique

INTRODUCTION

The history of space exploration is marked by significant technical challenges, among which propulsion of spacecraft in the vacuum of space holds a prominent position. This quest began in the late 19th century with the visionary work of Konstantin Tsiolkovsky, a pioneer in vacuum propulsion through rocket engines, inspired by Isaac Newton's principles of action and reaction. These engines propel spacecraft by expelling gases at high speeds in a given direction, without requiring an external point of support.

The design of propulsion nozzles constitutes a complex field, demanding expertise in fluid dynamics, thermodynamics, and considerations specific to flight conditions. Various methods, such as the RAO method, have been developed to design and optimize these nozzles, with the goal of maximizing thrust while minimizing their mass.

The RAO method, widely used, relies on an analysis of the vibrations generated by the flow of gases inside the nozzle, allowing for the optimization of its shape to maximize propulsion efficiency. However, this method has limitations in case of modifications to the nozzle contour or flow model, thus requiring a complete redesign of calculations.

With the evolution of space technologies, optimizing the performance of rocket engines has become crucial for increasing launcher payload and improving the efficiency of space missions. It is in this context that the double bell nozzles (DBN) have emerged as an innovative solution. Unlike conventional nozzles, DBNs allow for propulsion optimization throughout the flight trajectory, offering distinct operating modes for low and high altitudes, optimized for specific encountered conditions.

The concept of DBNs relies on modifying the nozzle geometry to maximize thrust at low altitude by forcing the flow to detach from the wall at a specific point, and then allowing for increased thrust at high altitude by gradually reattaching the flow to the wall. Despite persistent challenges such as weight, costs, and mechanical complexity, DBNs offer significant performance gains, as demonstrated by theoretical and experimental studies.

In the history of aerodynamics, remarkable progress has been made through multidisciplinary efforts, from early fluid-based propulsion concepts in antiquity to major developments in the 20th century. The pioneering work of Carl Gustaf Patrik de Laval in the 19th century laid the foundations for the design of convergent-divergent nozzles, while methods like those developed by Pierre Laval enabled significant advancements in optimization.

Since then, nozzles have continued to evolve, integrating technological advances such as the use of innovative materials and advanced numerical simulations to refine their

performances. These innovations have enhanced the efficiency of rocket engines and turbojets, contributing to the progress of aeronautics and space exploration.

The development of supersonic propulsion nozzles has been facilitated by research conducted worldwide, enabling notable advances in cutting-edge laboratories established in the United States, Europe, Russia, Japan, and China. These advancements have opened new perspectives for space exploration and launcher technology, thereby strengthening our ability to explore the surrounding universe.

Among the major players involved in research on supersonic nozzles are a multitude of research organizations, space agencies, and industrial enterprises. In the United States, institutions such as NASA, DLR, ONERA, and LEA-Poitier (PPRIME) have conducted cutting-edge research, while researchers such as Charles E. Tinney, Josef H. Ruf, and Ten-See Wang have contributed to advancing knowledge in this field. In Europe, countries like Germany, Sweden, the Netherlands, Italy, Spain, and France have also played a crucial role. Researchers like Gerald Hagemann in Germany, Jan Ostland in Sweden, Marcello Onofri in Italy, and Jose A. Morinigo in Spain have made significant contributions. In France, institutions such as ONERA-Meuden, CNES-Evry, University of Evry, University Paris VI, and CORIA-Rouen have been at the forefront of research, with researchers such as Jean Delery, Jean-Pierre Veuillot, Sebastien Deck, and many others contributing significantly to the progress made in the field of supersonic nozzles.

SUMMARY

Rocket nozzles are vital for space propulsion, converting the energy of combustion gases into forward thrust. Among various designs, double-bell nozzles stand out as a promising solution for enhancing first-stage rocket engines, offering two operating modes suited for different altitudes to reduce mismatch losses. Traditionally, these nozzles have a cylindrical section and have been studied through numerous experiments and simulations.

On the other hand, double-contoured nozzles represent a significant advancement in space propulsion, providing adaptive dynamic design to optimize the performance of rocket engines at different altitudes. With their ability to adjust shape for optimal expansion of exhaust gases at various altitudes, they enable increased efficiency throughout the flight. This adaptability can translate into payload increase or overall energy efficiency improvement of the propulsion system, thus opening promising prospects for the future of space exploration and

transportation.

By proposing an innovative approach with an elliptical outlet section dual bell nozzle, our work aims to broaden design possibilities and enhance rocket nozzle performance. A computational fluid dynamics (CFD) based numerical study will be undertaken to assess thermodynamic parameters and performance of this nozzle, providing insights into potential advantages of this innovative design. A comparative analysis will then be conducted with a conventional double-bell nozzle, thus offering insights into potential benefits of this innovative design.

RESEARCH PLAN

The study, following a general introduction to the subject, is divided into two parts. The first part, entitled "Literature Review and State of the Art," provides an in-depth exploration of rocket nozzles from various perspectives: historical background, functioning, design, and evolution. This section offers a comprehensive overview of existing knowledge on rocket nozzles, highlighting the advancements made in this crucial area of space engineering.

In this first part, subdivided into four subsections, we delve into different facets of rocket nozzles. The first subsection explores classical nozzles, showcasing past and current research efforts on profiles, design methodologies, and technical advancements. We also analyze the fundamental theories and principles underlying the operation of traditional rocket nozzles.

The second subsection provides an overview of the operating parameters of rocket nozzles, along with their performances. We examine the key factors influencing the efficiency and effectiveness of rocket nozzles, highlighting the design criteria and performance metrics used in the space industry.

The third subsection addresses the challenges associated with separation in rocket nozzles and explores various proposed solutions. We particularly focus on the concept of "altitude-compensating nozzles," which aim to optimize nozzle performance over a wide range of altitudes, thereby providing increased adaptability to variations in flight conditions.

Lastly, the fourth subsection concentrates on double-bell nozzles, a recent innovation in the field of space propulsion. We examine in detail the design, evolution, and future prospects of these nozzles, emphasizing their potential advantages over conventional designs. Additionally, we also discuss elliptical-section nozzles, exploring the opportunities they offer in terms of enhancing the performance of space propulsion systems.

In the second part of the study, we focused on proposing, for the first time, an elliptical-section double-bell nozzle, an idea hitherto unexplored in the literature. This innovation represents a novel contribution to the field, as no prior examples of such a design have been documented. Thus, we have the privilege of claiming pioneer status for this initiative.

Initially, our focus was on generating a profile for a conventional double-bell nozzle using an in-house code written in Fortran. The base profile is a TIC profile, while for the second profile, we worked with a CP (constant pressure) profile. Flow parameters, such as pressure and Mach number, were evaluated and studied within the scope of this investigation.

Subsequently, building upon this initial nozzle, we utilized our methodology to obtain

the profile of a double-bell nozzle with an elliptical outlet section. We followed the same approach as before, studying and optimizing the performance parameters of this elliptical nozzle, and then comparing them to those obtained for a conventional double-bell nozzle. The results of this comparison are detailed in this section.

In conclusion, this study comes to an end with a synthesis of the results and conclusions drawn from the analyses conducted.

PART I: LITERATURE REVIEW & STATE OF THE ART

RESUME

In this section of the study, titled "Literature Review and State of the Art," we conducted an in-depth review of the literature on nozzles in general, examining their history, design, evolution, and future prospects. This involved a comprehensive bibliographic search covering over a hundred articles and studies. Initially, we focused on classical nozzles, exploring the works and chronological milestones in this field, as well as operational parameters and modes of operation. Subsequently, we addressed altitude-compensating nozzles and the various types of nozzles developed to enhance their performance by predicting or avoiding wall separation. Double-bell nozzles and asymmetric nozzles were given particular attention due to the advantages they offer. This bibliographic study undoubtedly serves as a fundamental resource for students and researchers interested in this field.

I.1 THE CLASSIC NOZZLES

I.1.1 Introduction

The primary propulsion of a launcher relies on an engine fueled by liquid oxygen and hydrogen, also known as cryogenic propellants. These substances undergo combustion in a dedicated chamber, generating gases that are then channeled towards an expansion nozzle to create the necessary thrust. The nozzle, a crucial component, aims to transform the pressure energy "enthalpy" into kinetic energy of a fluid during an adiabatic expansion, thus inducing a pressure drop through judicious modification of the flow section. Typically, a nozzle, also referred to as an exhaust duct, is divided into three essential parts:

1. The convergent: upstream, narrows the nozzle, contributing to the acceleration of gases.
2. The throat: the narrowest section of the duct, establishing sonic conditions (M=1) and determining the engine's operating point.
3. The divergent: downstream, accelerates the flow to supersonic speeds in accordance with the Hugoniot relationship, once the throat is initiated.

The supersonic nozzle is called a De-Laval nozzle, as depicted in Figure I.1.

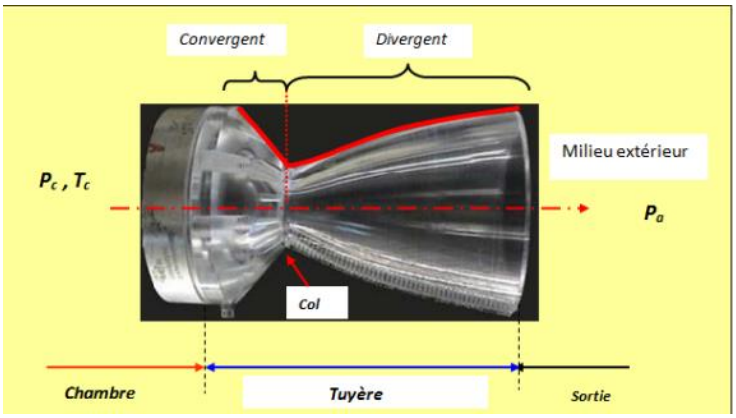

Figure I- 1: De Laval Nozzle.

This subdivision proves most appropriate due to the specific effects in each part when determining the developed proposition, and the varied analysis methods necessary to calculate the flow field in each of these regions. The nozzle configuration, initially presented by Carl De Laval, is often referred to as a "De Laval" nozzle or simply a CD (Converging-Diverging) nozzle. Carl De Laval introduced the characteristic nozzle configuration to enhance the efficiency of propulsion systems. Since then, nozzles have continuously evolved, incorporating technological advancements such as the use of innovative materials and the application of advanced numerical simulations to optimize performance. The nozzle must fulfill various

functions, and its role can be defined by the following conditions:

- It must ensure flow blocking at different engine operating regimes, whether with or without afterburning. This implies the ability to vary the throat area according to the flow rate, gas temperature, and pressure conditions to be evacuated.
- Additionally, the nozzle must ensure optimal expansion of combustion gases for maximum thrust in cruise mode. This task is complex, as the nozzle outlet section must be connected to the engine's master frame or to the aircraft structure via fairing. The shape of this fairing, and consequently the pressures it will experience in flight due to external flow, depend on the shape and size of the nozzle exit.
- Optimizing the nozzle on the test bench would be pointless if significant depressions were to persist in flight on the fairing. Thus, optimization studies require a comprehensive analysis of the aft-body.
- At intermediate flight regimes, it is essential that the nozzle does not cause excessive thrust losses due to mismatch. In these regimes, it is crucial to avoid overexpansion, requiring a thorough study of flow conditions.
- Apart from the engine's main flow, one or more secondary flows are typically observed, originating from cooling air or a boundary layer trap in the air intake. This flow, representing up to 5 or 6% of the total flow, must be ejected either in separate nozzles or in the main nozzle, as is the case with the Concorde.
- During landing, the nozzle can contribute to aircraft braking by organizing thrust reversal, similar to: Optimal expansion of combustion gases (maximum thrust in cruise mode). Minimum pressure losses when the nozzle is adapted to flight mode (nozzle adaptation regime).

Currently, research on supersonic nozzles primarily aims to improve the efficiency and performance of space propulsion systems by overcoming challenges such as controlling high-speed compressible flows, reducing energy losses, and optimizing nozzle geometry. This rapidly growing field has significant implications for space exploration and the development of advanced technologies, offering the opportunity to push current limits and open new prospects for humanity's future through ongoing research.

I.1.2 Chronological milestones in the evolution of classical ejection nozzles

The history of the nozzle traces back to antiquity when the Greek scholar Hero of Alexandria designed the aeolipile, a primitive form of a nozzle used to illustrate the principle of steam propulsion. In 1791, Italian engineer Giovanni Battista Venturi made a seminal

breakthrough by highlighting the principle bearing his name, thus paving the way for subsequent developments in fluid dynamics. The year 1883 marked a significant turning point with the invention of the convergent-divergent nozzle by Swedish engineer Carl Gustaf Patrik de Laval, enabling the achievement of supersonic gas velocities and revolutionizing both aviation and space exploration. The Wright brothers first utilized an ejection nozzle during their historic powered flight in 1903. In the 1920s, jet aircraft extensively adopted convergent-divergent nozzles for their superior performance. Subsequent decades witnessed the emergence of new technologies, including afterburning nozzles in the 1950s, thrust vectoring nozzles in the 1960s, and supercritical nozzles in the 1970s. In the 1980s, widespread use of composite materials began, while the 1990s saw the introduction of variable geometry nozzles for performance optimization. More recently, in the early 2000s, research intensified on quiet and environmentally friendly nozzles, reflecting growing environmental concerns. This chronology illustrates the continuous evolution and diversification of nozzle technologies over time.

The profil of the nozzle contour and the expansion ratio are key parameters influencing performance. Over the years, different types of rocket nozzles have been developed, each with its own characteristics and applications. The concept of the ideal nozzle represents an ideal in terms of thrust performance in rocket engine design, although its practical realization poses significant challenges. In theory, this nozzle would provide the maximum possible performance, but it is characterized by its significant length and weight, adding to the complexity of its manufacturing and integration into propulsion systems. Throughout the history of nozzle research and development, different shapes and concepts have been explored to optimize performance while striving to approach the theoretical ideal. For example, in the 1930s and 1940s, German scientists conducted significant research on nozzles, concluding that complex contours offered no major benefits for low-area ratio nozzles, such as the V-2, showing a preference for simpler shapes despite lower performance due to divergence losses. Subsequently, nozzle types such as conical, bell, plug, expansion-deflection (E-D), and double-bell were developed, each with its own advantages, limitations, and specific applications. However, the concept of the ideal nozzle remains an ultimate goal, guiding research towards innovative solutions to maximize propulsion efficiency in the aerospace domain.

I.1.2.1 Conical Nozzles

Pioneering work on conical nozzles began in 1962 with studies conducted by Migdal and Landis **[1],** who performed numerical analysis of these nozzles' performances. This initial investigation was followed in 1963 by Darwell and Badham **[2],** who also undertook numerical analysis but focused on shock formation inside these nozzles. In 1964, Sunley and Ferriman **[3]**

initiated an experimental approach to study jet separation in conical nozzles. The following year, in 1965, Migdal and Kosson **[4],** as well as Hoffman and Lorenc **[5],** continued with numerical studies, with the former focusing on shock predictions while the latter examined the effects of gas particle flow. In 1970, Wehofer and Moger **[6]** adopted an analytical method to explore inviscid transonic flow fields. After a period of hiatus in research, Khan and Shembharkar **[7]** resumed in 2008 with a numerical study pinpointing shocks in conical nozzles. In 2011, Balabel et al. **[8]** examined turbulent gas flow dynamics through numerical methods. Between 2014 and 2016, research intensified with Zmijanovic et al. **[9]** combining experimental and numerical approaches to study fluidic thrust vectorization, Zhang et al. **[10]** focusing on convergent conical nozzles in 2015, and finally, Jia et al. conducting two successive studies in 2015 **[11]** and 2016 **[12]** on flow separation and induced side loads by these nozzles. These studies illustrate an evolution of research themes, shifting from overall performance and shock formation to more specific aspects such as gas particle flow effects, inviscid transonic flow fields, and finally, side loads and fluidic thrust vectorization.

I.1.2.2 Profiled nozzles

Research on bell-shaped nozzles, also referred to as "bell nozzles," has followed a rich and varied trajectory since the 1950s. Pioneering three-dimensional analysis by Dillaway **[13]** in 1957 initiated this exploration, focusing on supersonic contours of nozzles. The following year, Rao **[14]** developed an analytical method to optimize nozzle wall geometries, marking the beginning of a trend towards optimization and efficient design. In 1960, Lands Baum **[15]** continued this path by numerically studying bell-shaped nozzle contours, while Farley and Campbell **[16]** adopted an experimental approach by examining cut sections of ideal nozzles.

In 1961, Ahlberg and colleagues **[17]** combined experimental and numerical approaches to optimize these truncated sections. Subsequently, focus shifted to flow separation phenomena and disturbed flow characteristics, as evidenced by Lawrence and Weynand's study **[18]** in 1968 on separated flow in 2D and axisymmetric nozzles, followed by several other studies exploring specific nozzle designs for low-density and high-speed conditions, as well as optimization of flow separation and generation of side loads in different types of nozzles.

This field experienced a resurgence of interest in the early 2000s, with works such as Terhardt et al. **[19]** in 2001, examining flow separation and side loads in TIC nozzles using experimental and analytical approaches. In 2002, studies conducted by Verma **[20]** and Hagemann et al. [21] focused on flow separation and the origin of side loads in various types of nozzles. The following years saw a series of in-depth experiments and numerical analyses on these issues, including Verma et al. in 2006 **[22]** and 2017 **[23],** as well as Stark and Wagner

[24] [25], who analyzed flow fields and boundary layer separation in TIC nozzles.

The year 2017 was also characterized by significant studies conducted by Frey et al. **[26]** and Baloni et al. **[27],** using numerical approaches to design and analyze TIC and TOP nozzles, as well as the aeroelastic stability demonstrated by Zhang et al., illustrating the diversity and continued depth of research in this essential field of rocket nozzle technology.

Investigations into plug nozzles began in 1959 with Krase's numerical study **[29],** aiming to design optimal contours for these nozzle types. This study paved the way for further research, such as that of Berman and Crimp **[30]** in 1961, who analytically analyzed nozzle end modifications. In the same year, Rao **[31]** conducted a numerical study focused on optimizing plug nozzle contours. In 1974, Johnson et al. **[32]** continued this trend by optimizing axisymmetric plug nozzles through numerical analysis. Interest in these nozzles remained high in the 1990s, with Rommel et al. **[33]** in 1997 studying flow development at different ambient pressures. In the same year, Ruf and McConnaughey **[34]** focused their research on plug nozzle truncation.

In the early 2000s, studies diversified and deepened with Ito et al.'s numerical analysis **[35]** in 2002, focusing on nozzle contour design. Simultaneously, Besnard et al. **[36]** conducted an experimental study on the design and testing of an abrasive aerodynamic tip engine (aerospike). Interest in the internal and external dynamics of truncated plug nozzles was rekindled by Lahouti and Tolouei **[37]** in 2006, with a particular focus on base bleed. Flow properties of aerospike nozzle shapes were explored by Shahrokhi and Noori **[38]** in 2010, marking a continued interest in more complex configurations.

In 2014, Chutkey et al. **[39]** took a new step by combining numerical and experimental approaches to study flow fields in truncated annular plug nozzles of different lengths. This exploration was closely followed in 2015 by Shanmuganathan et al. **[40],** who focused their numerical study on flow fields of linear and annular aerospike nozzles. Research on plug nozzles continued to progress with Kumar et al. **[41]** in 2017, where they developed a design procedure for aerospike nozzles based on both numerical and experimental approaches. This chronological overview highlights the continuous progression and evolution of studies on plug nozzles, underscoring the ongoing interest in optimizing these propulsion systems over the decades.

I.1.2.3 Expansion/deflection nozzles

The study of expansion-deflection (E-D) nozzles, a type of rocket nozzle designed to compensate for altitude variations by interacting with the atmosphere, reveals several crucial aspects of their operation and advantages over traditional nozzles. Unlike bell-shaped nozzles,

E-D nozzles incorporate a "pintle" or "central body" at the throat level, thereby redirecting the exhaust gas flow towards the wall. This mechanism allows for a significant reduction in nozzle size for the same expansion ratio compared to conventional nozzles.

E-D nozzles operate in two modes: closed and open. In the closed mode, the nozzle exit area is completely filled by the exhaust gases, while in the open mode, ambient pressure influences the exit area, thus allowing altitude compensation up to design pressure. Compared to plug nozzles, E-D nozzles offer similar performance under high chamber-to-ambient pressure ratios (pc/pa). However, at lower pressure ratios, the E-D nozzle adjusts its flow differently, aligned with the pressure behind the central body, unlike plug nozzles that adjust to the pressure at the exit lip. This feature, combined with a smaller combustion chamber, presents advantages in terms of cooling requirements and E-D nozzle weight **[42].**

I.1.2.4 Multi nozzle grid (MNG)

Investigations into the Multi Nozzle Grid (MNG) were initiated by the work of Chasman et al. **[43]** in 2005, who explored a Multi-Disciplinary Optimization (MDO) method for designing an MNG. This approach aimed to develop a thin and lightweight MNG plate, offering an effective alternative to long and heavy traditional single nozzles. In the same year **[44],** Chasman et al. conducted firing tests to evaluate nozzle erosion in an MNG configuration comprising 91 small nozzles (nozzlettes), highlighting notable erosion of tungsten infiltrated copper nozzles, at an average rate of 0.5 lb./sec. This observation underscored the importance of selecting materials suitable for propellant combustion environments. In 2012 **[45],** continuing their MNG research, Chasman et al. studied viscous losses in MNG hybrid engine tests, identifying crucial aspects of nozzle efficiency in the context of hybrid propulsion. These studies laid the groundwork for a better understanding and improvement of MNG design and operation in rocket engines, focusing on mass reduction and nozzle efficiency optimization through in-depth analysis of involved physical phenomena.

I.1.3 Different configurations (Profiles) of classical nozzles

The final design of a rocket nozzle configuration depends on numerous considerations, such as performance requirements, maximum engine mass, dimensional constraints, cooling performance, longevity, and manufacturing methods, among others. A thorough examination of these aspects requires expertise in multiple engineering domains. However, one fundamental requirement in the rocket nozzle design process lies in weight minimization. To achieve this objective, it is recommended to control the length and/or surface area of the nozzle. The primary challenge in gas dynamics lies in determining the optimal shape of the profile to maximize

efficiency, taking into account heat losses by radiation, chemical reactions due to incomplete combustion, and chemical properties of the exhaust gases. In the inviscid case, nozzle profiles can be classified into several types, each generating its own internal flow field. It is crucial for a designer to understand these characteristics as the internal flow field influences flow detachment and lateral load behavior. Figure I.2 presents examples of Mach contour for different nozzles:

- Conical nozzle: section ratio ε=43.4 and length L=20[cm];
- TIC, TOC, and TOP nozzles: length L=17.7[cm];
- With a design Mach of 4.67.

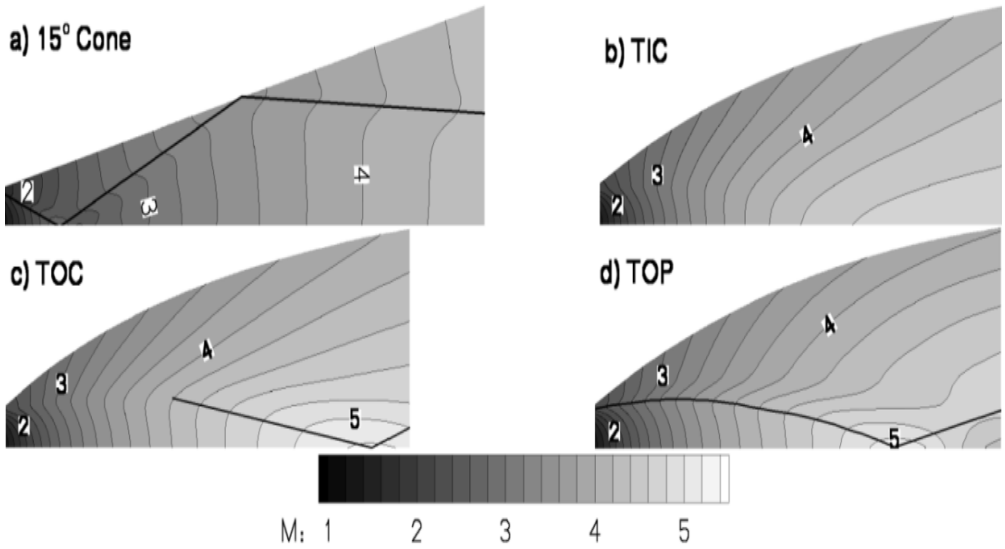

Figure I- 2: Mach contour in a 15° conical nozzle, TIC, TOC, and TOP with ε= 43.4. Bold lines indicate the approximate position of the internal shock [46].

Evidently, the most commonly used method by nozzle profile designers currently is the Method of Characteristics (MOC), which is based on solving the hyperbolic Euler equations **[47].** It allows for a design that takes into account certain specific physical characteristics, typically specified by the designer. The foundation of the Method of Characteristics (MOC) is the expansion zone (the Kernel region) determined by the area produced along the throat contour TN, as shown in Figure I.3 below. The subsonic/transonic flow field in the nozzle inlet and throat region must be computed. Generally, for conventional nozzles with a throat profile in the shape of a circular arc, the methods developed by Sauer R., Hall I. M., Kliegel J.R., & Levine J.N. are most appropriate **[48-49].** Conversely, for throat profiles of more complex shapes, the VNAP2 method developed by Cline M. C. **[50]** is recommended. It is based on transonic flow analysis, an initial TO line, a Mach number slightly greater than unity defined in the throat region. Considering the flow state along the initial TO line and the TN wall, a flow

field in the expansion zone TNKO can be computed using the Method of Characteristics **[51-52].** Given that the flow downstream of the TO line is supersonic, the core is entirely determined by the conditions at the throat. This, in turn, determines the flow character in the downstream region.

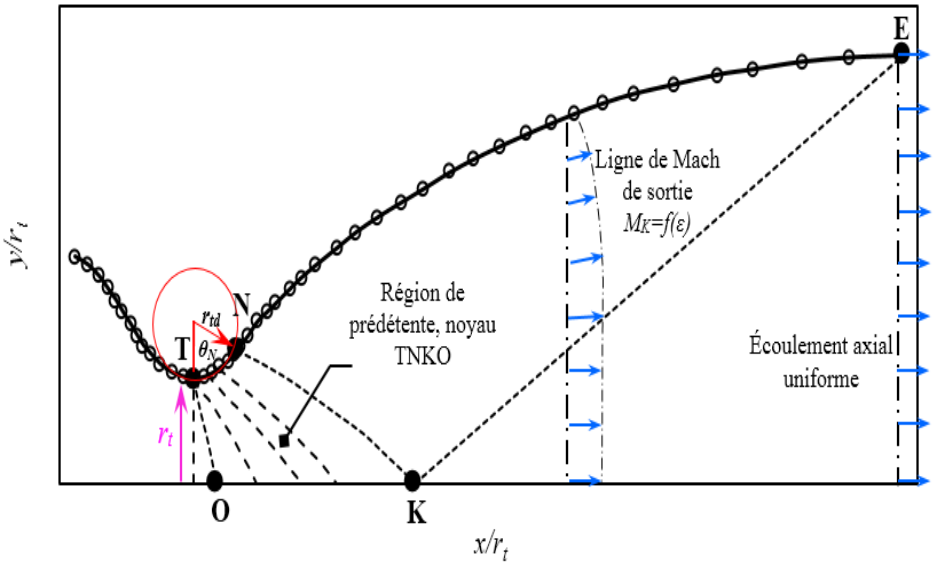

Figure I- 3: Basic components of an ideal profile.

I.1.3.1 Conical profile

The conical profile has always been the most widely used in rocket engines because it is simple and generally easy to manufacture. The exit jet velocity from the conical nozzle is approximately equal to the velocity calculated by a one-dimensional approach for the same area ratio. However, the flow is not axial over the entire exit surface. Efficiency loss is induced by flow divergence. Considering that the flow is conical at the exit, Malina F J. **[53]** showed that the geometric efficiency is given by the following relationship:

$$\eta_{geo} = \frac{1+\cos\alpha}{2} \qquad \textbf{(I .1)}$$

Where: α is the half cone angle, see Figure I.4.

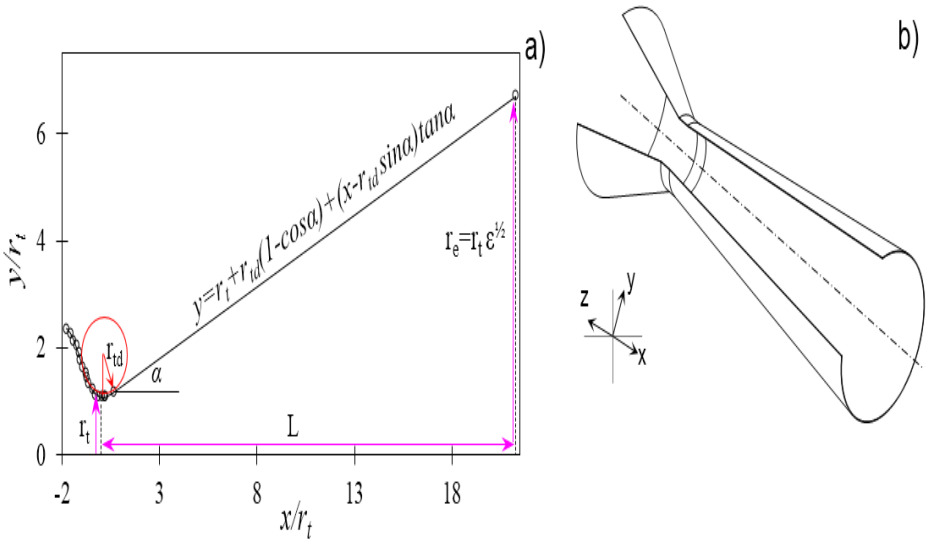

Figure I- 4: a) Definition of the conical profile, b) 3D diagram.

The length of the conical profile is obtained by the equation (1.2) below:

$$L_{\alpha^\circ,cone} = \frac{r_t\left(\sqrt{\varepsilon}-1\right)+r_{td}\left(\sec\alpha-1\right)}{\tan\alpha} \qquad \textbf{(I .2)}$$

In the design of nozzles for rocket engines, the area ratio (ε) represents the ratio between the exit area of the nozzle and the throat area, the nozzle radius (rt) measures the diameter of the nozzle, and the downstream curvature radius (rtd) describes the curvature of the nozzle exit section. Generally, the half-cone angle varies between 12° and 18°. However, the 15° conical profile is often used as a reference for comparing lengths and performances among different nozzle profiles. For a similar area ratio ε, the length of a curved profile is often given as a percentage compared to the length of a 15° conical profile. In the late 1930s, comprehensive studies were conducted by German scientists on various types of nozzle profiles. They considered all aspects of design and asserted that no significant advantage justifies the use of complex profiles. However, this assertion is valid only for nozzles with low area ratios like that of the V-2 rocket, presented in Figure I.5, due to the significant divergence losses they cause. The conical profile is now primarily used on short nozzles, such as those used in solid rocket boosters and small thrusters, where simple manufacturing is preferable to aerodynamic performance.

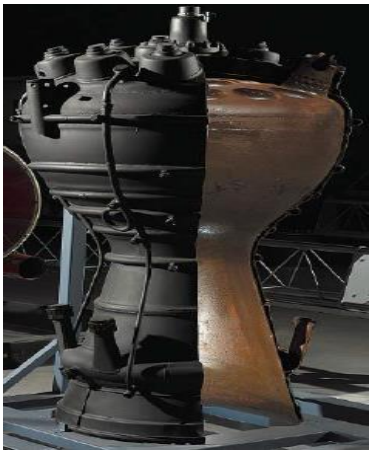

Figure I- 5: Conical nozzle of the V2 rocket.

I.1.3.2 Ideal profile

An ideal profile is one that produces an isentropic flow (without internal shocks) and a uniform velocity field at the exit of the nozzle, as shown in Figure I.3. Such a profile can be designed using the method of characteristics. The detailed procedure is outlined by Shapiro A.H**. [55],** Zurcow M. J. & Hoffman J. D. **[52],** and Anderson J.D. **[56].** After the expansion zone TN, the contour NE allows the flow to have an axial direction at the nozzle exit. Once the characteristic line NK is calculated with the condition that the line KE is a uniform exit characteristic, it is possible to use the method of characteristics (M.O.C) to construct the characteristic field between N and E. Figure I.6 depicts twelve (12) ideal profiles with iso-thrust coefficients at high altitude, iso-area ratios, and iso-wall pressure coefficients **[57].**

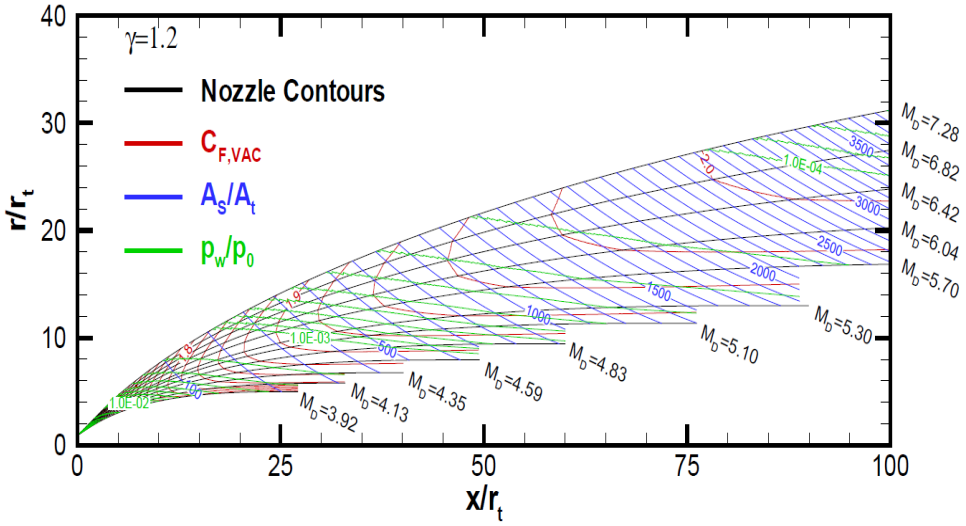

Figure I- 6: Chart of 12 ideal profiles with boundary layer calculation [57].

I.1.3.3 Truncated ideal contour (TIC) profile

A very long nozzle is necessary to produce a 1D flow. However, the latter is not suitable for aerospace applications where strict weight and structural limitations are imposed to increase payload capacity. In reality, the downstream portion of an ideal nozzle represents only a very small percentage of the total thrust, and its contribution can be neglected. Therefore, by truncating this nozzle, its use on rocket engines is facilitated without significant loss in performance due to non-uniformity of the flow at the exit. Such a profile is called a Truncated Ideal Contour (TIC) profile. The truncation can occur quite far upstream of the exit. As long as the expansion area is not truncated, the flow field will have a central portion where the exit velocity profile is axial and uniform. It will only diverge in the region near the wall, as shown in Figure I.7. The Mach contours in a TIC nozzle are depicted in Figure I.2b. This type of profile finds applications in actual nozzles such as the LR-115, Viking, and RD-0120 used respectively on the American Saturn C-1, European Ariane-4, and Russian Energia launch vehicles [46]. Ahlberg J.H. et al**. [58]** developed a graphical method for selecting optimal profiles from a family of TIC profiles. With this method on the same chart, they associated a set of ideal profiles with thrust coefficient isopleths, area ratio isopleths, diameter, and length, see Figures I.6 and 7. The profile shape is calculated using the Method of Characteristics (MOC). Note that this method takes into account the calculation of the thrust coefficient and all losses using a Two-Dimensional Kinetics nozzle performance code (T.D.K) proposed by Frey H.M. and Nickerson G. R. **[59].**

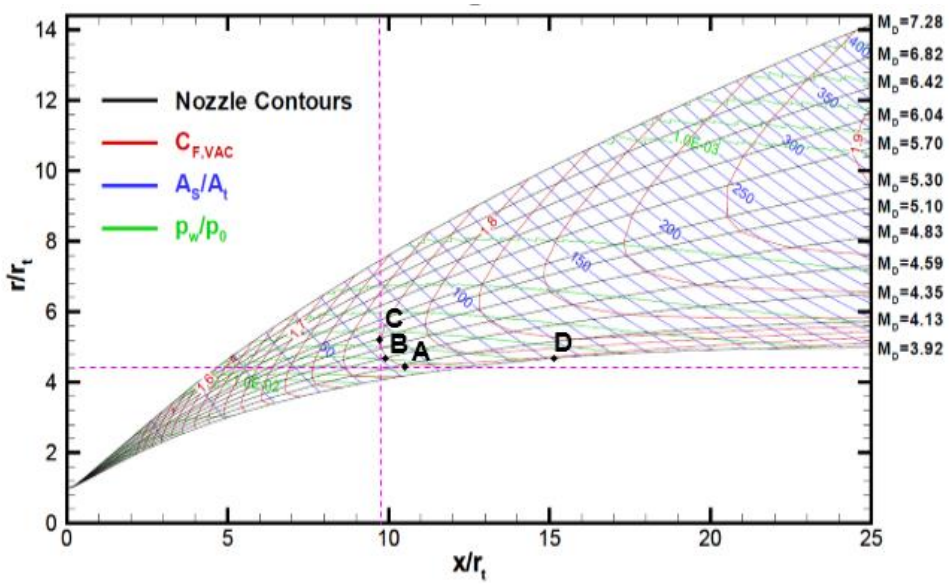

Figure I- 7: Ahlberg et al.'s Method for an Optimal TIC Profile [58].

I.1.3.4 Thrust-optimized contour (TOC)

Guderley K.G. et al. **[60]** formulated a mathematical model to determine the exit surface and profile shape that produces optimal thrust, for given values of length and ambient pressure. However, this approach was not widely followed until a simplified solution was presented by Rao G.V.R **[61].** Since then, this profile is often referred to as the Rao profile. In Russia, Shmyglevsky Yu. D. **[62-67]** independently formulated the same method. The basic idea of the Rao-Shmyglevsky profile **[61-66]** is the thrust-optimized profile (TOC) as illustrated in Figure I.8. Firstly, flow in the expansion region is generated using the method of characteristics MOC for a variety of θN (slope in the throat region) and Rtd (throat radius of curvature). For given design parameters (exit Mach number and ε area ratio or the length of the nozzle and ε area ratio), to obtain points P and N, it is necessary to simultaneously satisfy two conditions: ensuring that the mass flow rate through PE is equal to the mass flow rate through NP while maximizing thrust.

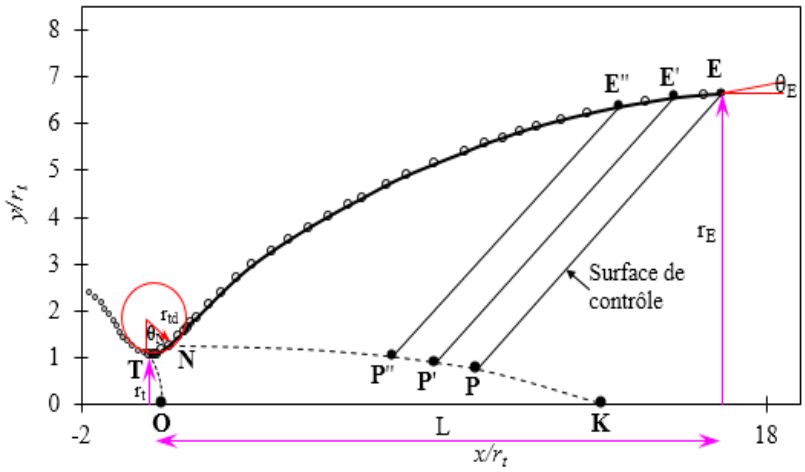

Figure I- 8: Definition of a TOC profile.

Using the calculus of variations, these conditions are formulated as specific relationships that must be satisfied along PE and NP **[61].** The length of a TOC profile is generally between 75% and 85% of the length of the conical profile. The index 80% is added to its notation (TOC80%). As mentioned earlier, the TOC profile depends on the slope θN. Figure I.9 illustrates a family of TOC profiles for 25°≤ θN ≤34° **[57].** In real applications, θN ranges between 25° and 28° **[67].**

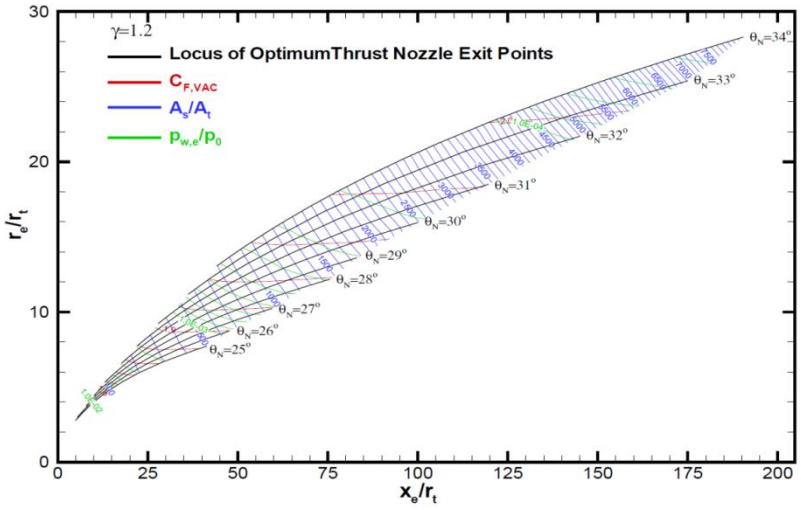

Figure I- 9: Family of TOC profiles for 25°≤ θN ≤34° [57].

The calculations leading to a TOC profile are quite intricate, and the resulting contour can only be described by a list of coordinates. Rao G.V.R **[67-68]** demonstrated that the TOC profile can be approximated by a parabola, with no significant loss in performance. This profile is often denoted as the Thrust Optimized Parabolic (TOP) profile. With such a parabola, the profile is fully defined using five independent variables, namely: Rtd, θN, L, Ys, and θs, as illustrated in Figure I.8. The major difference between the flow fields in TOC and TOP profile nozzles lies in the fact that the TOP profile presents a discontinuity at point N where the arc of the circle evolves into a parabolic curve. This curvature discontinuity generates compression waves that coalesce into an internal shock upstream of the last negative characteristic line C–, as shown in Figure I.10. In a TOC profile nozzle, the shock is formed downstream of the last negative characteristic line C–, as illustrated by the Mach contours in Figure I.2. Consequently, the wall pressure is influenced by the internal shock in the case of the TOP profile and by a slightly higher exit pressure in the case of the TOC profile. This particular property of the TOP profile proves very useful for nozzles operating at low altitudes to delay boundary layer separation. For this reason, the Vulcain and SSME (Space Shuttle Main Engine, respectively used on the European Ariane-5 launcher and the American Space Shuttle **[69])** nozzles are designed with TOP profiles. It is noteworthy that the initial design of the SSME profile was a TOC, and the change to the TOP profile resulted in a 24% increase in exit pressure with a loss of only 0.1% efficiency compared to the TOC nozzle.

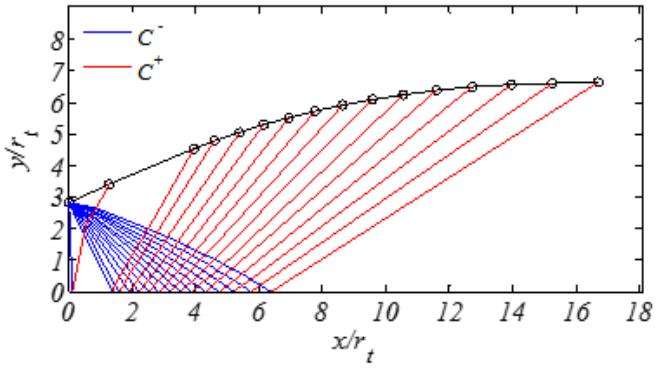

Figure I- 10: Characteristic lines C+ and C- in a nozzle profile.

I.1.3.5 Compressed truncated ideal contour (CTIC) profile

In 1966, Gogish L.V. **[69]** proposed compressing TIC profiles to design extremely short nozzles. He suggested that such a Compressed Truncated Ideal Contour (CTIC) profile could outperform a TOC profile for the same envelope (i.e., for the same length and area ratio). A CTIC profile is obtained by linearly compressing (with a factor C) a TIC profile in the axial direction to the desired length, as illustrated in Figure I.11. The CTIC profile exhibits rapid initial expansion followed by a more severe curvature compared to the TIC profile. Thus, strong compression waves are generated in the flow field. Sufficient compression leads to the focusing of characteristic lines to form an oblique shock. Wall pressure and thrust increase if the shock wave is near the nozzle wall. This mechanism was first proposed by Gogish L.V. **[70].** He suggested that a CTIC profile could offer better performance than a TOC profile; a proposition not shared by Hoffman J.D. **[71],** who emphasizes that the TOC profile always outperforms the CTIC profile. However, the performance gap between the two profiles is quite small (on the order of 0.04%) for certain models. Currently, this profile is used in the Mitsubishi LE-7A engine, which powers the Japanese H-IIA launcher **[69].** Figure I.12 presents a geometric comparison of various conventional nozzle profiles**.**

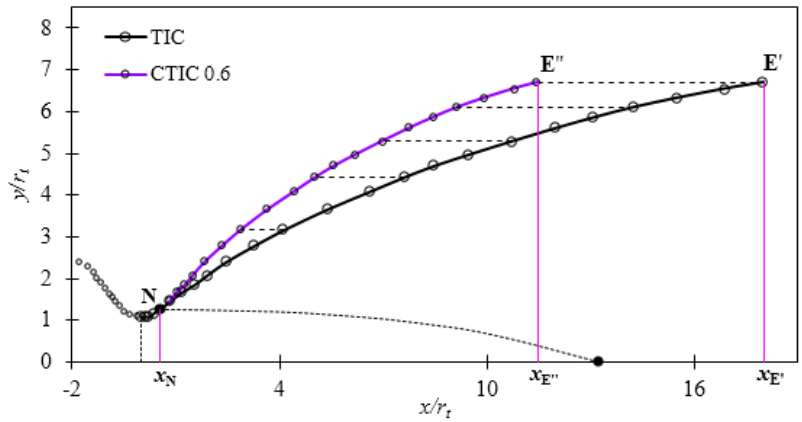

Figure I- 11: CTIC Profile with a Compression Factor $C = \frac{X_{e''} - X_n}{X_{e'} - X_n} = 0.6$, Compared to a TIC

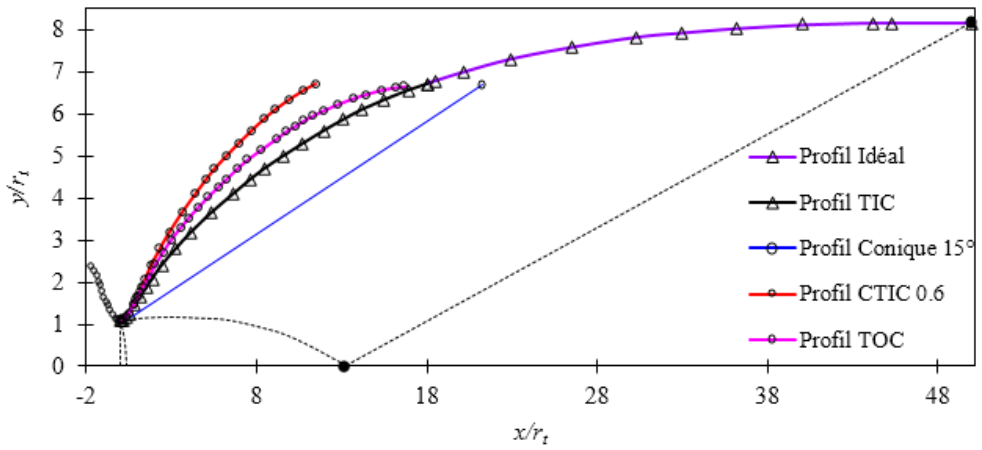

Figure I- 12: Comparison of Different Conventional Profiles.

I.1.4 Performance parameters

A rocket engine operates by propelling gases at high velocity to generate an opposite reaction and produce thrust. Propellant engines burn fuel and oxidizer in a combustion chamber, then direct the combustion products towards a nozzle where they are accelerated. The nozzle is defined from the point where the diameter of the chamber starts to decrease. Simply put, the nozzle exploits the temperature and pressure conditions of the combustion chamber to accelerate the combustion gases, thus generating thrust. The exit velocity (ve) depends on the expansion ratio of the nozzle (ε), which is defined as the ratio of the exit area to the throat area, ε = Ae / At.

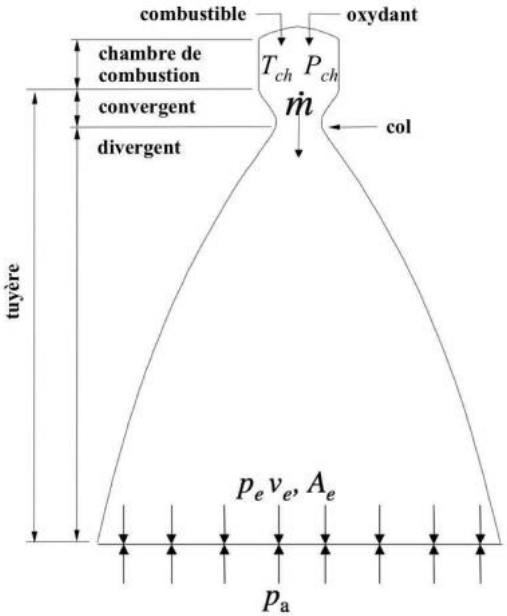

Figure I- 13: Principle of a Nozzle.

- Pch: Pressure in the combustion chamber considered as P0.
- Tch: Temperature in the combustion chamber considered as T0.

I.1.4.1 Flow rate

A nozzle, like any other orifice, allows the passage of a flow rate proportional to the passage area (throat area, At) and the upstream pressure (combustion pressure, P0). The proportionality coefficient, denoted by the term flow coefficient (CD), has dimensions of inverse velocity. Its inverse, commonly known as characteristic velocity (C*), is typically used. The associated mathematical formulations are as follows :

$$\dot{m} = C_D P_0 A_t = \frac{P_0 A_t \delta(\gamma)}{\sqrt{C_p T_0}} \qquad \textbf{(I .3)}$$

With:

$$\delta(\gamma) = \frac{\gamma}{\sqrt{\gamma - 1}} \left(\frac{\gamma + 1}{2}\right)^{\frac{1-\gamma}{2(\gamma-1)}} \qquad \textbf{(I .4)}$$

γ : Specific heat ratio at constant pressure and constant volume
Cp: Specific heat at constant pressure

$$C^* = \frac{P_0 A_t}{\dot{m}} \qquad \textbf{(I .5)}$$

A nozzle is said to be choked when the throat area is at sonic conditions. Under these conditions, the flow rate reaches its maximum value for a given P0.

I.1.4.2 The thrust

Thrust is the force generated by the nozzle, depending on the velocity of the ejected gases and the flow rate passing through it. This force, represented by the mathematical relationship, includes both dynamic thrust and pressure thrust. The total thrust (F) produced by the rocket engine resulting from the combination of these two components is described by the relationship:

$$F = \dot{m} v_e + (P_e - P_a) A_e \qquad \textbf{(I .6)}$$

where:

F: The thrust (N) ;
A_e: Nozzle exit area (m^2);
$\dot{m}$: Mass flow rate (kg/s).

I.1.4.3 The thrust coefficient

The thrust coefficient is defined as the ratio of thrust (F) to the product of the total pressure in the chamber and the area at the throat. This coefficient plays a characteristic role in the expansion of gases within the divergent section of the nozzle. It is a dimensionless quantity that expresses the relationship between the thrust force and the product of the generating pressure and the nozzle exit area, thereby providing an indication of performance.

$$C_F = \frac{F}{P_t S_c} \qquad \textbf{(I .7)}$$

With :

P_t : total pressure

S_c : Nozzle exit area

It corresponds to the increase in thrust in the nozzle compared to the thrust it would have at the throat (no divergent).

I.1.4.4 The discharge coefficient

The discharge coefficient, denoted Cd, is defined as the ratio of the actual flow rate to that determined from isentropic relations. When considering a fluid to be perfect and inviscid, or when assuming flow to be isentropic, it simplifies calculations and reduces the equations describing a phenomenon in aerodynamics or fluid mechanics in general. However, in reality, this assumption introduces an immediate error into the results. To correct for this, upon introducing the discharge coefficient, a dimensionless entity expressing the error made per unit of result

$$Cd = \frac{Débit\ actuel\ réel}{Débit\ actuel\ isentropique} \qquad \textbf{(I .8)}$$

$$\dot{m}_{rel} = C_d \,.\, \dot{m} \qquad \textbf{(I .9)}$$

And:

$$C_d = C_{dk} + C_{d\delta} \qquad \textbf{(I .10)}$$

C_{dk} : Effect of the nozzle throat geometry on the sonic line

$C_{d\delta}$: Effect of the boundary layer

I.1.4.5 Characteristic velocity

It's the velocity measured at the throat, denoted by C*, and it depends on the velocity, the nature of the fluid, and its generating temperature:

$$C^* = \frac{P_t A^*}{\dot{m}} \qquad \textbf{(I .11)}$$

I.1.4.6 Effective velocity

The effective velocity, noted V_{eff}, represents the adapted nozzle exit velocity, determined by the ratio of thrust to mass flow rate. It is the actual velocity measured at the exit of a nozzle, depending both on the thrust force generated by an adapted nozzle and the flow rate passing through it.

$$V_{eff} = \frac{F}{\dot{m}} \qquad \textbf{(I .12)}$$

I.1.4.7 Specific impulse

It's a highly significant parameter in the field of propulsion, denoted as I_s , often used for comparing the performance of various propulsion systems. It's measured by dividing the thrust by the product of the mass flow rate and gravitational acceleration.

$$I_s = \frac{F}{\dot{m}\, g} \qquad \textbf{(I .13)}$$

I.1.4.8 Total impulse

Total impulse, symbolized by I, is defined as the integral of thrust over the entire duration of operation.

$$I = \int_0^T F dt \qquad \textbf{(I .14)}$$

I.1.5 Operating regimes of a conventional nozzle

In a nozzle primed with a sonic state at the throat, the flow regime is exclusively determined by the relationship between the ambient pressure, noted as Pa (considered variable), and the static pressure at the exit Pe ,vac (indicating a vacuum reference). In practice, two types of flows are observed: those that remain attached and those that detach.

I.1.5.1 Non-detached flow

When the flow in the divergent remains attached to the wall, the pressure profile along the wall is not affected by the external ambient pressure, but depends primarily on the chamber pressure, pc, and the geometry of the nozzle used. This type of flow occurs when the engine operates at (or beyond) the altitude for which it was designed. In terms of pressure ratio, this corresponds to:

- $p_a / p_{e,vac} = 1$: Nozzle adapted to ambient pressure.
- $p_a / p_{e,vac} < 1$: Under expanded nozzle.

In this scenario, an expansion phenomenon occurs at the nozzle exit, as illustrated in Figure I.14.a. The adjustment of pressure between the jet emanating from the nozzle and the ambient environment must occur outside the divergent, through the formation of oblique shock waves. These shock waves generate a series of periodic diamond-shaped cells. The size of these cells increases as the ambient pressure, Pa decreases.

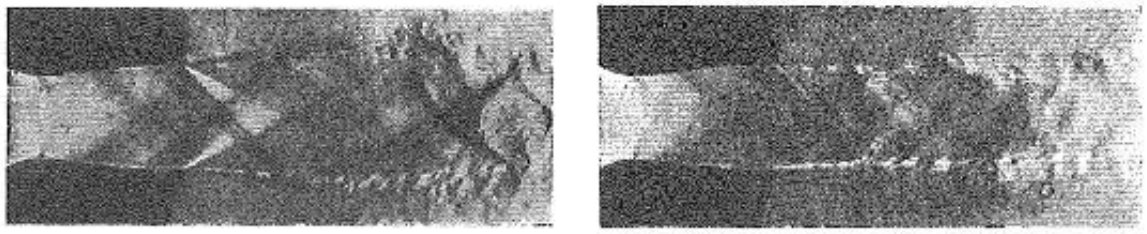

Figure I- 14: a) 2D nozzle in under expanded regime (pa /pe,vac =0.66), pa /pe,vac =0.66), b) 2D nozzle in over expanded regime with Mach reflections (pa /pe,vac >2.5), [72].

I.1.5.2 Flow with incipient separation

When the pressure ratio exceeds unity ($p_a / p_{e,vac} > 1$), the nozzle enters a state of overexpansion, generating a shock wave (compression or detachment) at its lip. In Figure I.14.b, it can be observed that the boundary layer experiences an adverse pressure gradient, thickening while remaining attached to the wall until the nozzle exit. Various shock structures, detailed later, can be observed in the jet**.**

I.1.5.3 Flow with actual separation

If the downstream pressure continues to increase beyond a defined threshold (, leading to a regime of strong over-expansion, as observed in practice **[77]),** there comes a point where the boundary layer can no longer withstand an excessive pressure gradient, causing its separation, as illustrated in Figure I.15.

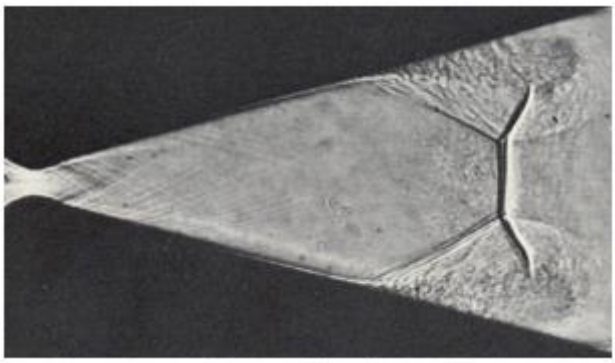

Figure I- 15: Effective Separation during Rapid Expansion [74].

As mentioned earlier, various shock structures can be observed in the jet.

1. When the nozzle profile exhibits a gentle evolution, as in the case of the TIC (Transition Into Cruise), the separation shock may reflect off the axis of symmetry. Two types of reflections can then occur:
2. A reflection called "regular," where the incident shock "I" reflects directly off the axis of symmetry as a reflected oblique shock "IR," as illustrated in Figure I.16.a. Although theoretically improbable in axisymmetric nozzles, it may happen that the Mach disk is small enough for the reflection to appear regular.
3. A reflection called "singular" or "Mach," where the incident shock "I" reflects forming a normal shock to the axis, creating a Mach disk, as illustrated in Figure I.16b. A slip line "SL" emanates from the triple point "TP," where the incident shock, the reflected shock, and the Mach disk meet. This iso-bar discontinuity separates the subsonic pocket downstream of the strong shock from the supersonic region downstream of the reflected shock "IR."

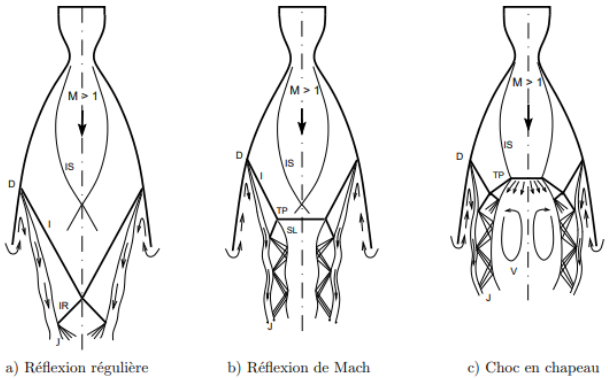

Figure I- 16: a) Regular Reflection, b) Mach Reflection, c) Hat Shock. I: Incident shock, IS: Focusing shock, IR: Reflected shock, J: Jet, SL: Slip line, TP: Triple point, D: Detachment point, V: Vortex. [74].

It is worth noting that the occurrence of either of these reflections is largely influenced by the pressure ratio and the nozzle configuration. Moreover, the transition between these reflections may result in a hysteresis phenomenon.

When the nozzle profile is specifically optimized for thrust, as in the cases of TOC (Takeoff Climb) or TOP (Takeoff Power), an internal focusing shock "IS" forms due to the modification of curvature at the throat (see above). The interaction between this internal shock and the detachment shock "I" can generate a complex shock structure called "hat shock" or "cap-shock," as illustrated in Figure I.16.c. This configuration would result from the interference between the detachment shock and the reverse reflection of the internal shock along the axis of symmetry. Again, the appearance of either of these structures is determined by the nozzle profile, pressure ratio, and also exhibits a hysteresis effect. Figure I.17 shows an image of the Vulcain operating on the ground on the DLR/Lampoldshausen P5 test stand, with the interpretation of the two shock structures.

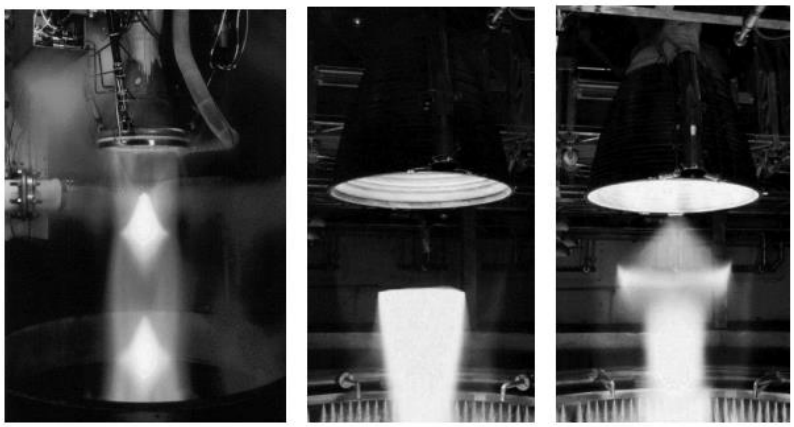

Figure I- 17: a) Mach disk structure, nominal pc, b) Cap-shock structure, 95% nominal pc [75].

I.1.5.4 Free, constrained, and transitional separations

Generally, the observed separation is of the free type, which means that the jet detaches

from the nozzle before reaching its exit lip and ejects autonomously. However, in the case of certain nozzle designs, another type of separation, known as "constrained separation," can also occur. This is characterized by a rapid reattachment of the boundary layer that had initially detached.

I.1.5.4.1 Free Separation Shock (FSS)

When it comes to free separation (FSS: Free Shock Separation), the over-expanded flow inside the nozzle completely detaches for a certain pressure ratio, pa/pw (where pw represents the wall pressure). At this separation point, a return flow forms downstream: a portion of the ambient fluid is "drawn in" to the separation point before being redirected and combined with the main jet emanating from the nozzle, as illustrated in Figure I.18.

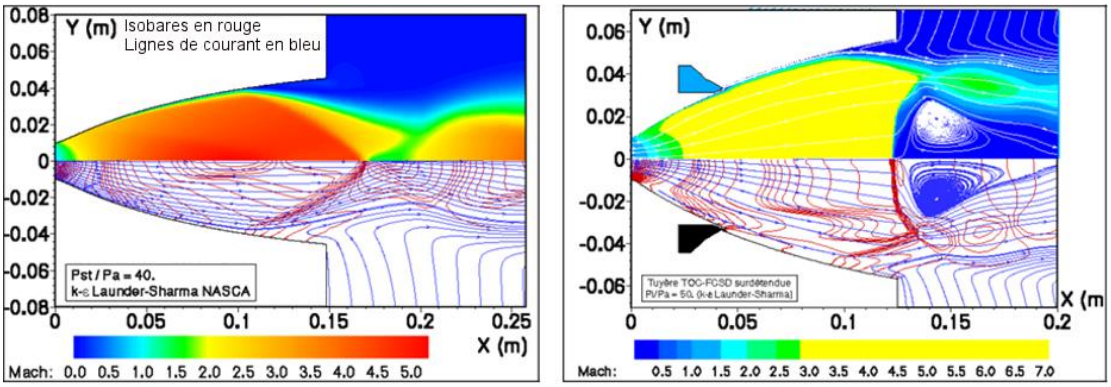

a) ONERA-TIC (p_{ij}/p_a=40) b) ONERA-TOC (p_{ij}/p_a=50)

Figure I- 18: Free Separation in Over-Expanded Nozzles. Iso-Mach contours on top, isobar contours, and streamlines below [75].

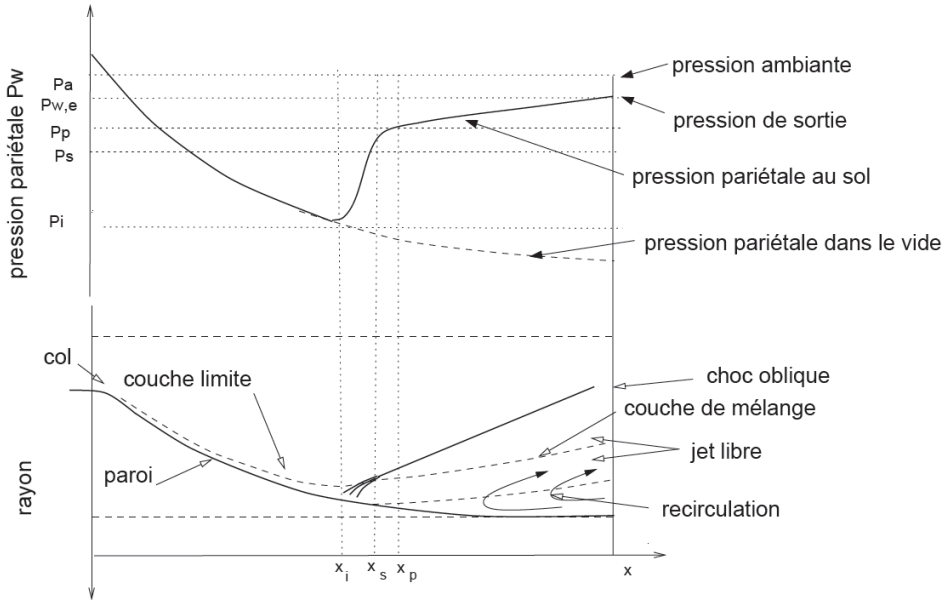

Figure I- 19: Schematic Representation of Free Separation, adapted from [76].

The variation in wall pressure, pw, can partly result from physical interactions between shock waves and the boundary layer in supersonic flow. The first deviation of wall pressure from its evolution in a vacuum, pw, vac, is termed as the incipient separation pressure and is

denoted by pi. Subsequently, the wall pressure rapidly increases until it reaches a pressure plateau pp., usually lower than the ambient pressure p. It is important to emphasize that effective separation occurs further downstream, at xs, slightly before reaching the plateau. The pressure rise between pp and pa, resulting from the recirculation zone, is significantly less pronounced, as shown in Figure I.19. Therefore, it emerges that free separation involves two distinct mechanisms. The first is associated with the detachment of the jet from the wall and is regulated by the pressure jump pi /pp, while the second is related to the ambient flow drawn into the recirculation zone, influencing the evolution of the ratio pp/pa.

I.1.5.4.2 Restricted separation

In the 1970s, Nave and Coffey identified a second type of separation configuration during their tests on scale models of the J-2S engine using cold gas. This new type of separation, named "restricted" (RSS: Restricted Shock Separation) due to its limited recirculation zone, was confirmed in 1994 by numerical simulations conducted by Chen et al. Subsequently, this phenomenon was observed not only on other small-scale models but also on real engines. Initially, researchers believed that this configuration only occurred on scaled-down models operating with cold gas. However, it is now established that this configuration is primarily influenced by the nozzle profile rather than its size.

For this flow regime, which occurs only at certain pressure ratios, the flow separates and then quickly reattaches to the nozzle wall. The evolution of the wall pressure downstream of the separation is irregular, sometimes exceeding ambient pressure, as illustrated in Figure I.20. This phenomenon is attributed to the reattachment of the detached flow, inducing compression and expansion waves in the supersonic jet.

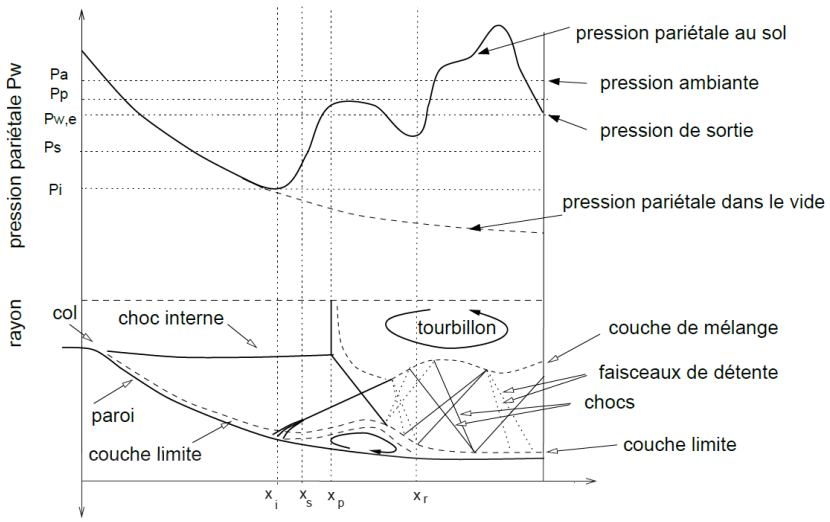

Figure I- 20: Schematic representation of restricted shock separation, adapted from [76]. The indices i, s, p, and r refer, respectively, to the point of incipient separation, the point of effective separation, the plateau, and the reattachment point.

I.1.5.4.3 Transition and "end effect"

When engines initially subjected to free shock separation are ignited, the transition to restricted shock separation occurs at a well-defined pressure ratio pc/pa. Restricted shock separation, as mentioned earlier, is characterized by a closed recirculation zone where pressures are lower than ambient pressure. This transition from free shock separation (FSS) to restricted shock separation (RSS) is accompanied by a sudden downstream movement of the separation point. As the generating pressure increases, the recirculation bubble also moves downstream, eventually reaching the nozzle exit. At this stage, the recirculation zone opens up to ambient fluid, resulting in a pressure rise in the return zone behind the separation shock. Consequently, the separation point is pushed upstream, and the recirculation zone may close again, leading to a new pressure drop and downstream movement of the separation point. Thus, a recurrent cycle, associated with the opening and closing of the recirculation zone, is observed. This transition from restricted shock separation to free shock separation is termed as "end effect" or "lip effect".

Similar phenomena can be observed during the engine shutdown phase, for example, during ground tests. However, in the case of a transition from free shock separation to restricted shock separation during ignition, the generating pressure ratio is the same as during startup. In contrast, the transition from restricted shock separation to free shock separation differs, thus illustrating a hysteresis effect.

Frey and Hagemann proposed an explanation of restricted shock separation based on experimental observations and numerical simulations. According to their findings, the cap-shaped shock structure would be the key element in the transition from free shock separation to restricted shock separation. They conclude that this transition can only occur in nozzles with an internal shock (i.e., TOC and TOP), a conclusion confirmed by numerical simulations, as illustrated in Figure I.21.

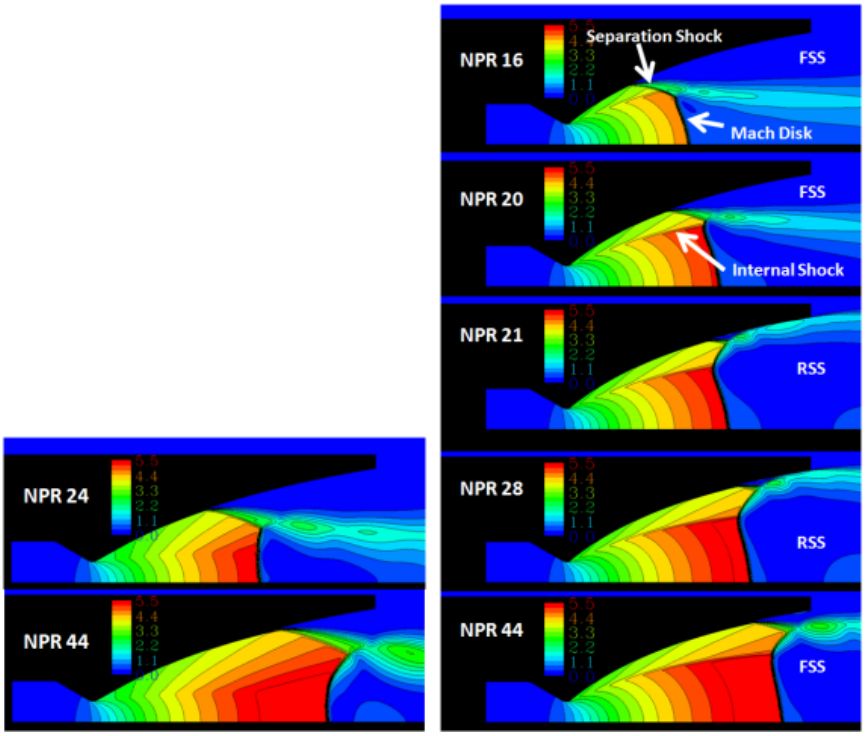

Figure I- 21: Transition from FSS to RSS to FSS in a TOP nozzle (left), and an FSS in a TIC nozzle (right), [77].

I.1.5.4.4 Asymmetry and Unsteadiness of Separation

We have outlined the main characteristics of free and restricted separations in steady-state flow. At this point, it is crucial to emphasize that these separations can exhibit asymmetries, as illustrated in Figure I.22.

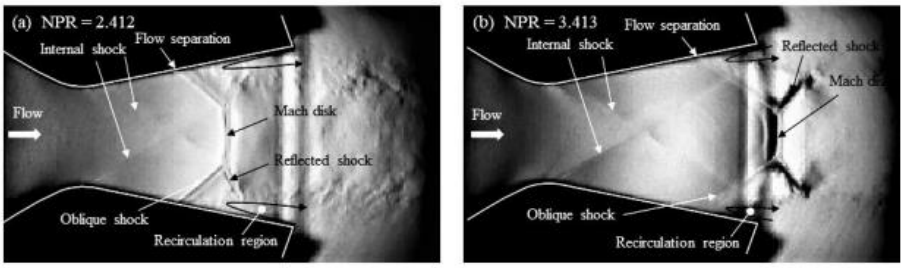

Figure I- 22: Shock waves in the experimental planar nozzle captured using Schlieren technique [78]: (a) NPR = 2,412 and (b) NPR = 3,413.

The asymmetric nature of the flow has been extensively examined, notably by Lawrence. His experiments revealed that asymmetric separations, whether stable or not, could occur in all types of nozzles, whether two-dimensional, axisymmetric, conical, contoured, with small or large area ratios. It was also observed that this asymmetric regime tended to appear generally in intermediate ranges of NPR, after or before phases of symmetric separation. Furthermore, the asymmetric nature of separation could be associated with a phenomenon of

tilting from one side to the other of the divergent. The study of the unsteadiness and asymmetry of separation in supersonic nozzles was revisited in the 2000s, as mentioned in, and more recently in the context of Laval nozzles. These researches highlight the inherent complexity in understanding and controlling the symmetry and stability of separation. It is also important to note that turbulent separation induced by shocks is inherently fluctuating (a comprehensive review on this subject is available in). This characteristic of separation plays a crucial role in the generation of lateral loads, hence the proposal of several separation prediction models.

I.1.6 Origin of side loads in optimized nozzles

The lateral forces observed in rocket engine nozzles can have various origins, as illustrated in Figure I.23.

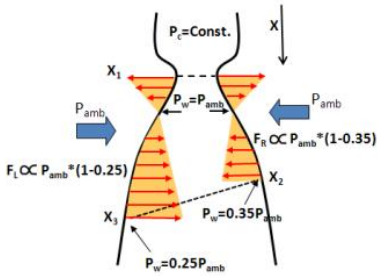

Figure I- 23: Simplified diagram of the aerodynamic forces contributing to lateral loads [77].

Self-sustained pressure fluctuations in the separation zone can induce non-axisymmetric oscillations of the shock and separation line, as depicted in Figure I.23. Therefore, even if, on average, the separation may be considered axisymmetric, fluctuating lateral forces can occur when these pressure fluctuations are not in phase.

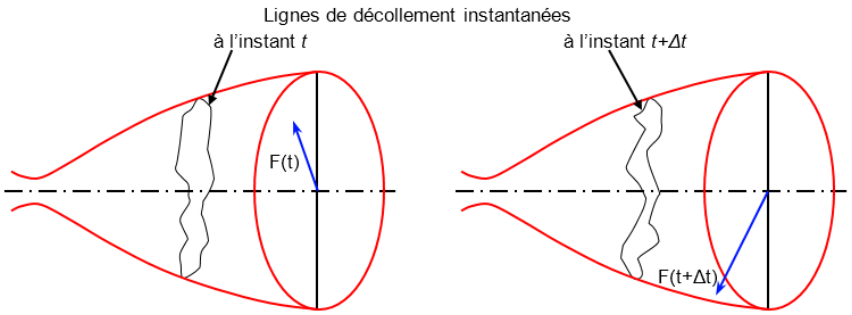

Figure I- 24: Schematic representation of the aerodynamic lateral force phenomenon, [77].

- Asymmetric tilting of the detached jet over a section of the nozzle can lead to highly asymmetric pressure and friction distributions along the wall, thus resulting in lateral forces. These tiltings can occur in nozzles with low divergence and under high over-expansions

- Non-axisymmetric disturbances originating upstream of the jet, such as those generated by combustion instabilities, can cause variations in local pressure and temperature that alter the position of the detachment shock.
- Aeroelastic coupling between the fluid and the structure on complex non-axisymmetric modes can amplify the vibratory behavior of the nozzle.
- Transitions between different detachment regimes, free and restricted, can induce lateral forces, particularly for certain forms of optimized nozzles.
- External pressure fluctuations around the nozzle can also contribute to lateral loads, either by acting directly on the external wall or by coupling with pressure fluctuations within the detachment inside the nozzle.

It is crucial to highlight, at the end of this section, the main performance losses in the currently used conventional nozzles. The performance losses of two typical high-performance engines, the SSME and the Vulcain-1 engine of Ariane-5, are presented in Table 1, **[77].**

Table I- 1: Performance losses in conventional nozzles [77].

Performance losses	**SSME**	**Vulcain 1**
Combustion incomplète	0.5 %	1.0 %
Boundary Layer	0.6 %	1.1 %
Exit flow divergence	1.0 %	1.2 %
Chemical non-equilibrium	0.1 %	0.2 %
Non-adapted flow	0–15 %	0–15 %

According to **[24],** losses related to viscous effects resulting from the turbulent boundary layer, flow divergence at the exit, and non-equilibrium chemical effects can be neglected in H2-O2 rocket engines with a chamber pressure pc ≤ 50 bars. However, the most significant performance losses stem from the mismatch of the flow at the nozzle exit.

I.2 ALTITUDE COMPENSATION NOZZLE

For most research endeavors, the objectives pursued involve describing and characterizing separation zones, defining design criteria, and enhancing existing ones to create nozzles capable of operating on the ground under overexpansion conditions without jet separation. A comprehensive compilation of all proposed criteria (mostly empirical or semi-empirical) has been gathered by Stark R. **[79].** All these studies underscore the significant role played by ambient pressure in jet separation occurrence in supersonic nozzles. The ratio between static pressure at the wall and ambient pressure is often used as a good correlation parameter to predict its occurrence. However, most control techniques proposed in these studies have only been tested in laboratories, on small surfaces, and under very low enthalpy flow conditions. Unfortunately, these conditions are not representative of those encountered in rocket engines. The proposed control techniques often seem inapplicable to these vehicles because they are too complex and inappropriate for their operating conditions. Below, we will present various ideas proposed for controlling, preventing, mastering, or reducing separation effects. Subsequently, a thorough exploration of research conducted to improve nozzle performance focuses particularly on studying different geometric shapes and their ability to function in multiple modes while anticipating the separation phenomenon.

1. Within the category of **controlled separation nozzles**, various concepts can be found, such as the nozzle with controlled internal roughness **[80].** This idea involves integrating angular sectors with increased roughness on the inner surface of the nozzle, aiming to limit the lateral forces that may be generated by a potential asymmetry of the separation line. However, there is no documentation in the literature confirming the effectiveness of this device. Moreover, continuous operation with a well-established separation line inside the nozzle could have adverse consequences on its thermomechanical resistance. Regarding the ***deployable or extendable divergent nozzle***, also known as the two-position nozzle, several numerical studies have been conducted. For example, Sato et al. **[81]** conducted tests on a scaled model to assess the lateral loads exerted on the movable part during deployment in flight. These loads constitute a major constraint for the mechanical design of the engine, especially for the deployment system and the divergent itself **[82].** The inability to ground-validate the engine design under flight-representative conditions poses a significant obstacle to the adoption of this type of concept without compromising the launcher's reliability.
2. Regarding **trigger-ring nozzles**, two subcategories can be distinguished based on the triggering mechanism of the ring. For example, **the fixed trigger-ring nozzle**, designed to control boundary layer separation, employs a trigger fixed on the inner wall of the divergent,

symmetrically disturbing the boundary layer and promoting its separation under overexpansion conditions (see Figure I.14.a). At very high altitudes where ambient pressure is very low, flow reattaches behind the trigger, allowing full utilization of the area ratio and resulting in thrust augmentation. The transition between the two modes (low altitude and high altitude) depends on various parameters, including trigger size **[83].** Although this nozzle exhibits performance practically equivalent to the double-bend concept **[46],** issues such as high-temperature resistance, precise trigger fixation, and uncertainty regarding the transition between operational modes have affected its performance. Consequently, interest in this concept has declined since the 1970s **[83-84].** Another subcategory is **the temporary trigger-ring nozzle**, equipped with a temporary trigger (insert) to control separation at low altitude. This trigger is removed in vacuum mode operation. Therefore, the trigger can be ejectable or ablative respectively **[85-86],** as shown in Figure I.14.b. The trigger can also be a total secondary nozzle or a partial insert fixed inside the nozzle wall. This type of triggers causes a slight performance loss in low altitude mode compared to a curved nozzle of the same area ratio **[86-88].** Hot tests of ejectable trigger nozzles have demonstrated the feasibility of this concept **[87].** However, it is important to note that this concept heavily relies on a reliable mechanism that provides abrupt and symmetrical detachment of the insert. Asymmetric ejection would lead to lateral loads generation. Moreover, there is a risk of downstream collision with the nozzle wall, as the inserts may also experience transverse movement towards the wall. These limitations of ejectable inserts have led to considering the use of ablative inserts (in consumable solid fuel) **[83, 86, 89].** During launcher ascent, the insert continuously reduces in size until complete consumption, resulting in a curved nozzle with better performance at high altitude operation. The main uncertainties of this concept lie in the consumption rate and the stability of the insert. Furthermore, uniform, symmetrical, and well-defined consumption over time must be ensured, despite possible local pressure and temperature fluctuations near the nozzle wall.

3. **The secondary flow injection nozzle** is divided into two distinct categories. Firstly, **the passive secondary injection** nozzle operates by controlling the jet detachment position through the injection of a secondary fluid flow, directly extracted from the external atmosphere, into the nozzle through slots in the metal wall, hence the name "Vented Nozzle**" [46]** (see Figure I.15a). At high altitudes, these slots close, allowing the nozzle to function suitably at different flight altitudes, thus enhancing overall engine performance. Parsley R.C. and Van-Stelle K.J. [90] conducted hot tests to characterize this concept. The

results showed that this nozzle behaves similarly to a TIC-profile nozzle at low altitudes. In 2007, Semenov V.V. et al. **[91]** carried out an experimental measurement campaign, revealing that the performance gain remains limited, in the range of 1 to 3%. Moreover, the presence of lateral loads at low altitudes and significant leakage of hot gases outward at high altitudes are major limitations for the application of this concept on a launcher. Secondly, **the active secondary injection nozzle** introduces gas at a defined pressure into the main flow of the nozzle, either perpendicularly or at an angle from the wall, thereby inducing separation of the overexpanded flow at the desired location (see Figure I.15.b). An experiment conducted by Ward J.J. & Musical N.T**. [92]** demonstrated that this method requires a large quantity of gas to induce significant flow separation. However, no clear improvement in efficiency is observed when considering the additional mass flow rate. Another approach to this concept was proposed by Bonniot C.E. **[93]** (see Figure I.16.a), with the main idea of reducing the external pressure at the nozzle exit section by placing a secondary nozzle near the exit of the main divergent. Although this proposition is promising, the curved secondary nozzle variant defined by the author **[93]** has not demonstrated significant effectiveness. For example, the Vulcain1 engine incorporates one of the variants proposed by the author, but its sensitivity to jet separation does not differ from that of other engines in the same category. More recently, Boccaletto L. **[94]** suggested installing a truncated central body nozzle (aerospike) at the end of the main nozzle, called BOCCAJET (see Figure I.16b). Cold gas experimental measurements as well as numerical simulations have indicated a potential performance improvement, although no operational results have been discussed.

4. **Vortex generator nozzles** aim to reduce lateral loads by proposing two distinct non-axisymmetric concepts, divided into two main categories. Firstly, **the concept of wavy-walled divergent,**the essence of this concept **[95]** lies in the idea of increasing resistance to separation by creating vortices using a wavy contour at the nozzle exit (see Figure I.24.a). This wavy contour is designed to slow down the lateral movement of the separation line by increasing drag in the critical area, while inducing longitudinal vortices that stabilize the circumferential flow structure (see Figure I.23). Cold gas tests on sub-scale models have shown that the wavy contour significantly reduces, and in some cases completely eliminates, separation induced by shock in the overexpanded flow **[96].** However, due to the high wall stress on the wavy surface and an increase in overexpansion losses, separation control is achieved at the expense of significant performance losses, ranging from 3.6–6.4%

compared to the fully separated case. Furthermore, the complexity of design and manufacturing significantly increases when transitioning from revolution geometry to a three-dimensional geometry. **The concept of polygonal divergent** aims to control jet separation by introducing edges along the divergent, promoting a gradual transition from the throat to the exit, and transitioning from a circular to a polygonal section of the nozzle **[97].** Experimental research on this concept was conducted within the FSCD working group, under the supervision of Östlund J. & Bigert M. **[98].** However, despite these efforts, the results obtained were not deemed convincing**.**

5. **Two-mode nozzles** have experienced significant success, notably **Dual-throat nozzles,** this concept proposes two completely concentric combustion chambers, as illustrated in Figure I.25.a. At low altitude, both chambers operate in parallel with a moderate expansion ratio. Conversely, at high altitude, only the inner chamber remains operational. Flow reattachment occurs on the outer wall, resulting in a higher expansion ratio than in the first mode, thus allowing for performance gains at high altitude. Combustion tests revealed the presence of separation at low altitude when the pressure ratio between the outer and inner nozzle is high **[99].** This separation is caused by high thermal loads on the inner nozzle. Additionally, profile mismatch at high altitude results in performance losses ranging from 0.8 to 4%, depending on the area ratio between the outer and inner throats **[100]. Concentric Dual-thrust engines** present two concentric engines, with the smaller one housed inside the larger one, as depicted in Figure I.25.b **[101].** Unlike previous configurations, the inner chamber is not fully contained within the outer chamber; the latter has an annular shape with an independent inner wall. In principle, the two operating modes are similar to those of a dual-throat nozzle **[100].** Numerical simulations have revealed the presence of compression waves near the exit lip of the inner nozzle at low altitude **[102-103].** These waves contribute to flow non-uniformity in the common mixing zone between the inner and outer nozzles, reflecting downstream in the flow field after interacting with the outer wall. In high-altitude mode, expansion waves appear at the exit of the outer nozzle when the area ratio increases abruptly, and the flow is directed towards the axis of symmetry. Near the axis, a shock forms, significantly increasing static pressure in the central region of the jet. This pressure increase generates subsonic and supersonic recirculation zones in the inner nozzle. Losses due to non-uniformity and compression shock remain comparable to those observed in conventional curved nozzles **[100].**

6. **Self-adaptive internal flow nozzles** are based on the concept of varying the area ratio of the nozzle by deploying its surface, which was previously folded **[104],** as shown in Figure I.26. This allows adapting the nozzle exit pressure to all flight altitudes. Although theoretically the most suitable solution to eliminate jet separation and maximize nozzle performance, its feasibility remains completely to be demonstrated. Nevertheless, similar technological solutions (overlapping petal nozzles) have been used on ballistic missiles and certain military aircraft nozzles. This technology allows for relatively modest area ratio variation rates and cannot be easily integrated into nozzles requiring active cooling of the metal wall. **Variable surface throat nozzles**, depicted in Figure I.27, utilize a conventional curved nozzle with a fixed exit section and a mechanical needle located in the combustion chamber and throat region to adjust the throat surface. The throat section, which takes on an annular shape between the needle and the outer wall, is modified by axially moving the needle. Initially developed for solid propellant engines to allow for variable thrust, this concept theoretically offers continuous throat section adaptation and thus optimal area ratios throughout the mission. However, its use requires sophisticated actuation devices and a complex control system. Disadvantages associated with this concept include increased engine weight, design complexity, challenges related to needle and throat wall cooling, and reliability issues. Performance losses for this type of nozzle are estimated between 1 to 2.5% compared to a conventional curved nozzle for the same area ratio **[104],** with losses varying depending on the needle position. **Expansion/deflection nozzles**, presented in Figure I. 28, primarily aim to reduce overall engine bulk, particularly in the longitudinal direction, and several variants of this concept have been proposed. The most famous involves positioning the combustion chamber and engine components at the center of the nozzle **[105].** In this configuration, combustion gases reach sonic velocity in an area where their flow direction undergoes significant deflection to be directed into the supersonic nozzle without generating shockwaves. This avoids concentrating a compression wave on the nozzle's metal wall, which would be detrimental to the thermomechanical resistance of the structure. The definition of the profile of the sonic region of the combustion chamber, as well as its cooling system, represents critical points of this concept. Despite this, a prototype was developed in Russia (RD-0126E engine), and firing tests were conducted in the 1990s, demonstrating the effectiveness of this type of engine. However, these nozzles are primarily intended for use in vacuum conditions, as they do not solve jet separation issues in atmospheric conditions.

7. Regarding **External Flow Self-Adapting Nozzles**, self-adaptation involves the nozzle's external boundary adjusting according to the external pressure Pa. The significance of plug nozzles compared to conventional nozzles becomes apparent during overexpansion regimes, where the external boundary adapts, channeling the jet through a variable effective area Aeff depending on external pressure. A plug nozzle operates with an adaptable effective area ratio Aeff/Ac, according to altitude, resulting in self-controlled expansion of propellant gases. Several studies in recent years have evaluated the optimal spine geometry, such as Dunn S. S. & Coats D. E. **[106],** Calabro M. & al. **[107],** Le Bozec A & al. **[108],** Wisse M. E. N. **[109-110],** Onofri M. **[111],** assessing the performances and limits of different possible architectures. Two types of these nozzles can be distinguished. **Ideal Central Body Nozzles**: This concept involves using an ideal axisymmetric central body, also known as a "full-length plug nozzle," with a conical or curved profile, as illustrated in Figure I.29. Profile calculation relies on the method developed by Rao G.V.R. **[60],** taking into account kinematic and boundary layer effects using the Two-Dimensional Kinetics (TDK) method **[106].** Compared to an ideal internal flow nozzle, the profile of an ideal spine is significantly longer and therefore heavier than a conventional ideal nozzle. This type of nozzle offers several advantages, including better performance at low altitude and equivalent performance at high altitude compared to a conventional nozzle with the same area ratio [54]. However, due to its weight and length, it is challenging to integrate into a launcher and requires high-technology cooling systems, especially at the spine's end. **Truncated Central Body Nozzles**, Compared to the previous concept, this one offers advantages in terms of mass and length, which are considered moderate. Additionally, the flow field behavior is different. At low altitude, the skirt region generates an open wake with a pressure very close to atmospheric pressure. In contrast, at high altitude, the skirt wake closes, and its length remains independent of atmospheric pressure. The transition between the two modes results in thrust loss because when the wake closes, the pressure at the skirt is slightly lower than atmospheric pressure. This thrust loss depends heavily on the truncation percentage. At low altitude, this nozzle offers nearly the same performance as one with an ideal central body. However, at high altitude, it is characterized by performance losses due to skirt drag **[100]. Linear Aerospike Nozzles**, Linear aerospike nozzles have been extensively studied from the 1980s to the 2000s. The most well-known example is probably the NASA XRS-2200 prototype, as shown in Figure I.31, tested in August 2001 at NASA's Stennis Space Center. However, after the termination of the X-33 project, to which this engine was intended, the work was discontinued. By design, this type of nozzle

allows the engine to operate with constantly attached supersonic flow, as the jet remains in pressure equilibrium with the atmosphere (regardless of flight altitude). At high altitudes with low static pressure, the propulsive performance of this nozzle decreases significantly. Moreover, several challenges must be overcome for future flight applications of this technology. Additionally, the necessity to control the shockwave network generated by the interaction of the propulsive jet with the atmosphere and the spine's metal surface during engine operation and at all flight altitudes is crucial. Not to mention, the need to properly cool the spine, especially its end, imposes design and manufacturing constraints that are difficult to meet.

I.3 DUALL BELL NOZZLE

Double Bell Nozzles (DBNs) represent significant advancements in the field of space and aerospace propulsion. They are designed to optimize rocket engine performance by dynamically adapting to different flight phases, thus offering increased efficiency at various atmospheric altitudes.

Unlike conventional fixed-geometry nozzles, double bell nozzles have the ability to alter their shape to optimize exhaust gas expansion based on the pressure and temperature conditions encountered during flight. This adaptive capability allows for optimizing rocket engine performance throughout the flight, resulting in increased payload capacity or improved overall energy efficiency of the propulsion system.

Double bell nozzles are configured with two distinct divergent sections: one for low altitudes and another for high altitudes. At low altitude, the nozzle facilitates rapid expansion of exhaust gases to maximize thrust in a high atmospheric pressure environment. As the rocket ascends and atmospheric pressure decreases, the shape of the nozzle changes to accommodate these new conditions, allowing for slower expansion of exhaust gases and optimal efficiency at high altitude.

Similarly, DBNs allow for more effective adaptation to variable flight conditions by switching between different operating modes, such as sea level mode and altitude mode. This ability to overcome the limitations of conventional nozzles makes them particularly attractive for modern space missions.

In summary, double bell nozzles and DBNs represent promising advancements in the field of space and aerospace propulsion, offering significant improvement opportunities for future exploration and space transportation missions. They help avoid redundancy by providing an innovative solution to challenges faced by conventional nozzles, especially in terms of performance at different altitudes and speeds.

In this introduction, we will explore the concept of DBNs in detail, examining their operation, design, and potential applications. We will also assess their innovative nature compared to conventional nozzles, highlighting the advantages and challenges associated with this promising technology.

The double bell nozzle (DBN) relies on the principle of forcing the flow to detach from the nozzle wall at the desired location by imposing an inflection point. This aims to increase the launcher's thrust at low altitudes. The inflection of the contour ensures controlled and

symmetrical detachment, thus limiting the production of strong lateral forces known in conventional nozzles. During ascent, the jet gradually expands to finally reattach to the nozzle wall downstream of the inflection point, as illustrated in Figure I.25. Once the flow is attached to the wall and the nozzle exit pressure exceeds ambient pressure, the high effective area ratio obtained increases performance for the rest of the ascent. In the ideal case, having two nozzles, each optimized for a different part of the flight trajectory, is desired. Experimental studies have shown that the performance of two-mode double bell nozzles (ACNs) is very close (between 1 and 3%) to the optimal efficiency of an ideal nozzle for a given maximum area ratio.

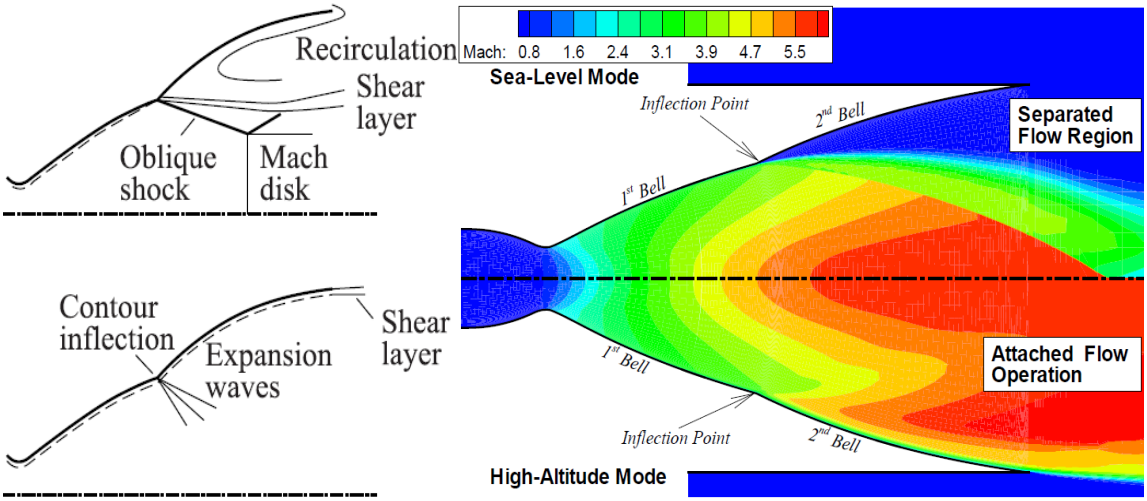

Figure I- 25: a) Operating modes of the left double bell nozzle [113], b) right [114].

In this concept, the design is relatively simpler than that of the Aerospike Engine (AE) to achieve altitude compensation, although this compensation is achieved discontinuously by switching between operating modes. The DB nozzles merge two distinct nozzle contours: the Ideal Truncated Contour (ITC) or the Thrust Optimized Contour (TOC) for the base portion of the nozzle, and the Constant Pressure Contour (CPC) or an Optimized Pressure Wall Contour for the extension. The base section of the nozzle is designed for sea-level operations, while the portion with fully attached flow is intended for vacuum operations. The transition between these two modes occurs at a specific Nozzle Pressure Ratio (NPR), but it exhibits hysteresis phenomena, making prediction and control difficult without resorting to active techniques.

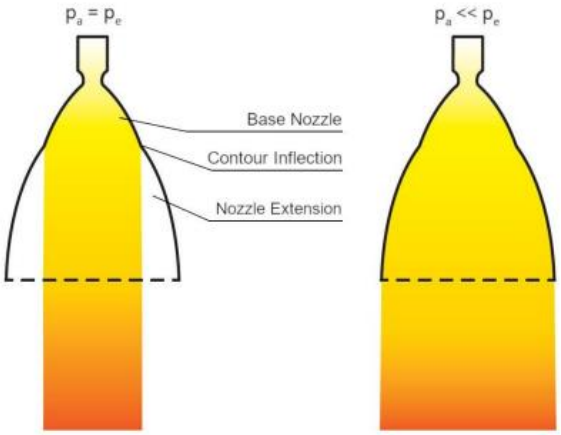

Figure I- 26: Dual-bell Nozzle in Different Operating Modes:Sea-level mode (left), Altitude mode (right).

Recent research initiatives led by research centers such as the SFB-TRR40 program and academic institutions like TUD, USR, and the Polytechnic of Turin have created a conducive environment for the in-depth exploration of DB nozzles, both in their design and their potential applications within successful reusable launch vehicle (RLV) programs. In addition to the anticipated payload gains resulting from improved performance compared to conventional nozzles, a significant advantage envisioned with the DB concept is its ability to facilitate safe and controlled flow separation during retro-propulsion maneuvers of the main stages during the vertical descent phase of RLVs. This concept relies on the ability to operate the nozzle in two distinct regimes. At low altitudes, only the first section of the nozzle operates in "full-flowing" mode, while the second section is fully detached. At higher altitudes, the entire nozzle operates in "full-flowing" mode, as illustrated in Figure I.27 enerated, as highlighted by Alziary et al**. [115].**

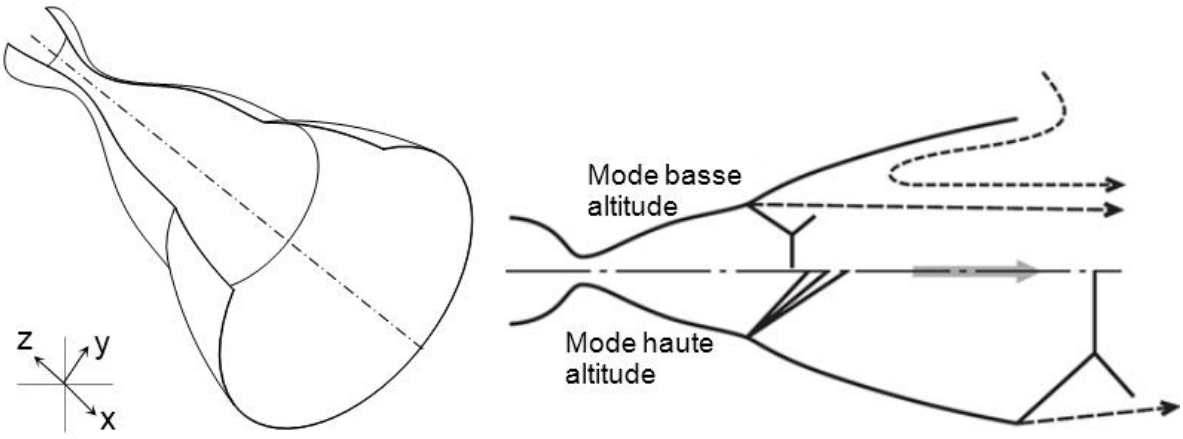

Figure I- 27: Dual Bell Nozzle.

I.3.1 The double-bell nozzle (DBN) concept

Foster C. & Cowles F. **[116]** were the first in 1949 to propose the concept of a nozzle with a profile inflection. The idea is to circumvent the limitation of the area ratio of the main launcher engine nozzles. Indeed, they have to withstand a wide range of ambient pressure. The first feasibility studies, both experimental and numerical, of the double-bell nozzle were undertaken by Horn M. & Fisher S. **[112]** and Hagemann G. et al**. [117]** during the 1990s. The double-bell nozzle offers two modes of operation, i.e., two altitudes where the engines can be optimized.

- The small area ratio at the end of the base nozzle profile offers safe operation at low altitudes with a thrust comparable to that of an optimized bell-shaped nozzle (TOC: Thrust-Optimized Contour) of the same area ratio.
- After transitioning to high altitude modes, the flow reattaches to the extension wall, utilizing the entire area ratio to generate increased thrust at high altitudes.

The performance gain obtained from these studies heavily depends on the chosen reference engine. Various assumptions have been proposed regarding the flow behavior in the double-bell nozzle. Frey M. & Hagemann G. **[118]** predicted a payload gain of up to 72%, if a double-bell nozzle was used on the FSS1 engine **[119].** Immich H. & Caporicci M. **[119-120]** indicated a payload gain of up to 33% or 1400 kg regardless of the launcher used. A specific impulse increase of 10s was calculated by Miyazawa M. **[121].** However, the DBN concept presents some inefficiency that reduces its performance from the theoretical optimum. Indeed, additional losses (of the order of 3%) are generated during low-altitude operation due to suction drag caused by the flow detachment on the nozzle extension. At high altitudes, losses (ranging from 0.1 to 1.2% compared to an optimized nozzle) due to the inflection of the nozzle profile **[117,119].** Figure I.28. shows the evolution of the specific impulse as a function of altitude for a double-bell nozzle compared with those of a TOC nozzle and an adapted nozzle.

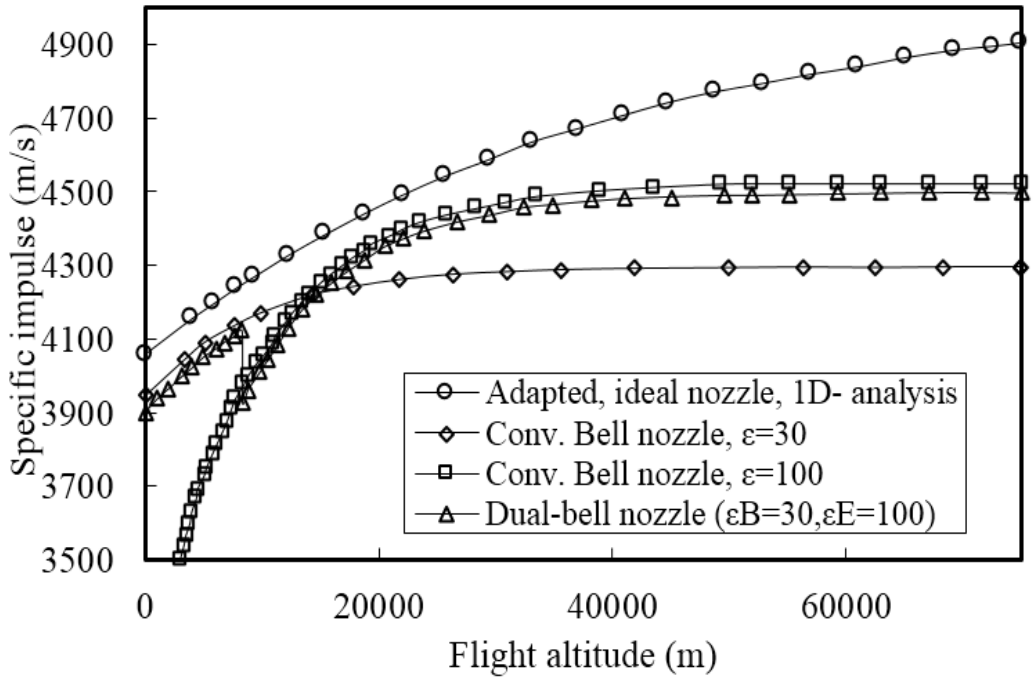

Figure I- 28: Comparison of the performance of the double-bell nozzle with that of the optimized bell-shaped nozzle [117].

I.3.2 Types of DBN concepts

Different design types regarding wall inflection and nozzle extension have been addressed in German analytical and experimental studies **[118, 122-123].** Special attention has been given to the dependence of the transition behavior between the two operating modes. Three types of extensions have been tested, namely: constant pressure extension, favorable pressure gradient extension, and adverse pressure gradient extension. A Truncated Ideal Contour (TIC) profile has been adopted for the first bell (Base Nozzle), with the three other configurations noted as TICCP, TICNP, and TICPP respectively. The wall pressure distribution of these three configurations is presented in Figure I.29. It is noteworthy that:

- The TICNP configuration, when used in a double-bell nozzle, can lead to uncontrolled separation inside the extension. This phenomenon can be observed similarly to what occurs in a conventional conical profile nozzle, also known by the acronym TOC **[122,124].** Uncontrolled separation can have detrimental effects on the performance and stability of the propulsion system.
- Conversely, the TICCP and TICPP configurations offer a more favorable alternative by allowing a smoother transition between the two operating modes: low altitude and high altitude **[118].** This smooth transition between modes helps optimize the efficiency and

overall performance of the double-bell nozzle, thereby enhancing the maneuverability and energy efficiency of the aircraft or spacecraft equipped with this propulsion system.

However, previous experiments on conventional nozzles with adverse pressure gradient have revealed significant sidewall loads issues. Thus, the TICCP configuration has been chosen as the most promising for further research.

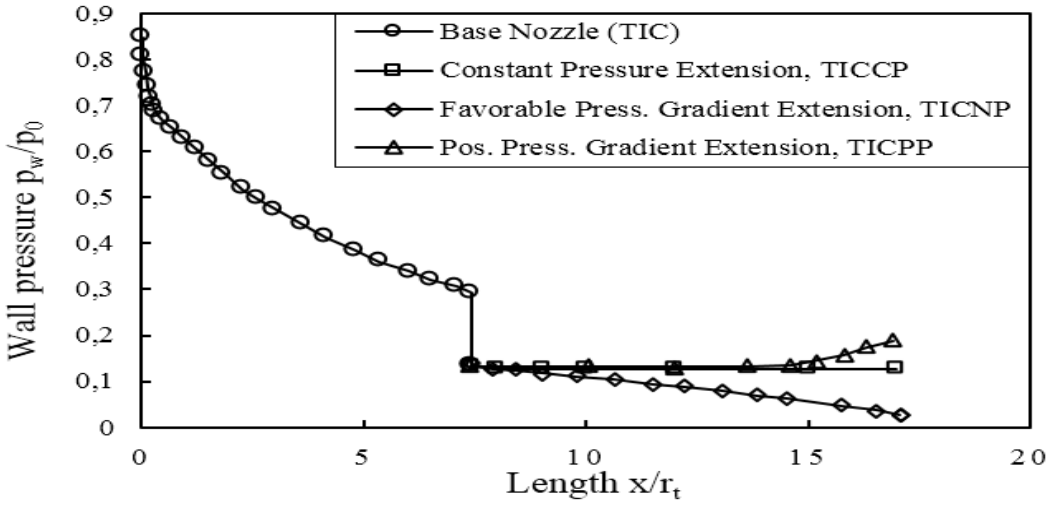

Figure I- 29: Wall pressure distribution in the three double-bell nozzle concepts [122].

Several experimental studies, both cold-gas and hot-fire tests, along with numerical simulations, have been conducted to investigate the TICCP configuration during its two operating modes and the transition between them **[123,125],** see Figure I.30. Several effects have been analyzed, including:

- Effect of extension divergence angle **[126-127**]: The divergence angle of the extension in an aerospace nozzle plays a crucial role in the overall performance of the propulsion system. An optimal divergence angle can contribute to maximizing energy efficiency by ensuring adequate expansion of exhaust gases. Studies **[126-127]** have demonstrated that subtle variations in this angle can have a significant impact on nozzle performance, particularly in terms of generated thrust and specific impulse. Thus, optimizing the divergence angle is an important consideration in nozzle design and engineering to ensure optimal propulsion system performance.
- Effect of cold gas density **[128]:** The density of cold gases, or ambient gases, surrounding the nozzle, directly influences its operation. Studies **[128]** have examined how variations in cold gas density can affect nozzle performance, especially in different atmospheric environments or during altitude changes. Increased cold gas density can lead to an increase

in ambient pressure, which can affect the exhaust gas exit velocity and thus the generated thrust. Understanding this effect is essential for adjusting nozzle parameters based on the environmental conditions encountered during flight operations.

- Effect of gas injection at the inflection point on the transition **[127]:** Gas injection at the inflection point of a double-bell nozzle can significantly influence the transition between different operating modes. Research **[127]** has explored how this practice can be used to optimize the transition between low-altitude and high-altitude modes, thereby adjusting propulsion system performance according to specific operational needs. By precisely controlling gas injection at this critical point, it is possible to improve nozzle stability and overall efficiency, thereby providing better maneuverability and more efficient fuel utilization.

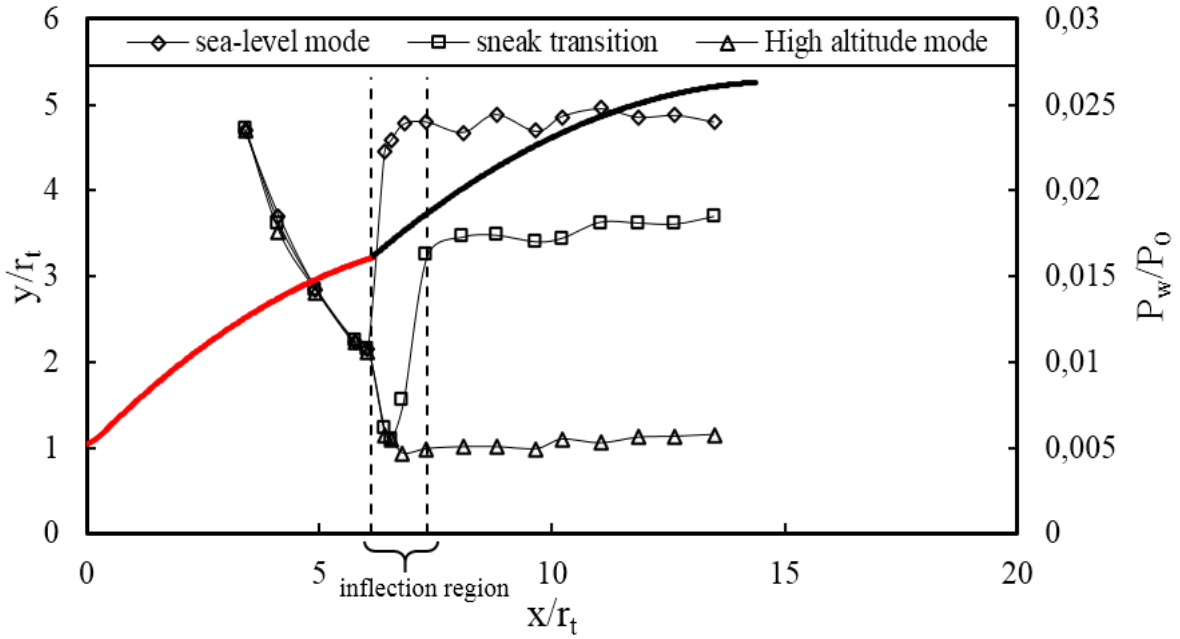

Figure I- 30: Wall pressure distribution in a TICCP during low-altitude mode, transition, and high-altitude mode [126-127].

A significant disturbance has been observed around the transition pressure ratio (NPRtr), with a higher value during startup. This hysteresis effect favors the TICCP concept, as it prevents interaction between the two modes of operation **[127].** Figure I.31 illustrates the theoretical and experimental wall pressure distribution obtained from viscous CFD calculations at high altitudes **[116,129].** Due to viscosity effects within the boundary layer, the pressure follows a negative slope rather than a discontinuity as predicted by theory. This effect was previously predicted by Martelli E. et al. **[129].** The extension must then be divided into two parts: the inflection region, where the pressure gradient is negative, and the residual part, where

the wall pressure is constant **[126].** Martelli E. et al. identified a third region with a negative pressure gradient located at the end of the extension.

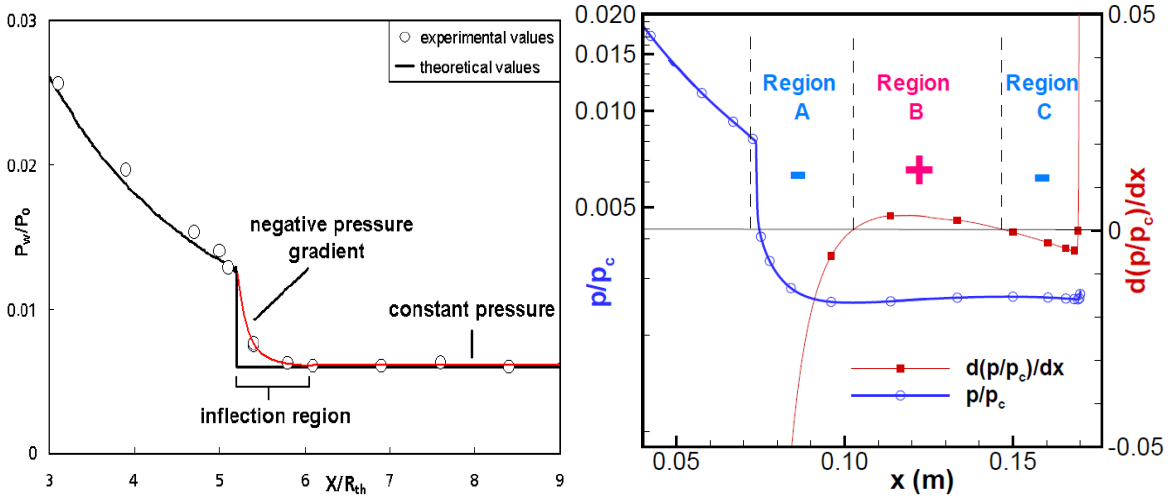

Figure I- 31: Pressure variation in the second operating mode of the double-bell nozzle, comparison of viscous vs. non-viscous flow (left) [126], viscous CFD (right) [114].

Stark R & Génin C. **[126]** noticed that before the actual transition where the flow abruptly reattaches over the entire extension, the wall pressure drops in the inflection region, see Figure I.20, and the separation point moves downstream of the inflection. This evolution preceding the actual transition is termed as "sneak transition." During ascent, the total pressure remains constant for a real rocket engine application. The variation in NPR is solely due to the change in ambient pressure with altitude. This variation is very slow, making the "sneak transition" a crucial issue for choosing the DBN concept. The "sneak transition" can be the source of very high lateral loads of the same order of magnitude as those encountered during the start-up phase, as shown in Figure (I.32) **[126].**

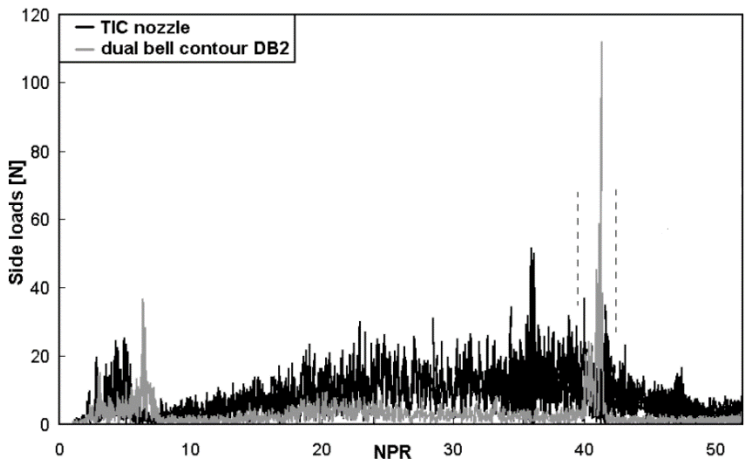

Figure I- 32: Comparison of lateral load level between the double bell nozzle and the conventional TIC nozzle [126].

Numerous projects and studies aimed at improving, studying, and optimizing DBN nozzles have been conducted in various laboratories and research centers. For instance, Mubarak A.K. et al. conducted a study titled "Design of a Supersonic Double Parabola Nozzle and Performance Evaluation by Experimental and Numerical Methods" **[130**] in 2018, published by Tide P.S. The objective of this study was to examine the design and performance evaluation of a supersonic double parabola nozzle compared to conventional nozzle designs (conical and bell-shaped). The aim was to enhance thrust performance using both experimental and numerical methods. The throat and divergent length dimensions of the three types of nozzles (conical, bell-shaped, and double parabola) were kept identical for fair comparison. The design of the double parabola nozzle was inspired by the Prandtl Meyer angle, aiming for a maximum slope of one-third of this angle. Tests were conducted at a nozzle pressure ratio (NPR) of 5 as well as at design conditions (NPR = 3.7). Experimental results and numerical simulations showed reasonable agreement, revealing increased thrust for the double parabola nozzle compared to other nozzle types. In particular, the double parabola nozzle generated slightly higher total thrust, which could potentially offer advantages in terms of fuel economy and payload capacity. Simulations were performed using a density-based solver with RANS equations and an SST k-ω turbulence model. However, although numerical predictions captured shock cell parameters well, they failed to capture shock oscillations. This study demonstrates the significant advantages of the double parabola nozzle design, especially in terms of improved thrust efficiency compared to conventional designs. These findings could have significant implications for the aerospace industry. In 2020, Nikolaus A. et al. **[131]** conducted a study summarizing the major successes of the Collaborative Research Center Transregio 40 (TRR40), funded by the German Research Foundation (DFG) from July 2008 to June 2020. TRR40 brought together teams from five German universities in collaboration with the German Aerospace Center (DLR) and industrial partner ArianeGroup to conduct fundamental research on liquid-propelled rocket propulsion systems. The main objectives were to understand dominant phenomena in liquid-propelled rocket engine systems, improve existing technologies, develop new solutions, and lay the scientific groundwork for future space transport systems. Research was divided into five main areas covering all aspects of thrust chamber assemblies: structural cooling, downstream flow, combustion chamber, nozzle, and thrust chamber assembly. The document also addresses the impact of double bell nozzles on turbulent flows and dynamic loads under transonic and supersonic flow conditions, as well as the efficiency of different cooling systems to protect the structural integrity of modern launcher engines. Numerical simulations and modal analyses reveal that using azimuthally distributed jets to

control flow significantly reduces buffet dynamic loads on the nozzle surface. Chloé Génin et al. **[132]** conducted a study in 2021 exploring the concept and design of double bell nozzles for space launchers. This innovation aims to improve rocket engine efficiency by adapting their performance to variations in atmospheric pressure encountered during space flight. The authors focused their efforts on the optimized design of these nozzles, using both experimental and numerical methods to study flow behavior, transition between operating modes, and the effect of film cooling. Through wind tunnel tests and hot firing tests, they validated their design, demonstrating a significant increase in thrust at high altitude as well as improved operational stability. This research, conducted as part of a collaboration within the SFB TRR40 of the German Research Foundation, highlights the potential of double bell nozzles to enhance the performance of space launchers by providing effective adaptation to altitude. In the study titled "Parametrical Investigation of Transverse Injection in a Dual-Bell Nozzle During Altitude-Varying Conditions" **[133]** in 2023, explores the effectiveness of secondary injection in a dual-bell nozzle (DBN) to improve the performance of space launchers by adjusting their behavior to changes in atmospheric pressure encountered during ascent or descent through the atmosphere. Previous research has focused on experimental and numerical studies of DBNs without active flow control, indicating issues such as early transition and unstable lateral forces. This article proposes the use of radial injection of secondary fluid as a solution to control transition and retransition, thereby offering increased stability and improved efficiency. Experiments were conducted with a subscale DBN in the EDITH wind tunnel, adjusting ambient pressure and varying the secondary mass flow rate, to assess the impact of these changes on nozzle transition and lateral force generation. The results show that secondary injection increases the transition pressure ratio by nearly 24% and reduces lateral forces to less than 1% of nozzle thrust, significantly improving performance compared to a smooth nozzle (without secondary injection slot). In conclusion, the article highlights the potential of secondary injection in double bell nozzles for space propulsion, enhancing adaptation to atmospheric pressure variations and minimizing unstable lateral forces. Despite the need for additional experiments, including numerical studies and extensive parametric investigation, the results provide encouraging proof of concept for the use of secondary radial injection in scaled-down, cold DBN models.

I.4 ASYMMETRIC NOZZLES

Asymmetric propulsion nozzles are a type of nozzle design used in aerospace applications where the geometry of the nozzle is intentionally modified in a non-uniform or asymmetric manner. Unlike traditional symmetrical nozzles, which have uniform shapes, asymmetric nozzles exhibit variations in their geometry that can lead to improved performance, maneuverability, or other specific characteristics. The asymmetry of these nozzles can take different forms, such as variations in throat area, divergent section shape, or the introduction of additional features like ramps, corners, or secondary flow paths. The main purpose of these modifications is to adjust the flow expansion and pressure distribution to achieve specific aerodynamic effects or performance advantages.

The resolution of profiles where the installed system did not generate too much thrust or drag loss was the central concern in the design of jet engine exhaust nozzles in the 1960s and early 1970s. Axisymmetric configurations exhibit high internal performance but with penalties of thrust and low drag. However, they show poor efficiency in terms of thrust to drag when integrated into complex propulsion systems with non-symmetric area constraints that increasingly require careful integration of fuselage/engine **[134].** The advent of hypersonic air-breathing propulsion systems operating at speeds greater than Mach 5 and offering higher specific impulses than available with rocket engines has sparked interest in asymmetric nozzle design **[135-136].** Additionally, non-axisymmetric supersonic nozzles are becoming a significant part of hypersonic air-breathing vehicles as they offer excellent integrated aerodynamic performance **[137].** Moreover, they appear to be much better integrated with propulsion engines having non-symmetric area constraints, enhancing their performance. Issues associated with designing optimal contours of asymmetric planar nozzles have been considered **[138-139].** In this case, i.e., for short lengths, the problem was resolved using the controlled contour method. It was demonstrated that substituting the centered wave with a very low-intensity compression wave significantly reduced nozzle thrust. Yang et al **[141]** studied the effect of nozzle asymmetry on the aerodynamic heating of a hypersonic vehicle while Thangaraj & Kaushik **[142]** examined the impact of two non-circular nozzle exit shapes (elliptical and square) on the efficiency of mix augmentation under subsonic and sonic flow conditions. It was found that the elliptical nozzle was superior in terms of shortening the potential core length. It achieved a maximum core length reduction of 18.75% with rapid jet decay. Due to hypersonic vehicle applications, nozzles need to be designed to fly at altitudes lower than conventional nozzles. This implies that the size and shape of the nozzle must be adjusted to accommodate

these conditions. Vianna Moizes et al. **[143]** examined various nozzles, with designs aimed at increasing thrust while minimizing surface and hence, nozzle production cost is garnering increasing interest. The maneuverability and efficiency of supersonic and hypersonic aircraft have also led to interest in asymmetric nozzle configurations. Casper **[144]** conducted a study on the design of an asymmetric supersonic nozzle for improved thrust vectoring. It was found that the asymmetric design would result in a 20% increase in nozzle performance compared to a symmetrical design. A numerical survey conducted on scramjet propulsion-designed asymmetric nozzles by Matveev & Semenov **[145]** revealed that asymmetric configurations offered a significant increase in thrust compared to a symmetrical design while also reducing the size and weight of the nozzle. Pal & Chattopadhyay **[146]** conducted a design optimization study on an asymmetric supersonic nozzle. They found that the optimized asymmetric design offered better thrust and pressure recovery compared to a symmetrical nozzle. Overall, asymmetric nozzles are becoming a significant part of hypersonic air-breathing vehicles as they offer excellent integrated aerodynamic performance, particularly in terms of thrust and energy efficiency (Zhu et al. **[147].**

I.4.1 Elliptical nozzle

Elliptical propulsion nozzles are valuable components in aerospace engineering. They play a critical role in the performance and functionality of various aerospace vehicles, and offer diverse advantages in terms of precise control and maneuverability (Bajpai & Rathakrishnan, **[148].** For instance, they can provide higher levels of thrust vectoring efficiency compared to certain other designs, primarily by altering the exhaust gas flow through the elliptical shape. Additionally, they can help manage shock waves generated by supersonic or hypersonic flows more effectively, resulting in reduced separation and flow losses. In terms of supersonic combustion, elliptical nozzles can enhance its efficiency by maintaining stable and efficient supersonic combustion and providing better expansion of combustion gases required in air-breathing engines such as scramjets. Lastly, the shape of the elliptical nozzle can be tailored to specific flight conditions, allowing for efficient performance across a range of mission requirements. Figure I.33 illustrates an elliptical C-D nozzle with an aspect ratio of 2:1 (Kumar & Rathakrishnan, **[149].**

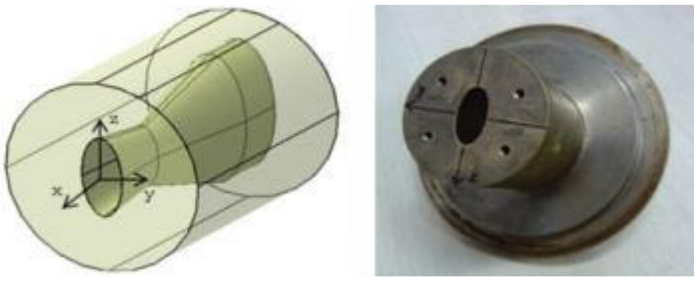

Figure I- 33 : Elliptical C-D Nozzle (Kumar & Rathakrishnan, [149]) a) Cross-sectional view of the exit (AR=2:1), b) Photographic view of the cross-sectional exit.

The applications of elliptical propulsion nozzles are diverse and extend to various types of vehicles operating at different speed regimes and altitudes. Scramjet engines, operating at high speeds in the atmosphere, can benefit from the optimized expansion characteristics of elliptical nozzles, which could enhance their combustion efficiency and thrust. The thrust vectoring capability of elliptical nozzles may be present in various drones designed for agile maneuvers, reconnaissance, and surveillance. Stealth aircraft requiring low radar cross-sections can benefit from elliptical nozzles capable of reducing their detectability by radar systems.

PART II: NUMERICAL INVESTIGATION AND PERFORMANCE EVALUATION OF AN INNOVATIVE THREE-DIMENSIONAL DUAL-BELL NOZZLE WITH ELLIPTICAL SECTION DESIGN

SUMMARY

In the second part of the study, we focused on proposing, for the first time, an elliptical-section double-bell nozzle, an idea hitherto unexplored in the literature. This innovation represents a novel contribution to the field, as no prior examples of such a design have been documented. Thus, we have the privilege of claiming pioneer status for this initiative. Initially, our focus was on generating a profile for a conventional double-bell nozzle using an in-house code written in Fortran. The base profile is a TIC profile, while for the second profile, we worked with a CP (constant pressure) profile. Flow parameters, such as pressure and Mach number, were evaluated and studied within the scope of this investigation. Subsequently, building upon this initial nozzle, we utilized our methodology to obtain the profile of a double-bell nozzle with an elliptical outlet section. We followed the same approach as before, studying and optimizing the performance parameters of this elliptical nozzle, and then comparing them to those obtained for a conventional double-bell nozzle. The results of this comparison are detailed in this section.

II.1 NUMERICAL FLUID DYNAMICS: ADVANCED SIMULATION FOR AERODYNAMIC AND TECHNOLOGICAL OPTIMIZATION

Computational Fluid Dynamics (CFD), a crucial advancement in scientific and technological research, enables the in-depth study of complex fluid behaviors by solving partial differential equations. This approach discretizes continuous space into a grid of points, providing the fundamental capability to model various types of flows, both internal and external. Simulation of flows in supersonic nozzles, characterized by transitions between subsonic and supersonic regimes and compressibility effects, presents a distinct challenge requiring careful attention.

Software tools such as ANSYS and FLUENT are essential for conducting these simulations. For instance, ANSYS 19 facilitates the creation of two and three-dimensional geometries and conducts simulations across various domains, while FLUENT focuses specifically on compressible and incompressible flow simulations, including complex phenomena such as turbulence and heat transfer. These tools streamline the modeling and simulation of flows around supersonic nozzles.

The standard methodology divides the simulation process into several stages, from geometric modeling to analysis/visualization, through to solving the equations. Additionally, the method of characteristics offers an alternative by transforming partial differential equations into systems of ordinary differential equations to facilitate their resolution. These simulations enable the understanding of internal system structure, its interaction with the environment, and prediction of its behavior under different conditions, providing significant efficiency and cost advantages for device design and optimization.

Computational Fluid Dynamics, or CFD, represents an indispensable technology enabling precise simulation and analysis of fluid flows around structures. By solving the Navier-Stokes equations, it models complex phenomena such as turbulence, shock waves, and flow separation, offering detailed visualization of pressure, velocity, and temperature fields. Used for optimizing aircraft aerodynamics, it reduces costs and time associated with wind tunnel tests and flight trials by simulating different scenarios and configurations even before a prototype is built.

Typical steps involved in simulating an aerodynamic problem are as follows:

1. Geometric Preparation and Modeling:
   - Creation of a geometric model of the vehicle, structure, or object under study.
   - Definition of boundary conditions and material properties.

2. Meshing:
   - Transformation of the continuous geometry into a discrete structure of points (mesh).
   - Selection of mesh type suitable for the problem (structured, unstructured, hybrid).

3. Preparation of Initial Conditions and Boundaries:
   - Definition of initial conditions for the problem (e.g., initial velocity, initial pressure).
   - Specification of boundary conditions for each part of the model surface (e.g., inlet/outlet conditions for flows).

4. Model Selection and Numerical Resolution:
   - Selection of appropriate turbulence model (e.g., k-epsilon model, LES model).
   - Numerical resolution of the fundamental equations (Navier-Stokes equations) using suitable numerical methods (e.g., finite volume method, finite element method).

5. Simulation and Post-processing:
   - Execution of the simulation to compute pressure, velocity, and temperature fields.
   - Analysis of results to extract relevant data on flow behavior (e.g., streamline visualization, aerodynamic coefficient analysis).
   - Validation of results through comparison with available experimental data.

6. Optimization and Analysis:
   - Utilization of results to optimize the design or performance of the studied object.
   - Analysis of results to meet specific project objectives (e.g., drag reduction, lift enhancement).

Each of these steps requires deep expertise in computational fluid dynamics and a detailed understanding of the physical problem being solved.

In this part of the study, we will first focus on a conventional double-bend nozzle with a circular exit section, a current topic that has been extensively researched under the supervision of our supervisor. Subsequently, building upon this configuration, we will propose an innovative concept: a double-bend nozzle with an elliptical exit section. This concept has not been explored before, making it a novel subject. Our study will also include a comparative analysis of the two concepts.

II.2 DUAL BELL NOZZLE WITH CIRCULAR SECTION

The selected profile pertains to the divergent section of a profiled axisymmetric nozzle. At the throat, this profile consists of two arcs of circles with identical radius of curvature, placed upstream and downstream respectively. The downstream circular arc is tangentially connected to the throat at its junction point. This specific profile for the base nozzle is an Ideal Truncated Conical (ITC) profile. The profile of the second profile is determined for a constant wall pressure P2. Assuming an inviscid fluid, this profile corresponds to the isobaric streamline of the perfect fluid under pressure P2. This streamline is obtained using the direct method of characteristics, specifically applied for a Prandtl-Meyer expansion wave of intensity P2/P1 at the junction point

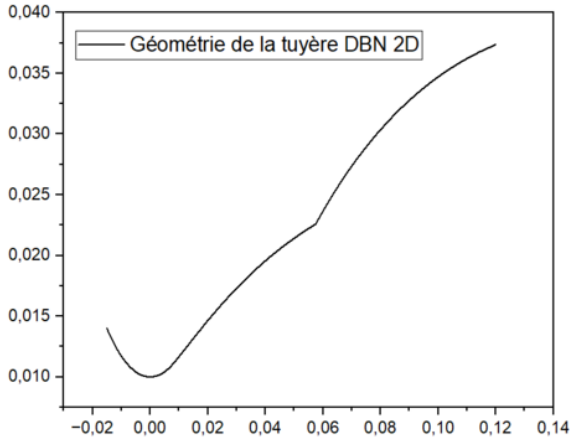

Figure II- 1: Geometry of the 2D cylindrical double-bell nozzle (DBN).

The axisymmetric DBN nozzle with a cylindrical section possesses several key geometric parameters. The inlet width of the nozzle (Win) is 0.014019 m. This dimension is crucial for determining the incoming air flow rate, as a smaller inlet width can limit the mass flow rate of air and directly influence nozzle performance. The outlet width of the nozzle (Wout) is 0.03736 m. A larger outlet width allows for expansion of the air flow, which is critical for generating thrust in propulsion applications. The length of the nozzle, measured from inlet to outlet (L), is 0.13485 m. This dimension affects the residence time of the fluid as well as pressure and temperature gradients along the nozzle. The maximum width of the nozzle (W) is 0.03736 m. This dimension influences the overall bulkiness of the nozzle and is relevant for compact design considerations. The radius at the narrowest point of the nozzle, known as the throat (Rth), is 0.01 m. This point is crucial for flow rate control and conditions transitioning between subsonic and supersonic flow. Points where the curvature of the nozzle changes (PI) are located at 0.0575 m and 0.0226 m. These points are essential for aerodynamic design as

they affect pressure distribution and flow separation. The cross-sectional area of the nozzle (A) is 0.0030939 m². A larger cross-sectional area allows for greater fluid expansion capacity, potentially increasing thrust efficiency. The internal volume of the nozzle (V) is negligible, which is correct for a two-dimensional simulation where volume is not considered. These geometric parameters of the nozzle are summarized in the table below.

Table II- 1 : Geometric Parameters of the Axisymmetric Nozzle.

Parameters	Symbol	Value	Description
Inlet width	$W_{in(}$ (m)	0,014019	Inlet nozzle width.
Exit width	W_{out} (m)	0,03736	Nozzle exit width.
Total length	L (m)	0,13485	Length of the nozzle from inlet to outlet.
Total width	W (m)	0,03736	Width of the nozzle from inlet to outlet.
Throat radius	R_{th}(m)	0,01	Throat radius of the nozzle.
Inflection point	PI (m)	0,0575 0,0226	The two inflection points of the nozzle.
Surface	A (m^2)	0,0030939	The surface of the nozzle.
Volume	V (m^3)	0	The volume of the nozzle.

The DBN nozzle is also characterized by several key thermodynamic parameters. The initial pressure P0 is 30 bars, representing the pressure at the inlet of the combustion chamber. The initial temperature T0 is 243 Kelvin, indicating the temperature at the inlet of the combustion chamber. The specific heat ratio Cp is 1006.43 Joule/kg·Kelvin, a crucial value for defining the thermodynamic properties of the fluid. The adiabatic index γ is 1.4, representing the ratio of specific heats of air. The exit pressure Pe is 0.23 bars, measured at the exit of the combustion chamber. The exit Mach number Me is 3.71, indicating the flow velocity in terms of multiples of the speed of sound. These parameters are essential for modeling and analyzing nozzle performance, directly influencing the efficiency and flow dynamics in propulsion applications. Ensuring the accuracy and consistency of these values relative to nozzle operational conditions is paramount to achieving reliable results in simulations.

These thermodynamic parameters of the nozzle are presented in the table below

Table II- 2: Thermodynamic Parameters of the Axisymmetric Nozzle.

Parameters	Symbole	Value	Description
Initiale pressure	P0 (Bar)	30	The pressure at the inlet of the combustion chamber.
Initiale temperature	T0 (Kelvin)	243	The temperature at the inlet of the combustion chamber.
The ratio of specific heats	Cp Joule/Kg*Kelvin	1006,43	The ratio of specific heats.
Gamma	ɣ	1,4	adiabatic index
Pression de sortie	Pe (Bar)	0,23	The pressure at the outlet of the combustion chamber.
Nombre de mach à la sortie	Me	3,71	The Mach number at the exit of the combustion chamber.

II.2.1 Inviscid calculations

II.2.1.1 Methodology

In this section, we describe the methodology used to simulate flow in double-bend nozzles. We conducted a detailed simulation of flow in a cylindrical axisymmetric DBN nozzle using a perfect fluid model. The simulation process was rigorously conducted, starting with the import of geometric data of the nozzle into ANSYS software. This step was crucial to establish an accurate representation of the nozzle geometry in the simulation environment.

Once the geometry was properly defined, we generated a suitable mesh to discretize the computational domain, ensuring precise resolution of the fluid dynamics equations. Thorough tests were performed on the mesh to ensure its quality and suitability for simulation objectives.

Subsequently, we proceeded with the numerical resolution of the fluid dynamics equations, thereby obtaining pressure, velocity, and temperature fields inside the nozzle. This resolution phase required significant computational power and careful attention to ensure accurate and reliable results. The obtained results were then analyzed in depth and presented in the form of graphs and visualizations to enhance understanding of flow characteristics.

- ***Geometry***

In ANSYS, geometry represents the structure and shapes of modeled components for analysis or simulation purposes. To create the geometry of the DBN nozzle, several precise

steps were followed:

- Importation of DAT file: The DAT file containing nozzle data was imported into the ANSYS modeling environment to serve as a reference for creating the nozzle geometry.
- Creation of reference points: Two points were created on the horizontal X-axis, positioned at a distance equivalent to twice the length of the nozzle. These points serve as markers to define the ends of the nozzle.
- Connecting points to form a line: The two points were connected by a straight line, representing the axis of the nozzle. This line forms the basis for constructing the nozzle geometry.
- Projection of start and end points of the nozzle: The start and end points of the nozzle, defined in the DAT file, were projected onto the previously created line to determine their exact positioning on the nozzle axis.
- Drawing the nozzle geometry: Using the "Create Line from Points" function, the nozzle geometry was drawn by connecting the projected start and end points on the line, thus defining the shape of the nozzle.
- Generation of the nozzle surface: The lines defined earlier were used to generate the surface of the nozzle, creating a solid and continuous representation of the nozzle geometry.
- Removal of wireframe body: The initial wireframe body used as a reference for creating the geometry was deleted, leaving only the surface of the nozzle.
- Assignment of surface body as fluid: Finally, the resulting nozzle surface was assigned as fluid, allowing for the definition of fluid properties for the subsequent simulation of flow within the nozzle.

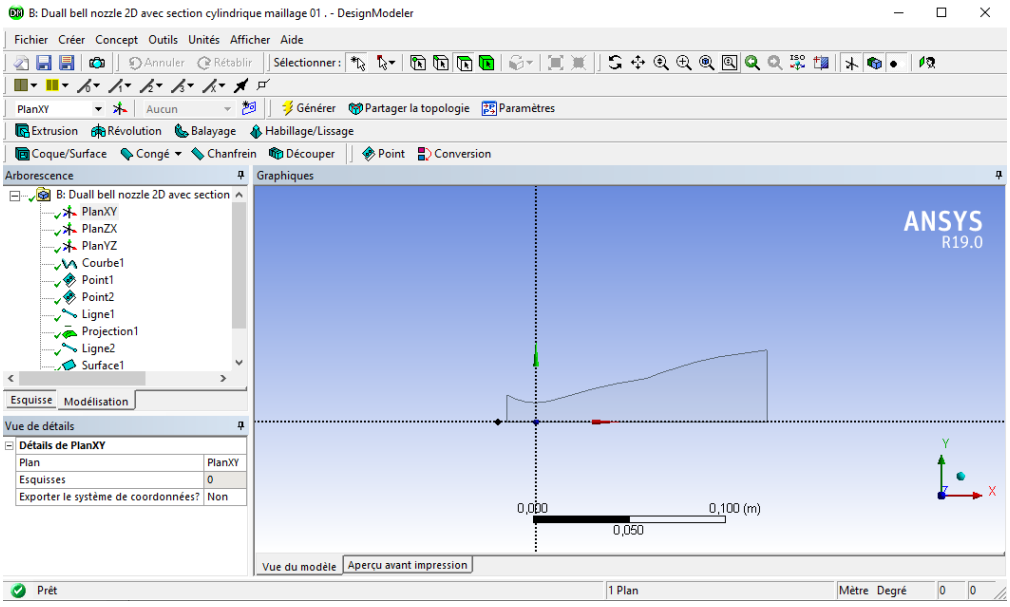

Figure II- 2: Axisymmetric DBN Geometry.

➢ ***Mesh Study***

- After creating the nozzle geometry, the meshing process was undertaken to discretize the computational domain and prepare the model for simulation. Here are the detailed steps followed to achieve the meshing:
- Surface Meshing: Initially, a surface mesh was created to represent the nozzle geometry using surface elements.
- Mesh Size Function Change: To obtain quadrilateral elements and ensure better mesh quality, the mesh size function was changed to uniform mode.
- Mesh Refinement: To increase resolution and achieve a more precise mesh, refinement was applied by reducing the maximum element size to 0.0005m.
- Generation of New Mesh: After adjusting mesh parameters, a new mesh was generated, ensuring a better representation of the nozzle geometry.
- Mesh Verification: The obtained mesh was verified to ensure its quality and compliance with simulation requirements. Special attention was given to critical zones, particularly at the inflection points of the nozzle

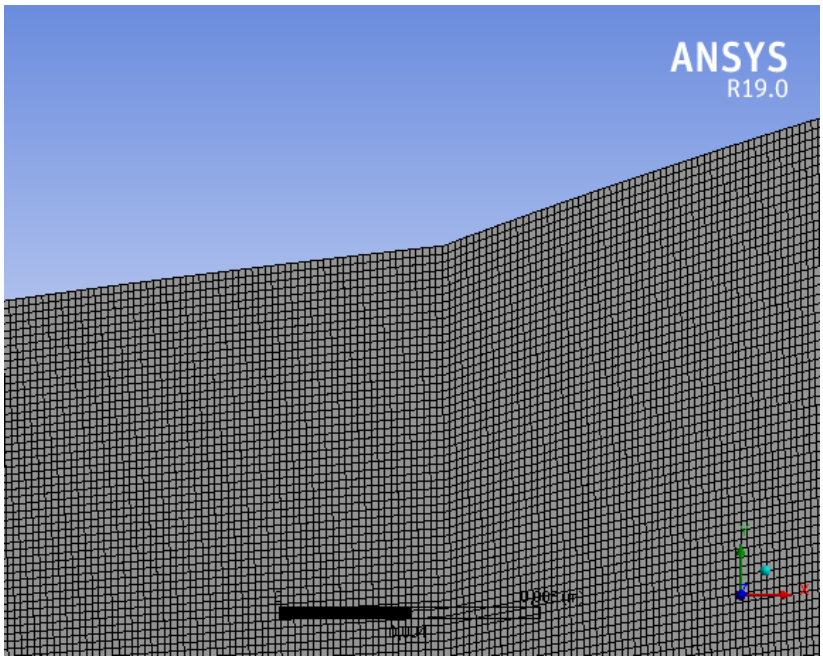

Figure II- 3: Mesh of the axisymmetric cylindrical DBN nozzle.

The characteristics of the mesh used are summarized in the table below:

Table II- 3:Mesh Data Configured for the Axisymmetric DBN.

Parameters	Description
Type of mesh	Surface mesh.
Type of elements	Quadrilateral.
Mesh size function	Uniforme
Maximum element size	0,0005 m
Total number of elements	11782 éléments
Orthogonal quality of mesh	0,99038
Refinement	Critical zones refined with a maximum size of 0.0005 m.
Verification	Mesh verified for quality and compliance with simulation requirements.
Critical zones	Inflection points of the nozzle, inlet and outlet zones.

II.2.1.2 Results & interpretation

- ***Configuration***

After creating and selecting a mesh, the simulation setup was initiated to define the initial conditions and simulation parameters. Here are the steps followed for this configuration:

- First of all, since the simulation is conducted under ideal gas conditions, we chose the solver that follows

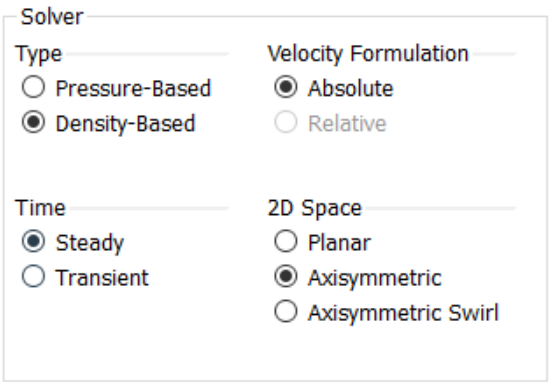

Figure II- 4: The CFD Solver in ANSYS.

    - For perfect gas, a compressible supersonic flow is considered.
    - The flow is steady (time-independent).
- Energy activation: Initially, energy was activated in the simulation setup, assuming the fluid to be non-viscous, to account for thermal effects in the flow.
- Choice of air properties: Air properties were selected for the simulation, considering an ideal gas to represent the thermodynamic behavior of the fluid.
- Definition of boundary conditions: Boundary conditions were defined for different zones of the model. At the inlet of the nozzle (inlet), a pressure of 30 bars and a temperature of 243 Kelvin were specified.
- Initialization of the simulation: Prior to launching the simulation, a calculation initialization was performed to set the starting conditions for the flow. This step prepares the model for numerical resolution.
- Selection of iteration count: An appropriate number of iterations was chosen to control the accuracy and convergence of the simulation. This value determines how many iterations the solver will perform to achieve a stable solution.
- Launching the calculation: Finally, after all configurations were completed, the calculation was launched to solve the equations of fluid dynamics and obtain the fields of pressure, velocity, and temperature inside the nozzle.

The results of the simulation of the axisymmetric DBN nozzle for perfect flow enabled plotting profiles of several important parameters: static pressure, Mach number, static temperature, and density. For a detailed analysis, we extracted the values of these parameters at critical points of the nozzle, namely the inlet, the junction point (throat of the nozzle), and the outlet.

- **Wall pressure évolution**

After successfully completing the simulation, it converged to a specified number of iterations, indicating the stabilization of the solution. The results obtained were analyzed and presented in the form of graphs, providing a clear visualization of the flow characteristics in the DBN nozzle**.**

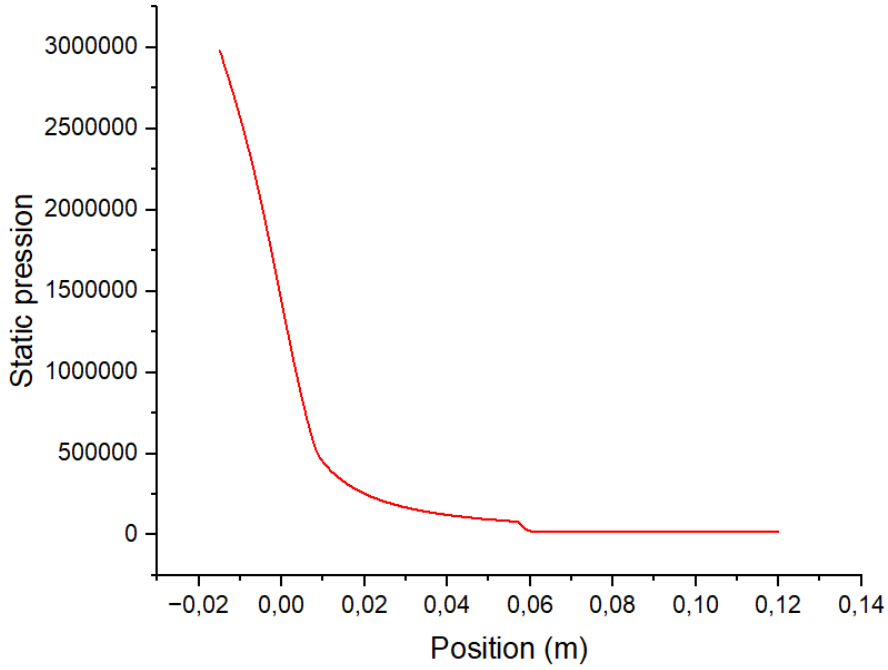

Figure II- 5: Static pressure evolution along the wall.

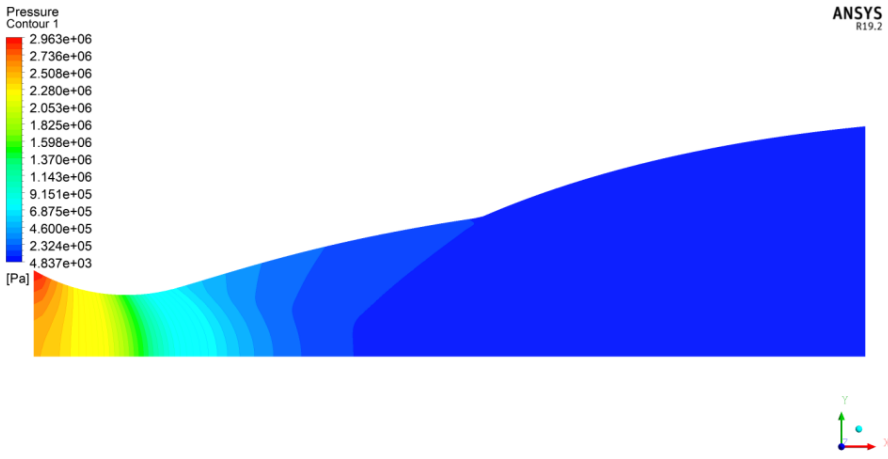

Figure II- 6: Contour of static pressure along the cylindrical DBN nozzle.

Figures II-5 and II-6 respectively depict the evolution of wall pressure along the nozzle and the contour of pressures inside it, illustrating the distribution of static pressure within a nozzle. The second figure is a contour map of static pressure generated by ANSYS, where variations in static pressure are represented by a color scale.

At the nozzle inlet, a high pressure of approximately 2,888,000 Pa is observed, gradually decreasing towards the exit to reach very low values in the range of a few thousand pascals. The transition from red to blue colors clearly indicates the fluid decompression as it traverses the nozzle, converting pressure energy into kinetic energy.

The first graph showing static pressure as a function of position along the nozzle. This graph confirms observations from the contour map, with initially high pressure sharply dropping after the nozzle inlet, stabilizing at a value close to zero towards the exit. This curve shows a rapid pressure decrease between -0.02 m and 0.04 m, followed by stabilization around 0 Pa, corroborating the visual analysis of the contour map.

Both figures consistently demonstrate the distribution and evolution of static pressure throughout the nozzle, indicating significant decompression and fluid acceleration as expected for a well-designed nozzle. These results highlight the typical energy conversion behavior from pressure energy to kinetic energy within a nozzle.

- **Temperature Evolution**

The graph of static temperature and its contour map below visualize the distribution of temperature within the simulation domain, providing crucial insights into thermal variations.

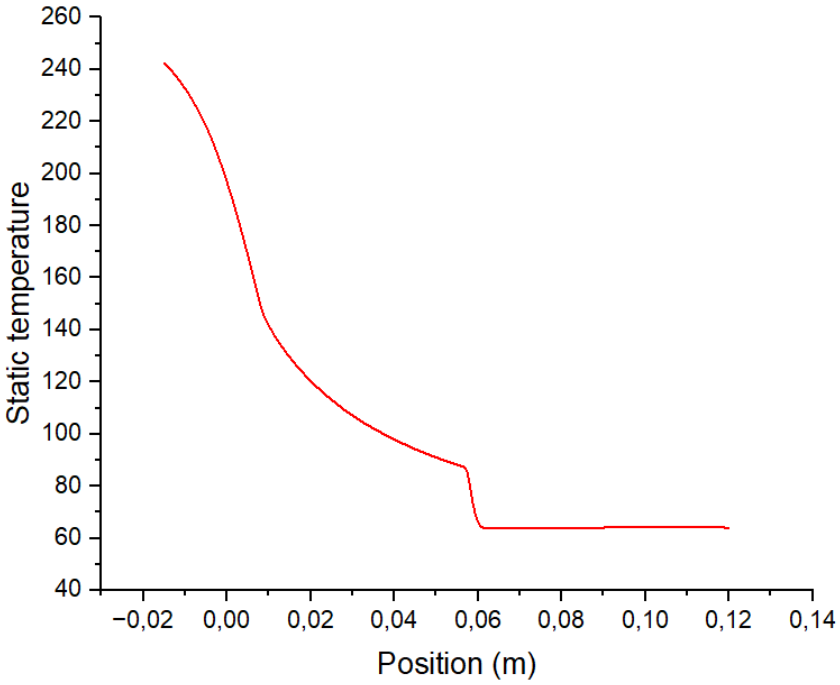

Figure II- 7: Static temperature evolution along the nozzle.

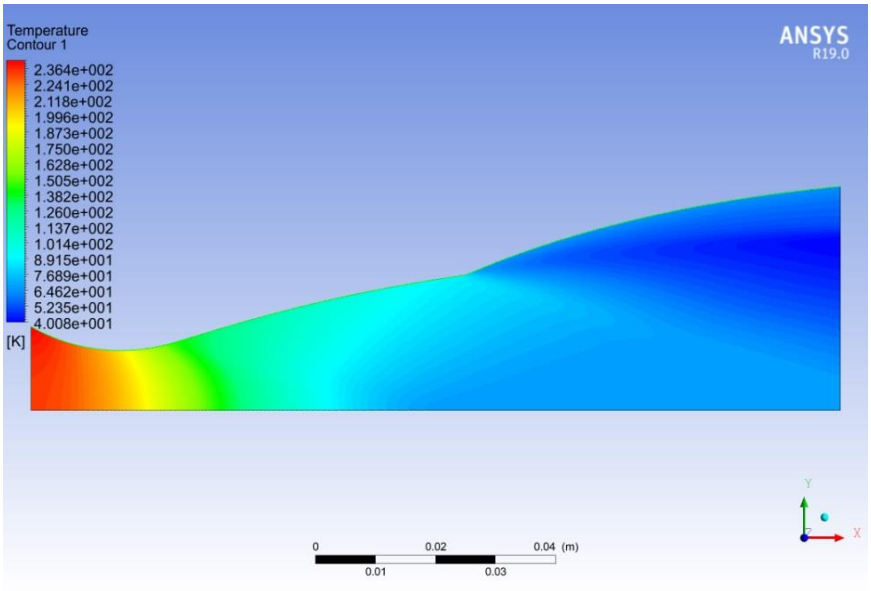

Figure II- 8: Contour of static temperature along the cylindrical DBN nozzle.

It is observed that the temperature follows the same trend as the pressure, decreasing from the inlet to its minimum value at the exit of the nozzle. Knowing this value allows me to select the appropriate material for the design and construction of the nozzle.

- **Number Mach evolution**

Next, the Mach number graph and its contour plot below provide a representation of fluid velocity variations, establishing the relationship between local velocity and the speed of sound.

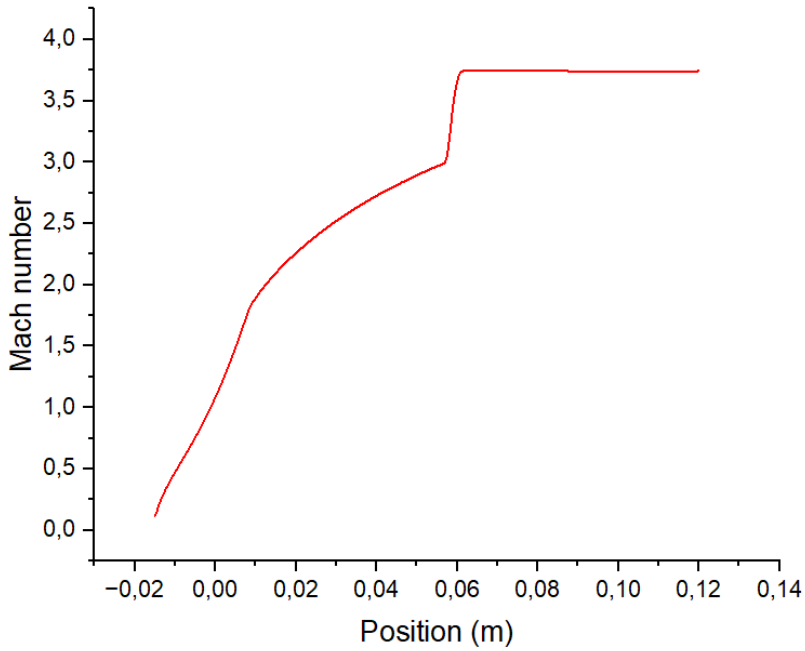

Figure II- 9: Mach number evolution along the nozzle wall.

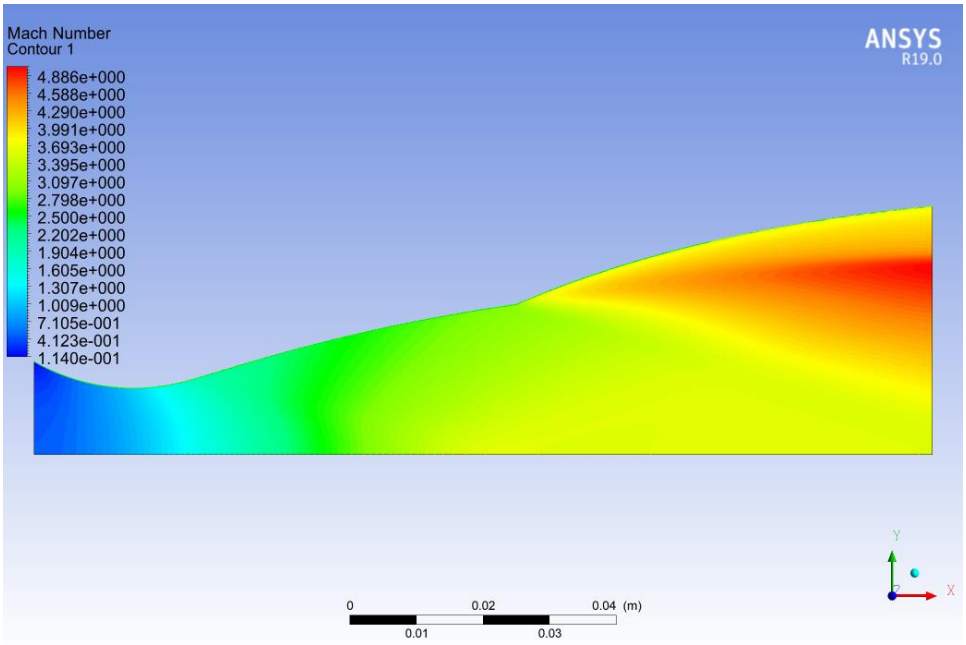

Figure II- 10: Mach number contour along the cylindrical DBN nozzle.

The two figures provide complementary information on the distribution and evolution of the Mach number in a nozzle.

Figure II-9 shows the graph illustrating the evolution of Mach number along the nozzle wall shows a gradual increase in Mach number with respect to position. Initially, at the entry, the Mach number is close to zero, indicating subsonic flow. As the position progresses towards the junction point, the Mach number steadily risen to about 2.5. At the junction point, there is a rapid increase, with the Mach number reaching approximately 3.8, suggesting a transition to supersonic flow. Beyond the junction point, the Mach number stabilizes slightly as it moves towards the exit.

In contrast, Figure II-10 is a graph illustrating the variation of the contour image of the Mach number displays the distribution of flow speed along the cylindrical DBN nozzle. At the entry, the flow starts at a subsonic speed with relatively low Mach numbers. As the flow progresses along the nozzle towards the junction point, the Mach number increases progressively. At the junction point and beyond, the Mach number reaches higher values towards the exit, indicating supersonic flow. This transition is clearly visible, corresponding to the regions where the Mach number reaches and exceeds.

In summary, both the Mach number evolution along the nozzle wall and the Mach number contour illustrate a gradual transition from subsonic to supersonic flow, with a marked

increase around the junction point and stabilization towards the exit. At the junction point, the Mach number takes two different values due to the Prandtl-Meyer expansion.

- **Density Evolution**

Finally, the density graph below illustrates the distribution of fluid density within the nozzle:

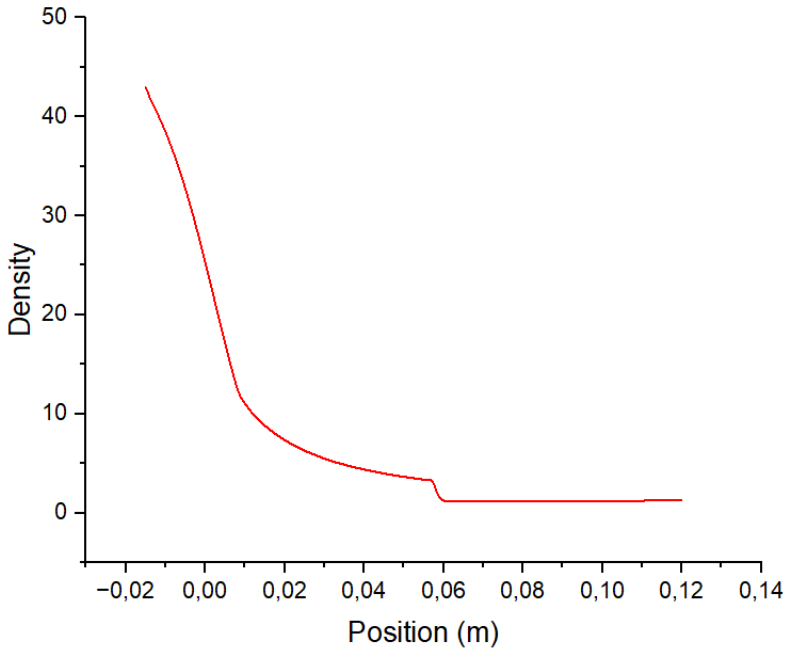

Figure II- 11: Density evolution along the nozzle.

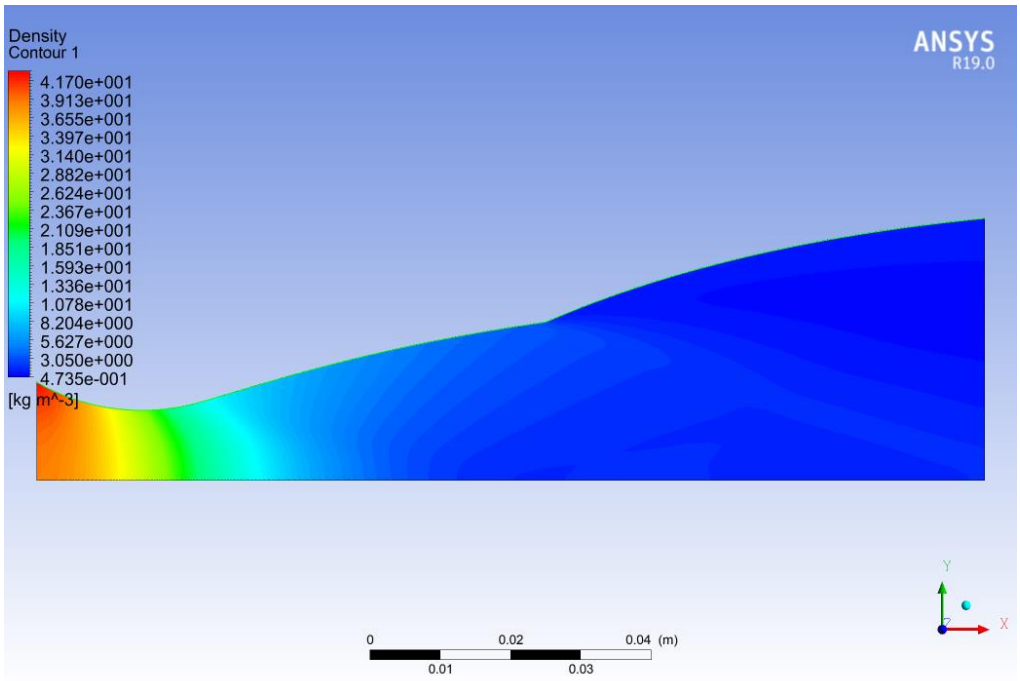

Figure II- 12 : Density contour along the cylindrical DBN nozzle.

The figures II-11 and II-12 provide a representation of density as a function of position.

At the entrance of the nozzle, the density is very high (around 40 kg/m³) and decreases rapidly as one moves further along. This is confirmed by the contour image, where warm colors (red and yellow) indicate high density. At the junction point, the density begins to stabilize after the initial steep drop, as seen on the graph around the 0.03 to 0.05 m mark. In the contour image, this transition is shown by the shift from warm to cooler colors. At the nozzle exit, the density continues to decrease but at a much slower rate, approaching nearly zero. On the graph, this trend is visible from 0.05 m to 0.14 m, where the curve flattens out. In the contour image, the density in this region is represented by blue colors, indicating low density. This overall pattern suggests that as the gases expand within the nozzle, their density decreases as they accelerate and occupy a larger volume.

II.2.2 Viscous calculations

II.2.2.1 Mesh sensitivity study

Mesh sensitivity study is essential for evaluating the accuracy of numerical simulations in the context of solving incompressible Navier-Stokes equations for perfect flow in a nozzle. Three distinct meshes were used: a fine mesh (Mesh 3), a medium mesh (Mesh 2), and a coarse mesh (Mesh 1). These meshes differ in their number of elements, orthogonal quality, and element dimensions of the nozzle, directly influencing the simulation results.

Table II- 4 : Mesh sensitivity.

Mesh	Number of elements	Orthogonal quality of mesh	Inlet pressure	Pressure at the inflection points.	Outlet pressure
Mesh 1	84881	0,98625	2.98952e+06	33845,2	15471.5
Mesh 2	66676	0,99228	2.97826e+06	29168,5	34734.2
Mesh 3	261508	0,81361	2.99483e+06	27140,1	30829.1

The provided table presents results for various thermodynamic parameters, including pressure at the inlet, inflection point, and outlet of the nozzle. It is crucial to observe how these values vary with mesh refinement to determine which mesh provides solution-independent results:

- **Coarse Mesh (Mesh 1):** Composed of 84,881 elements with an orthogonal quality of 0.98625, this mesh shows an inlet pressure of 2,989,520 Pa, an inflection point pressure of 33,845.2 Pa, and an outlet pressure of 15,471.5 Pa.

- **Medium Mesh (Mesh 2):** Composed of 66,676 elements and possessing the best orthogonal quality (0.99228), this mesh gives an inlet pressure of 2,978,260 Pa, an inflection point pressure of 29,168.5 Pa, and an outlet pressure of 34,734.2 Pa.
- **Fine Mesh (Mesh 3):** The most refined with 261,508 elements but a lower orthogonal quality (0.81361). The inlet pressure is 2,994,830 Pa, the inflection point pressure is 27,140.1 Pa, and the outlet pressure is 30,829.1 Pa.

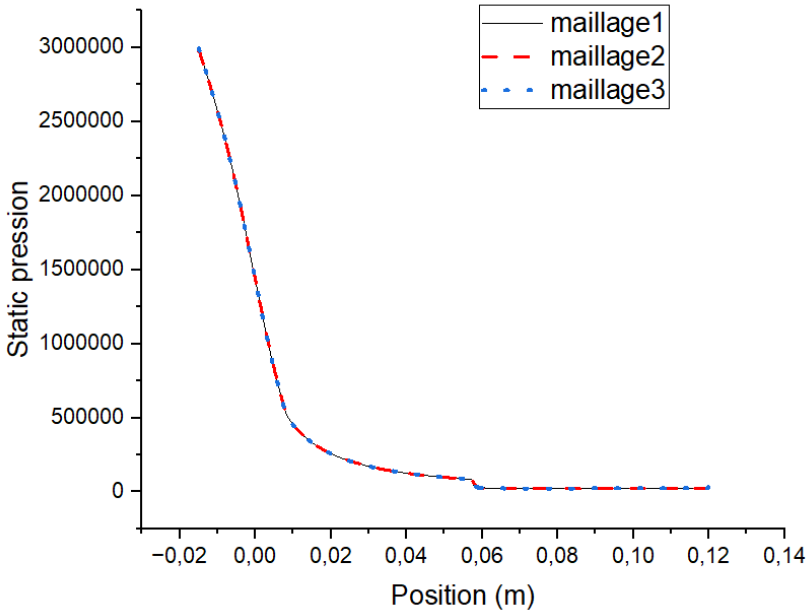

Figure II- 13: The evolution of static pressure for three types of meshing.

Comparative analysis of the results shows that the fine mesh and the medium mesh produce more stable and consistent results with each other, despite slight variations in measured pressures. In contrast, the coarse mesh exhibits more significant discrepancies, suggesting lower accuracy.

It is noteworthy that although the medium mesh has fewer elements compared to the fine mesh, it has superior orthogonal quality, contributing to result accuracy. Therefore, the medium mesh (Mesh 2) appears to offer a good balance between precision and computational resources, as its results closely align with those obtained from the finest mesh.

Thus, determining a mesh-independent solution can be approached by noting that results from the medium and fine meshes converge, indicating that additional refinement beyond the medium mesh does not yield significant precision gains. This conclusion validates the use of the medium mesh for precise simulations while optimizing computational time and resources.

II.2.2.2 Study of turbulence model influence

The study of turbulence model influence on simulation typically proceeds through several stages:

1. Turbulence Model Selection: Choosing an appropriate turbulence model based on flow conditions, geometry complexity, and simulation goals (e.g., k-epsilon model, LES model, RANS model, etc.).
2. Model Validation: Verifying the turbulence model's ability to reproduce consistent results with experimental data or well-established reference cases. This often involves comparisons of velocity profiles, turbulence fields, and other key parameters.
3. Sensitivity to Model Parameters: Analyzing the turbulence model's sensitivity to specific parameters it uses, such as turbulence constants or transport coefficients. Parametric studies may be conducted to assess the impact of these parameters on simulation results.
4. Performance Evaluation: Comparing the turbulence model's performance across different flow conditions (e.g., laminar flow, weak turbulence, strong turbulence). This helps understand the model's application limits and behaviors under various flow regimes.
5. Influence Analysis on Results: Studying the turbulence model's influence on final simulation results, including velocity fields, turbulence profiles, pressure gradients, etc. This analysis can reveal significant differences between models and their implications for prediction accuracy.
6. Optimization and Model Selection: Using the results to optimize the choice of turbulence model based on specific project requirements, such as required accuracy, available computational resources, and performance goals of the system under study.

The study of turbulence model influence involves a thorough evaluation of its ability to accurately represent turbulent phenomena in the simulated flow, as well as its impact on simulation reliability and accuracy.

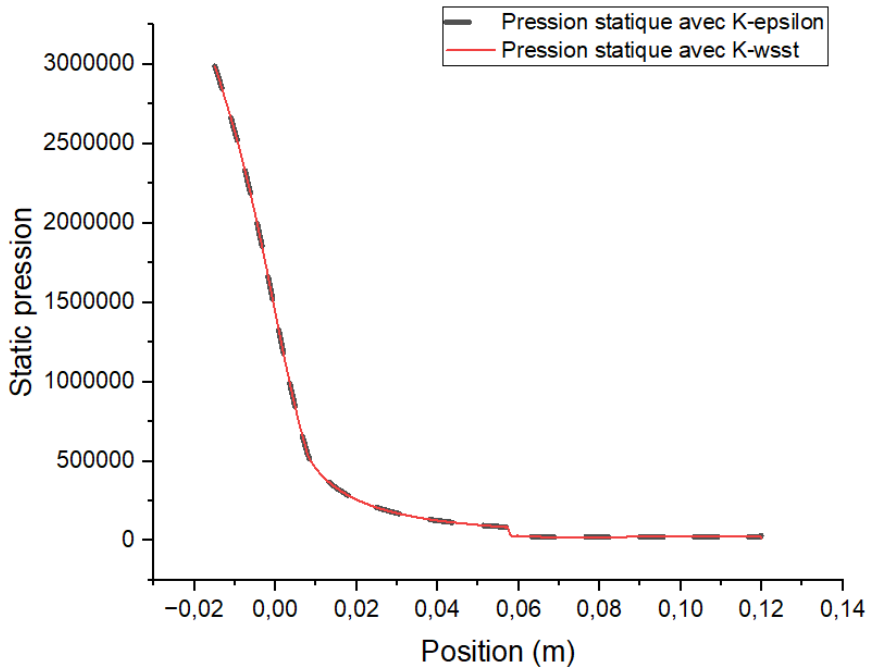

Figure II- 14: The evolution of pressure using the turbulence models k-w sst and k-epsilon.

Figure II-14 depicts the influence of turbulence models on the distribution of wall pressure for two turbulence models, Kw-sst and k-epsilon.

Initially, at the inlet of the nozzle, the static pressure is extremely high, reaching 30 bars. This pressure decreases rapidly, indicating a strong acceleration of the fluid as it enters the first bend of the nozzle. This drastic pressure drop reflects the expansion of the fluid and the conversion of potential pressure energy into kinetic energy.

At the junction between the first and second bends, there is an area where the static pressure temporarily stabilizes before continuing to decrease. This phenomenon is due to slight compression and the fluid adjusting to changes in geometry at this junction. This transition between the two bends is crucial for regulating flow and pressure.

At the outlet of the nozzle, the static pressure stabilizes and reaches a relatively low value. This stabilization indicates that the fluid has reached a maximum speed compatible with the cylindrical outlet section, and that most of the pressure energy has been converted into kinetic energy. The design of the double-bend nozzle facilitates an efficient transition from pressure to velocity, optimizing flow conditions and fluid ejection.

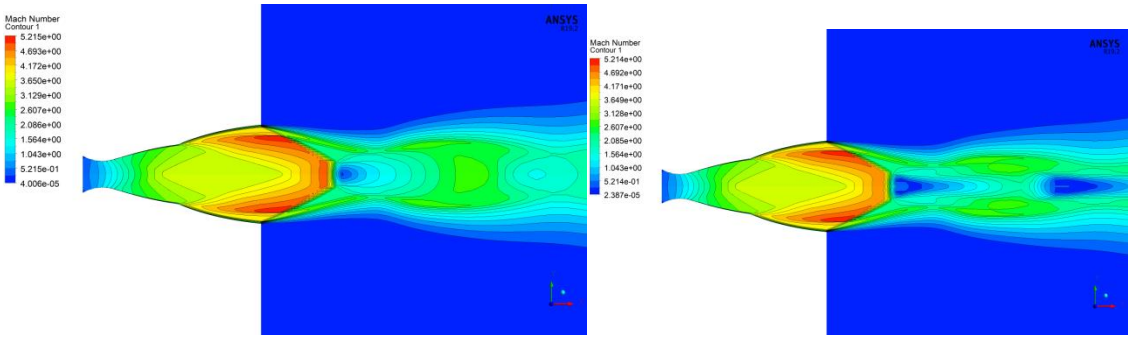

Figure II- 15: Mach number contour calculated with standard k-ε turbulence model and SST k-ω turbulence model.

For the k-ε turbulence model, at the entrance of the double-bell nozzle, the static pressure starts at a high level of approximately 3,000,000 Pa and decreases rapidly. Progressing through the first bell, this pressure decrease continues, reaching nearly zero around x = 0.03 m. At the junction between the first and second bells, slight pressure oscillations are observed, suggesting local fluctuations. Moving through the second bell, the static pressure stabilizes near zero, with small persistent variations along the nozzle exit.

Comparing the k-ε and k-ω SST turbulence models for the evolution of static pressure through the double-bell nozzle highlights significant differences in terms of accuracy and ability to resolve turbulent effects.

The k-ε model shows a rapid decrease in static pressure right from the nozzle entrance, nearing zero by x = 0.03 m, with subsequent slight oscillations. These oscillations could result from unresolved turbulence fluctuations or dissipation effects. Near the bell junction, the k-ε model exhibits slight fluctuations, indicating difficulty in precisely capturing effects of geometry changes. Downstream, the pressure stabilizes near zero with minor variations, suggesting insufficient resolution of turbulent effects over the nozzle length.

In contrast, the k-ω SST model also demonstrates a rapid decrease in static pressure but with a smoother transition and fewer oscillations. This suggests better capability in capturing turbulent effects near walls and in regions with high pressure gradients. At the bell junction, the transition is continuous without pronounced oscillations, illustrating superior performance for complex geometries. Downstream, the pressure stabilizes without the variations seen with the k-ε model, indicating a more consistent and stable simulation.

Advantages of the k-ω SST model include better resolution of turbulent effects, more accurate representation of geometry changes, and increased simulation stability. These features make the k-ω SST model a superior choice for simulations involving complex nozzle geometries, offering higher precision and finer resolution of turbulent phenomena.

In conclusion, the k-ω SST model is recommended for future studies due to its superior performance in representing turbulent effects and complex geometries.

II.2.2.3 Methodology

The analysis of flow in a double-bell nozzle with a cylindrical section is expanded to include the effects of viscosity and turbulence, transitioning from a perfect to a viscous flow state. Following conclusive results for inviscid flow, integrating viscosity and turbulence effects becomes central. The simulation setup is adjusted to address the viscous case by introducing sophisticated turbulence models, including the k-ε and k-ω SST models, known for their accuracy in capturing turbulent phenomena.

The simulation begins with the activation of viscous effects and the specification of fluid properties using suitable turbulence models. The same geometry as in the inviscid case is maintained, with an additional outer domain to better capture viscosity and turbulence effects. Separate simulations are conducted for each turbulence model to analyze turbulent flow characteristics within the nozzle.

Results from simulations using both turbulence models are compared in terms of performance and accuracy, based on criteria such as pressure fields, velocity fields, temperature profiles, and turbulence profiles. Comparing the distributions of thermodynamic parameters and flow structure determines which model better represents physical phenomena and refines results correctly. This crucial step ensures that viscous effects are accurately represented, and the most appropriate turbulence model for simulating viscous flow in the nozzle is selected based on the obtained results.

- ***Geometry***

- The geometry is generated by inputting the nozzle profile coordinates into the DesignModeler interface using the command Concept → 3D Curve → XY Plane → Coordinate File, and then opening the geometry file.
- Four points were placed on the horizontal X and Y axes: -0.02 m on the X-axis, 1.2 m on the X-axis, 1.2 m on the X-axis, and 0.6 m on the Y-axis, and 0.6 m on the Y-axis. These points serve as reference points to define the ends of the nozzle as well as to create the outer domain. The outer domain plays a crucial role in accurately capturing the effects of boundary conditions on the flow. The outer domain, often referred
- to as the control domain, allows simulation of the environment around the nozzle, ensuring that interactions between internal nozzle flow and ambient flow are properly represented. It also minimizes the influence of artificial boundary conditions imposed at the simulation domain boundaries, thereby ensuring more accurate and realistic results in terms of pressure

distribution, velocity, and turbulence characteristics. Overall, it ensures faithful modeling of the complex physical phenomena associated with viscous flow inside and around the nozzle.

- Linking and projecting points using the Concept → Lines from Point command as well as the Tools → Projection command defining the geometry shape.
- The surface of the geometry was generated using the lines defined previously.
- Using the Tools → Face Split command to split the geometry into two parts: the nozzle and the outer domain.
- Removal of the wireframe body: The original wireframe body, which served as a reference to construct the geometry, was removed, leaving only the surface of the geometry.
- The resulting geometry surface was designated as fluid, facilitating the definition of fluid properties for simulating the flow.

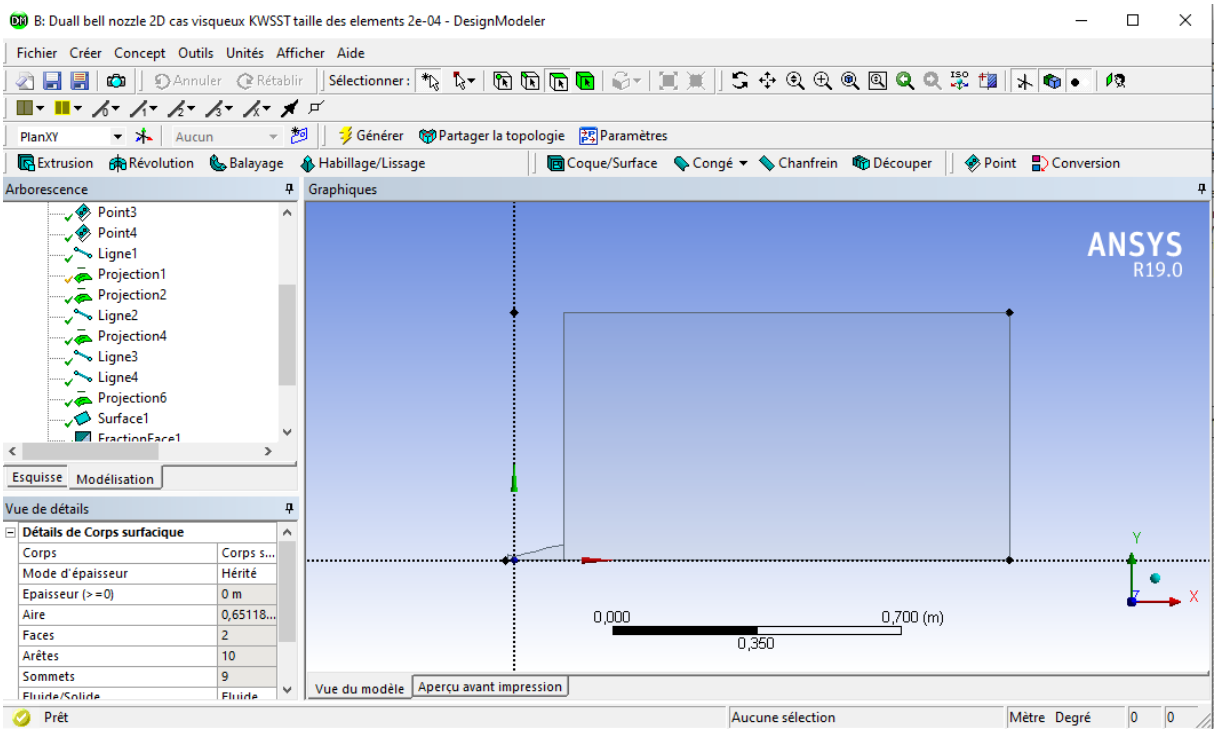

Figure II- 16: Geometry creation

Table II- 5: Geometric parameters for the viscous case.

Parameters	Symbole	Value	Description
Inlet width	W_{in} (m)	0,014019	Width of the inlet section of the nozzle.
Outlet width	W_{out} (m)	0,03736	Width of the outlet section of the nozzle.
Total lenght	L (m)	0,13485	Length of the nozzle from inlet to outlet.
Total width	W (m)	0,03736	Width of the nozzle from inlet to outlet.
Throat radius	R_{th} (m)	0,01	Throat radius of the nozzle.
Inflection point	PI (m)	0,0573025 0,0581962	The two inflection points of the nozzle.
Surface	A (m^2)	0,65118 m^2	The surface area of the geometry.
Volume	V (m^3)	0	The volume of the nozzle.
Width of the external domain	Wd (m)	0,6	Width of the external domain.
Lenght of the external domain	Ld (m)	1,0801	Length of the external domain.

➢ ***Mesh Study***

- In the Meshing interface [ANSYS AUTODYN PrepPost], using the mesh control command → face meshing → select our geometry and generate a mesh.
- In the mesh control command → sizing → select the nozzle face, impose behavior, and set element size to 0,0004 → generate a mesh.
- Mesh details → Sizing → size function: uniform → generate a mesh.
- In the mesh control command → sizing → select the edges of the outer domain and refine them on the nozzle section side using the division size type with 200 divisions, impose behavior, bias option with a bias factor of 200 → generate a mesh.

Finally, five named selections were created: WALL, DBN, AXIS, INLET, OUTLET.

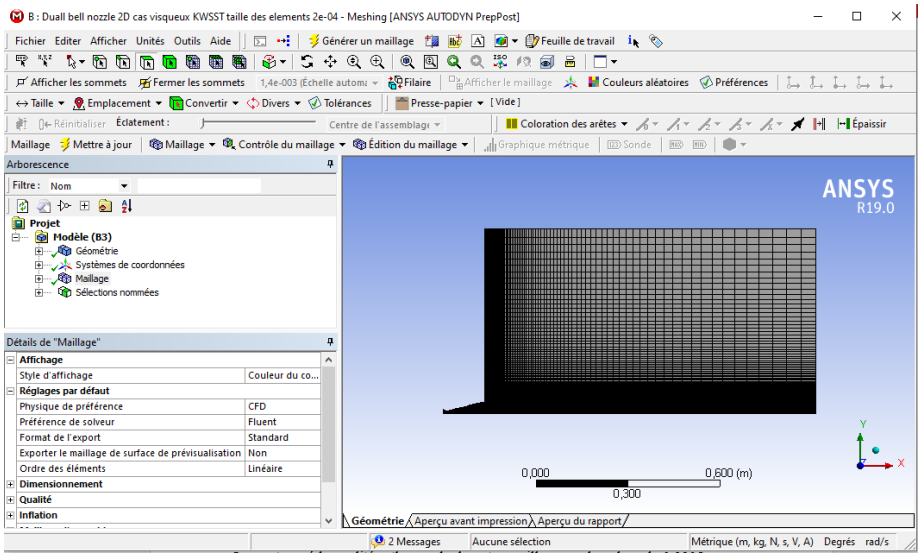

Figure II- 17: Mesh of the double-bend nozzle with cylindrical section.

The mesh quality used in this study was evaluated based on several important criteria. The mesh consists of a total of 66676 elements and 67442 nodes. A key measure of mesh quality, the orthogonality index, was determined to be 0,99228. This value indicates good mesh orthogonality, crucial for ensuring accurate representation of flow conditions and fluid-structure interactions in the simulation.

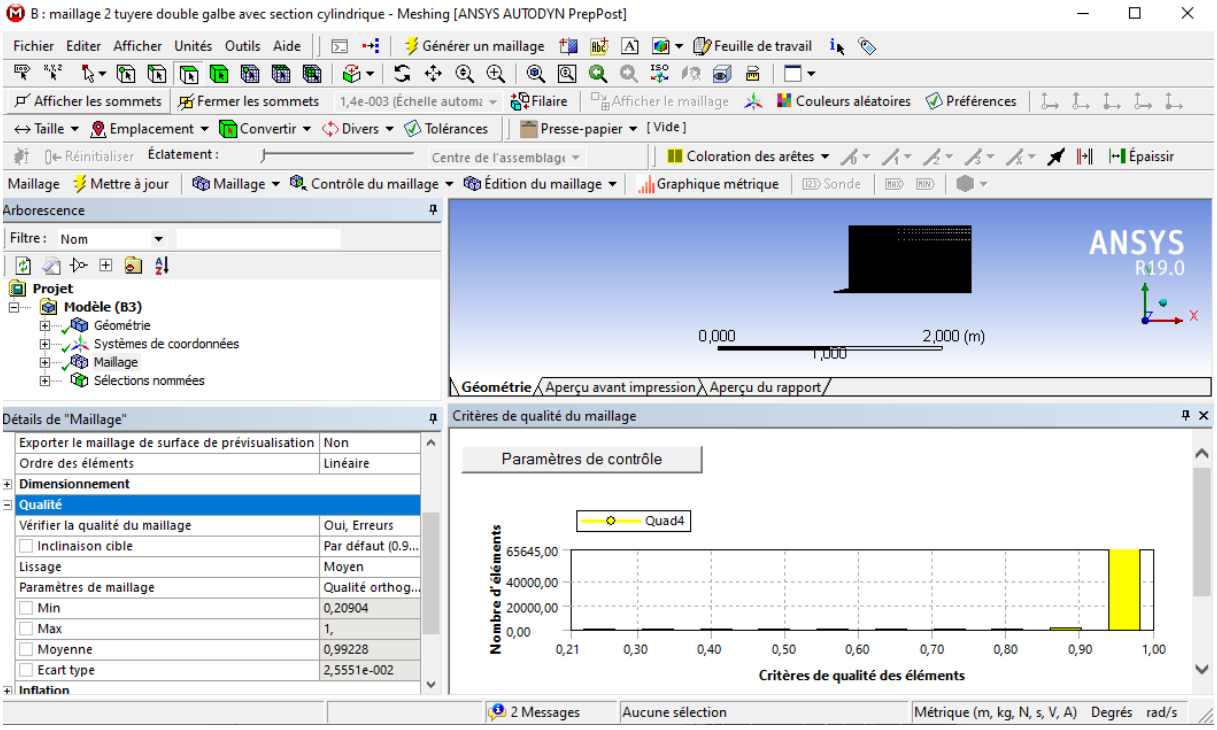

Figure II- 18: Mesh Orthogonality Quality.

Based on the figure below showing the mesh orthogonality values, we conclude that our mesh is excellent.

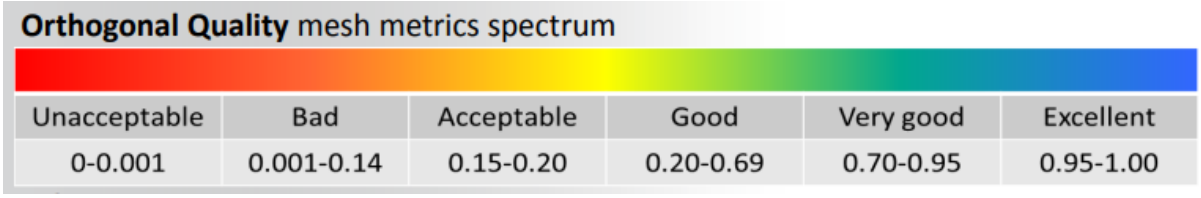

Figure II- 19: Range of values for the orthogonal quality of a mesh.

II.2.2.4 Results & interpretation

- General: Solver type: density-based (incompressible flow), velocity formulation: absolute, time: steady (time-independent), 2D space: axisymmetric for fluid mechanics equations resolution.
- Model: Energy → activation of energy equation.

- Model: Viscous → k-ω SST (Shear Stress Transport) turbulence model chosen to represent turbulence effects in the flow.
- Materials: Air → perfect gas.
- Boundary Conditions: Operating pressure: 0 Pascal, Inlet → gauge total pressure: 30 bars, supersonic/initial gauge pressure: 29.99790009, total temperature: 243 Kelvin, Outlet → total temperature: 243 Kelvin, gauge pressure: 0.4 bars.
- Solution: Method → pressure-velocity coupling, scheme: coupled, spatial discretization → gradient: least squares cell-based, pressure: second order, density: second order upwind, turbulence kinetic energy: second order upwind, specific dissipation rate: second order upwind, energy: second order upwind / pseudo-transient selected.
- Initialization: Initialization method: standard initialization, compute from: inlet, axial velocity: 3.124877 m/s, radial velocity: 2.14505e-14 m/s, turbulence kinetic energy: 0.03661821 m^2/s^2, specific dissipation rate: 8801.236 1/s → initialization.

To ensure accuracy and convergence of the simulation, an appropriate number of iterations was chosen, determining how many times the solver iterates to achieve a stable solution. Once all configurations were defined, the computation was initiated to solve the fluid dynamics equations, thereby determining pressure, velocity, and temperature fields inside the nozzle.

➢ **The Boundary Layer** :

Table II- 6: Thermodynamic Parameters of the Geometry for the Viscous Case.

Parameters	Symbole	Value	Description
Initial pressre	P0 (P)	30e+05	The pressure at the inlet of the combustion chamber.
Initial temperature	T0 (K)	243	The temperature at the inlet of the combustion chamber.
The ratio of specific heats	Cp Joule/Kg*Kelvin	1006,43	The ratio of specific heats.
Gamma	ɣ	1,4	adiabatic index.
Outlet pressure	Pe (P)	15471.5	The pressure at the outlet of the combustion chamber.

To assess the accuracy of our 2D axisymmetric DBN nozzle flow simulation, we compared our results with those obtained using the method of characteristics provided by our supervisor. This comparison was conducted by overlaying graphs of key variables such as static

pressure, static temperature, and Mach number on the same plot.

- **Static Pressure évolution**

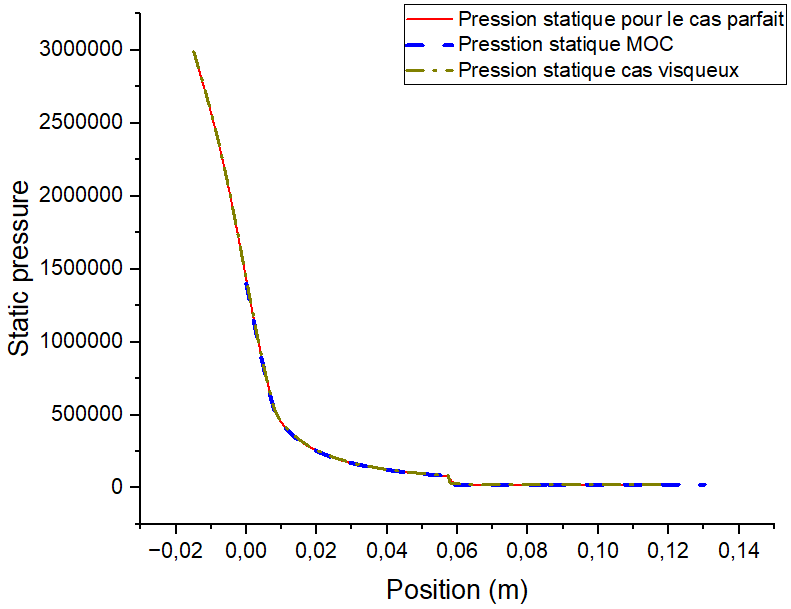

Figure II- 20: Comparison between static pressure obtained by the MOC method and CFD simulation.

The static pressure values for each station (inlet, junction point, and outlet) are presented in the table below:

Table II- 7: Static pressure values between simulation results and MOC.

Parameters	Inlet	Junction point	Outlet
Static pressure in the ideal case (Pa)	2,98312^{e}+06	82533,4 25186,5	22709,4
Static pressure in the viscous case (Pa)	2,98952e+06	75274,5 42228	15471,5
Static pressure MOC (Pa)	1400342	81629,51 22809	22809

At the inlet of the nozzle, the static pressure values are comparable between the perfect and viscous cases, but the Method of Characteristics (MOC) shows a significantly lower

pressure. At the junction point, the pressures in the perfect and viscous cases are similar, with a slight reduction in the viscous case due to friction effects, while the Method of Characteristics aligns closely with the perfect case. At the outlet, the viscous case exhibits higher pressure due to friction, whereas the perfect and MOC cases show pressures that are similar and slightly lower than that of the viscous case. Overall, the differences observed between the methods highlight the significant impact of viscosity and simulation conditions on static pressure results

- **Mach number evolution**

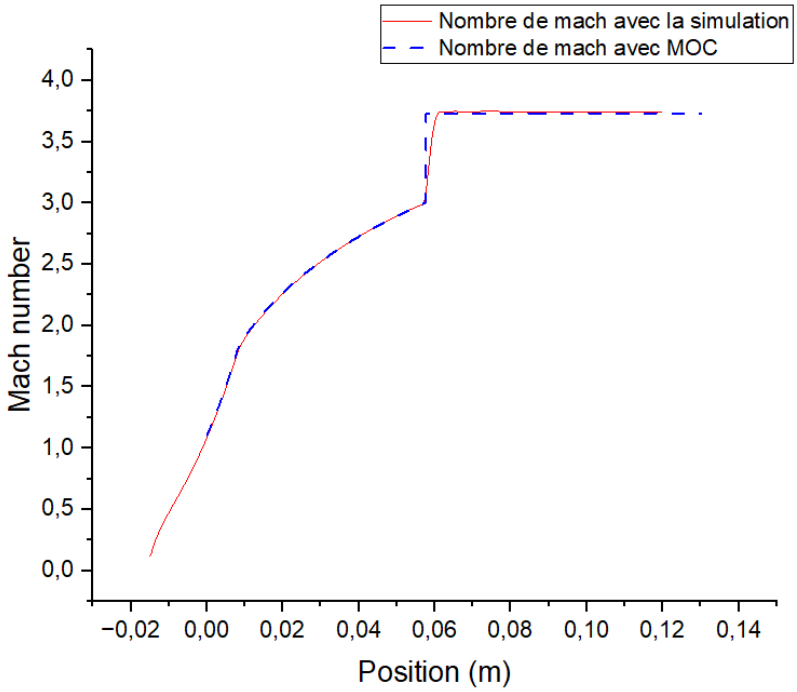

Figure II- 21: Comparison between the Mach number obtained using the MOC method and CFD simulation.

The table below presents the Mach number values for each station (inlet, junction point, and outlet).

Table II- 8 : Mach Number Values Comparison between Simulation and MOC Results.

Parameters	Inlet	Junction point	Outlet
Mach number ideal case	0,114026	3,0338 3,722	3,74281
Mach number MOC	1,102712	3,000339 3,73	3,73

At the inlet, the Mach number for the perfect gas case (0.114026) is significantly lower than that obtained by the Method of Characteristics (MOC) (1.102712), indicating a significant difference in initial conditions or simulation assumptions. At the junction point, the values are very close: 3.0338 for the perfect gas case and 3.000339 for the MOC, demonstrating good agreement between the two methods at this station. At the outlet, the values are also similar, with 3.722 for the perfect gas case and 3.73 for the MOC, suggesting that both methods predict similar flow behavior at this point. Overall, these differences and similarities highlight the impact of initial conditions and specific assumptions of each method on Mach number results. The relative error between the number obtained by the Method of Characteristics and that obtained by simulation is 0.34%, indicating a very satisfactory result.

- **Static Temperature evolution**

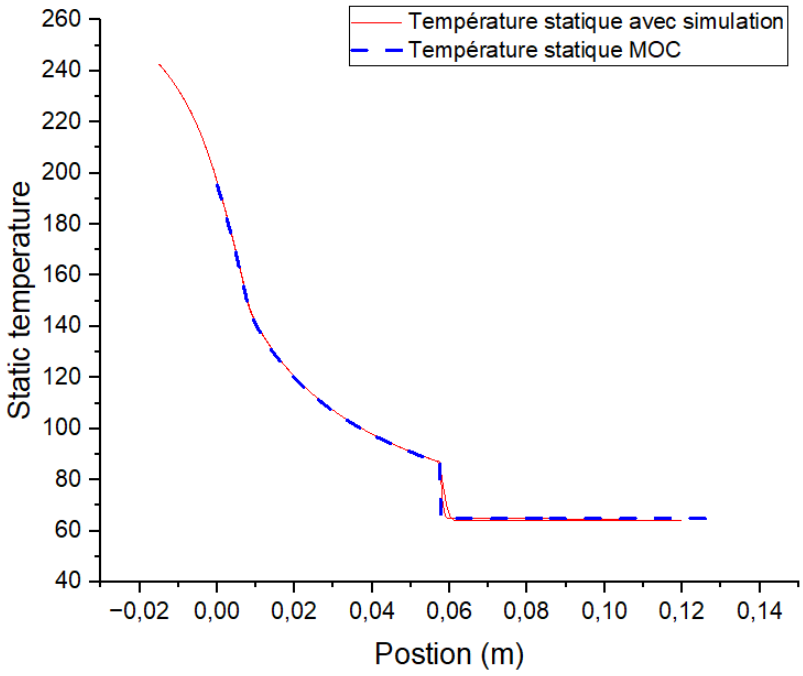

Figure II- 22: Comparison of static temperature obtained by the MOC method & CFD simulation.

The values of static temperature for each station (inlet, junction point, and outlet) are presented in the table below

Table II- 9: Static temperature values between CFD simulation and MOC results.

Parameters	Inlet	Junction point	Outlet
Static temperature ideal case (K)	242,444	87,337 64,558	64,0328
Static temperature MOC (K)	195,4641	86,7731 64,9098	64,9098

At the inlet, the static temperature for the perfect case (242.444 K) is higher than that obtained by the Method of Characteristics (MOC) (195.4641 K), suggesting a difference in initial conditions or simulation assumptions. At the junction point, the temperatures are very close: 87.337 K for the perfect case and 86.7731 K for the MOC, indicating good agreement between the two methods at this station. At the outlet, the values are also similar, with 64.558 K for the perfect case and 64.9098 K for the MOC, suggesting that both methods predict nearly identical static temperatures at this point. Overall, these differences and similarities highlight the significant impact of initial conditions and specific assumptions of each method on static temperature results.

- **Density evolution**

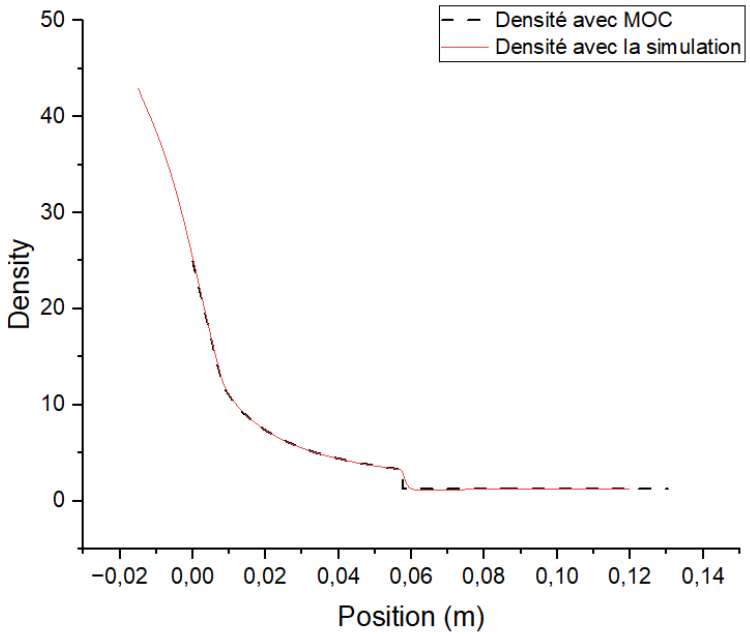

Figure II- 23: Comparison of density between the MOC method & CFD simulation.

The density values for each station (inlet, junction point, and outlet) are presented in the table below

Table II- 10: Density values between simulation results and MOC.

Parameters	Inlet	Junction point	Outlet
Density ideal case	42,9918	3,292 1,44	1,2356
Density MOC	24,91446	3,2715 1,2436	1,2436

At the inlet, the density for the perfect case (42.9918) is significantly higher than that obtained by the Method of Characteristics (MOC) (24.91446), indicating notable differences in initial conditions or simulation assumptions. At the junction point, the values are very close: 3.292 for the perfect case and 3.2715 for the MOC, demonstrating good agreement between the two methods at this station. At the outlet, the values differ slightly, with 1.44 for the perfect case and 1.2436 for the MOC, suggesting that the MOC predicts a slightly lower density at this point. Overall, these differences and similarities highlight the significant impact of initial conditions and specific assumptions of each method on density results.

In conclusion, the graphical comparison of results between our CFD simulation and the Method of Characteristics reveals overall good agreement, despite differences primarily attributable to modeling turbulent and diffusive effects in numerical simulation. The Method of Characteristics results show sharper, more analytical transitions, while CFD simulation presents smoother and more realistic variations, reflecting the complexities of turbulent flows under real-world conditions. The relative errors between values obtained by simulations and those obtained by the Method of Characteristics are very low, primarily due to methodological differences. This comparative analysis validates the numerical approach used while emphasizing the crucial importance of accurately modeling physical phenomena for a comprehensive understanding of flows in aerospace nozzle

II.3 COMPARISON STUDY OF AN INNOVATIVE AXISYMMETRIC DUAL-BELL ELLIPTICAL NOZZLE WITH CONVENTIONAL DUAL-BELL CYLINDRICAL NOZZLE

II.3.1 Introduction

Asymmetric propulsion nozzles are a type of engine nozzle design used in aerospace applications where the geometry of the nozzle is intentionally modified in a non-uniform or asymmetric manner. Unlike traditional symmetric nozzles that have uniform shapes, asymmetric nozzles exhibit variations in their geometry that can lead to improved performance, maneuverability, or other specific characteristics. The asymmetry of these nozzles can take various forms, such as variations in throat section, divergent section shape, or the introduction of additional features like ramps, corners, or secondary flow paths. The primary purpose of these modifications is to tailor the flow expansion and pressure distribution to achieve specific aerodynamic effects or performance benefits.

In the 1960s and early 1970s, the main concern in the design of jet engine exhaust nozzles was to achieve profiles where the installed system would not generate excessive thrust loss or drag. Axisymmetric configurations offer high internal performance but come with penalties of reduced thrust and low drag efficiency when integrated into complex propulsion engines with non-symmetric zone constraints requiring careful integration of the airframe/propulsion system. The advent of hypersonic air-breathing propulsion systems, operating at speeds exceeding Mach 5 and offering higher specific impulses than rocket engines, has sparked growing interest in asymmetric nozzle design. Moreover, non-axisymmetric supersonic nozzles have become an integral part of hypersonic air-breathing vehicles as they offer excellent integrated aerodynamic performance. They also seem to integrate much better with propulsion engines having non-symmetric zone constraints, leading to performance improvement. Numerous studies have been conducted in this field to study the feasibility and performance of this type of nozzle (see literature review). Several designs have been proposed in this regard, including elliptical nozzles.

Elliptical propulsion nozzles are valuable components in aerospace engineering. They play a critical role in the performance and functionality of various aerospace vehicles, offering diverse advantages in terms of precise control and maneuverability. For example, they can provide higher levels of thrust vector efficiency compared to other designs primarily by altering the exhaust gas flow through their elliptical shape. They can also help manage shock waves

generated by supersonic or hypersonic flows more effectively, resulting in reduced separation and flow losses. Regarding supersonic combustion, elliptical nozzles can enhance its efficiency by maintaining stable and efficient supersonic combustion and offering better expansion of combustion gases required in air-breathing engines like scramjets. Finally, the shape of the elliptical nozzle can be tailored to specific flight conditions, leading to efficient performance that meets a range of mission needs. The applications of elliptical propulsion nozzles are diverse and extend to different types of vehicles operating at various speed regimes and altitudes. Scramjet engines, operating at high speeds in the atmosphere, can benefit from the optimized expansion characteristics of elliptical nozzles, improving their combustion efficiency and thrust. The thrust vectoring capability of elliptical nozzles is also present in various drones designed for agile maneuvers, reconnaissance, and surveillance. Stealth aircraft, which require low radar cross-sections, can benefit from elliptical nozzles capable of reducing their detectability by radar systems.

II.3.2 Methodology

The initial step involves designing the axisymmetric dual-bell nozzle contour using a proprietary method of characteristics (MOC) code developed in-house. This contour is structured with a truncated ideal contour (TIC) serving as the base nozzle and a constant pressure (CP) section as the extension nozzle, as depicted in Figure II-24. The output of this design process is a file containing the coordinates of the nozzle design points X_{DBN_MOC} and Y_{DBN_MOC}, which define the shape and dimensions of the nozzle profile. This file serves as a crucial reference for further analysis and refinement of the nozzle geometry to optimize its performance characteristics in aerospace applications.

The following figure represents the axisymmetric MOC design of the dual-bell nozzle which is **the base** of the two designed 3D dual-bell nozzles with circular and elliptical cross sections.

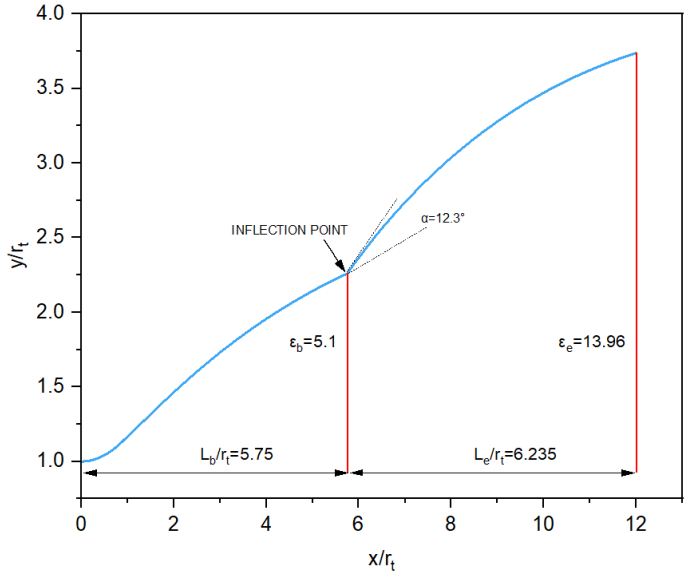

Figure II- 24: DBN divergent profile with geometrical details.

Table II- 11: 3D DBN geometrical parameters.

Parmeters	Value
Throat radius	r_{th} = 0.01 m
Base nozzle geometry (TIC)	Length: l_b/r_{th} = 5.75 Expansion ratio: ε_b = 5.1
Extension nozzle geometry (CP)	Length: l_e/r_{th} = 6.235 Expansion ratio: ε_e = 13.96
Inflection angle	α = 12.3 deg
Inflection point	Location: {5.75; 2.26} · r_{th}

Table II-11 and Table II-12 respectively summarize the geometric and thermodynamic parameters of our baseline nozzle.

Table II- 12: 3D DBN thermodynamical parameters.

Parmeters	Value
Stagnation (chamber) pressure	P_0 = 30 bars
Stagnation (chamber) temperature	T_0 = 243 K
Specie	Air
Specific heat ratio	γ = 1.4
Thermal capacity	C_p = 1006.43 J/Kg K

The second step involves designing elliptical sections at each position X_{DBN_MOC} of the dual-bell nozzle using specific equations.

$$\frac{y^2}{a}+\frac{z^2}{b}=c \qquad \text{(Eq. 1)}$$

With:

$$a = Y_{DBN\_MOC} \quad \text{(Eq. 2)} \qquad b = 2 \times Y_{DBN\_MOC} \quad \text{(Eq. 3)}$$

$$c = a \quad \text{(Eq. 4)} \qquad x_{DBN\_Elliptic} = X_{DBN\_MOC} \quad \text{(Eq. 5)}$$

a and b represent the radius of the elliptical sections according to the y-axis and z-axis respectively.

We have from the first equation:

$$y_{DBN\_Elliptic} = \sqrt{a \times \left(c - \frac{\left(z_{DBN\_Elliptic}\right)^2}{b}\right)} \qquad \text{(Eq. 6)}$$

$x_{DBN\_Elliptic}$ represents the coordinate of the elliptical sections according to the x-axis.

$y_{DBN\_Elliptic}$ represents the coordinate of the elliptical sections according to the y-axis.

$z_{DBN\_Elliptic}$ represents the coordinate of the elliptical sections according to the z-axis with a fixed marching step:

$$z_{DBN\_Elliptic} = z_{DBN\_Elliptic} + \frac{b}{10} \qquad \text{(Eq. 7)}$$

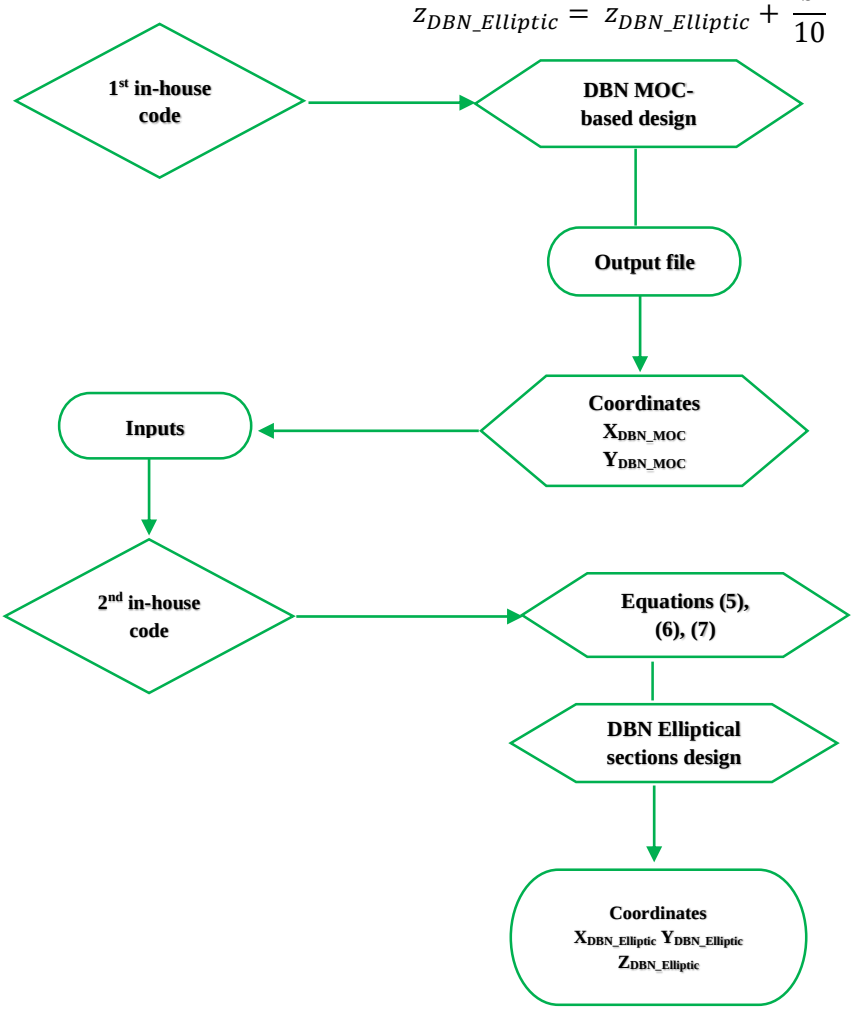

Figure II- 25: Flowchart (diagram) of the elliptical dual-bell nozzle design code.

II.3.3 Simulation of flow in a dual-bell nozzle with elliptical cross-section

This section presents a simulation of flow in a 3D dual-bell nozzle with an elliptical cross-section, an innovative design aimed at optimizing nozzle performance. The focus here is on validating the results obtained using the method of characteristics (MOC). Multiple simulations were conducted using Fluent software, with each test case discussed individually. A comparison of flow properties, including Mach number distribution, among different test cases in the project will be made against those obtained by MOC.

The geometry of the elliptical nozzle was precisely defined using 3D modeling tools, followed by the generation of a suitable mesh to discretize the computational domain, ensuring adequate resolution of the computational fluid dynamics (CFD) equations. CFD equations, including Navier-Stokes and energy conservation equations, were numerically solved using advanced CFD software. Robust solution algorithms were employed to ensure convergence and solution accuracy.

Pressure, velocity, and temperature fields obtained from the simulation were analyzed in detail, with graphs and visualizations created to illustrate flow characteristics, identifying recirculation zones, pressure gradients, and areas of acceleration and deceleration.

Simulation results highlighted the advantages of the elliptical nozzle design, such as uniform pressure distribution, reduced pressure losses, and overall efficiency improvement.

- ***Geometry creation***

The geometry is created by inserting the coordinates of the nozzle profile into the Design Modeler interface using the command Concept → 3D Curve → XY Plane → Coordinate File → Open the geometry file.

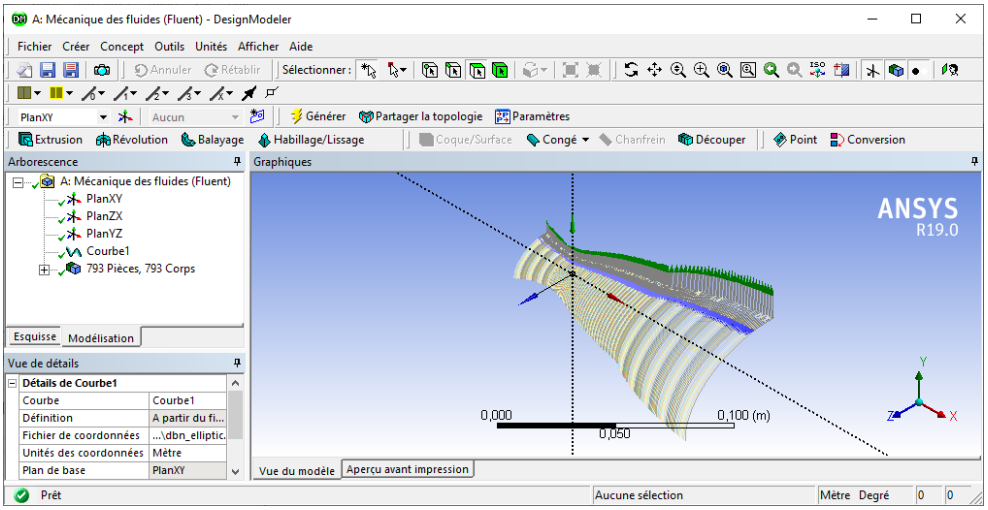

Figure II- 26: Importing the geometry into DesignModeler.

- Using the Create → Body Transformation → Mirror command: select all wireframe bodies. First, choose the XY plane as the mirror plane, then repeat the same operation for the ZX plane.
- In the Dress-Up/Smooth command → Select all wireframe bodies → Merge topology → Yes
- In the tree structure, select all wireframe bodies → Disable body
- In the tree structure, select solid → In the Fluid/Solid command, select Fluid
- In the Cut command → XY base plane → Generate
- The result is a geometry with 2 solids. For the solid representing the left side of the double-bell nozzle → In the tree structure → Disable body.

➢ ***Meshing the geometry:***

In the Meshing interface [ANSYS AUTODYN PrepPost], using the Mesh Control command → Method → select our geometry: multizone method → generate mesh.

Definition of multizone mesh: Multizone meshing is a technique used in finite element numerical simulation to divide a complex geometry into distinct zones, each meshed according to its characteristics. This provides flexibility, accuracy, and efficiency, thereby improving results and reducing computation time. Common types of multizone meshing include structured, unstructured, and hybrid meshes.

- Mesh Details → Sizing → Maximum face size 0.003 → generate mesh
- In the Mesh Control command → Sizing → Geometry: select outlet face, Behavior: Imposed, Element size: 0.0007 → generate mesh
- Finally, five named selections were created: symmetry, outlet, inlet, upper dual-bell nozzle, lower dual-bell nozzle.

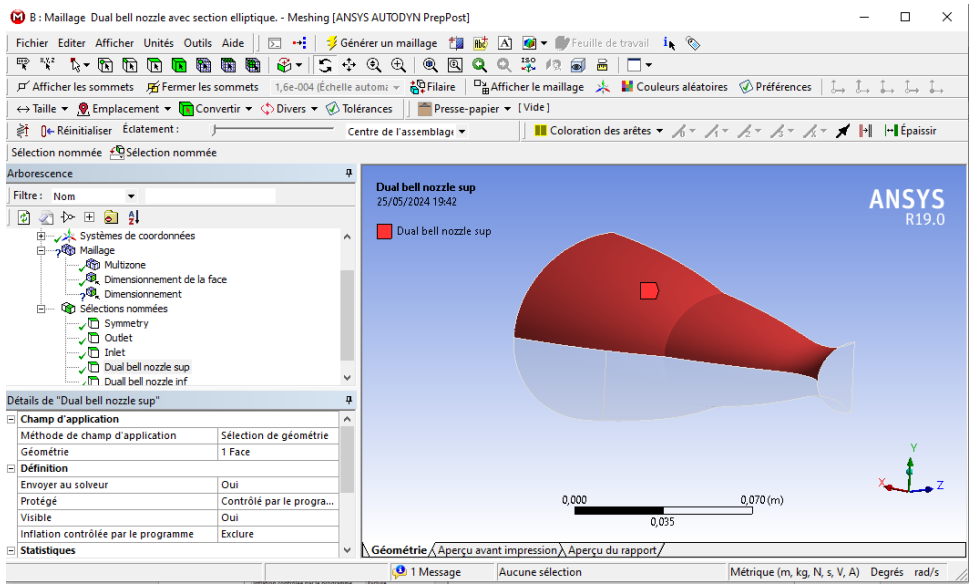

Figure II- 27: Creation of named selections.

Orthogonal quality: Orthogonal quality assesses the quality of a mesh element by measuring the angles between its edges. A perfectly orthogonal element displays a quality of 1, where edges form right angles, while a degenerate element with collinear edges will have a quality of 0. High orthogonal quality is crucial to ensure accuracy, convergence, and stability in finite element simulations.

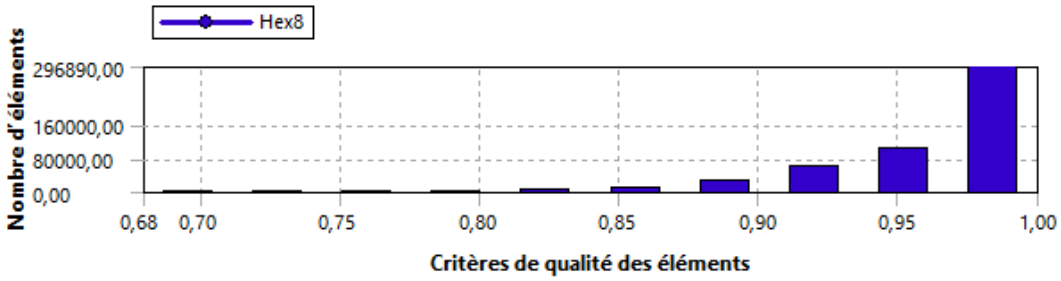

Figure II- 28: Mesh quality criteria.

➢ Resolution using Fluent:

The resolution is performed using the Fluent solver, in the general command → the solver type is chosen as density-based, time: steady.

- In the Models command → the energy equation is activated, model: inviscid.
- In the Materials command → air: ideal gas.
- In the boundary conditions command → operating pressure: 0, pressure inlet:
- Gauge total pressure (pascal): 30e+05 Supersonic/initial gauge pressure (pascal): 30e+05, thermal: total temperature (K): 243.

- In the solution command → initialization: initialize.
- Once the calculation method and number of iterations have been selected, the calculation is started using the "Run Calculation" function.
- After the simulation results have converged, flow variables are visualized either as field (contour) plots using the Graphics function or as graphs using the "Plots" function.

II.3.4 Results and interpretations

II.3.4.1 Design

Table II.13 compares the geometric characteristics of the proposed elliptical nozzle with those of the dual-bell nozzle with circular cross-section. It is evident that both nozzles have the same length, measuring 0.1198544 units. However, the cross-sectional areas at the throat, junction point, and exit have all increased by 29.3%.

To further clarify and expand on this comparison, it is observed that although the total lengths of both nozzles are identical, the elliptical nozzle exhibits larger cross-sectional areas at strategic points such as the throat, junction point, and exit. This 29.3% increase in cross-sectional areas suggests a potential for increased fluid flow or improved performance compared to the dual-bell nozzle with circular cross-section.

Table II- 13: Geometrical parameters comparison.

	Dual-bell nozzle with elliptical cross sections	**Dual-bell nozzle with circular cross sections**
Total Length (m)	0.1198544	0.1198544
Inlet Section Area (m^2)	0.00087326	0.00061745
Throat Section Area (m^2)	0.00044435	0.00031416
Inflection point Section Area (m^2)	0.0022686	0.0016037
Exit Section Area (m^2)	0.0062017	0.0043849
Weight (Kg)	0.435	0.376

Regarding the weight of the elliptical nozzle, it has increased by 13.56% compared to the weight of the circular nozzle. This increase represents a significant disadvantage in the aerospace field.

To delve deeper into this observation, it is important to note that the increased weight of the elliptical nozzle can have significant implications in aerospace applications. A 13.56% increase can compromise critical weight reduction goals for aerospace and space applications,

where every additional kilogram can impact the performance, efficiency, and fuel consumption of spacecraft or aircraft.

The figure below presents front, plan, and cross-sectional views of the two nozzles simulated in Fluent.

To enrich this description, it is essential to highlight that these views allow for a detailed analysis of the geometry and configuration of the studied nozzles. The front view provides a direct perspective on the shape and dimensions of the nozzle, while the plan view gives an insight into the spatial distribution of the cross-sectional areas. Finally, the cross-sectional view reveals the internal details of each nozzle, including flow profiles and geometric features crucial for the analysis of aerodynamic and thermodynamic performance.

This multidimensional approach enables a thorough comparison of the two nozzle configurations, providing valuable visual data to evaluate their effectiveness and behavior under different simulated operating condition

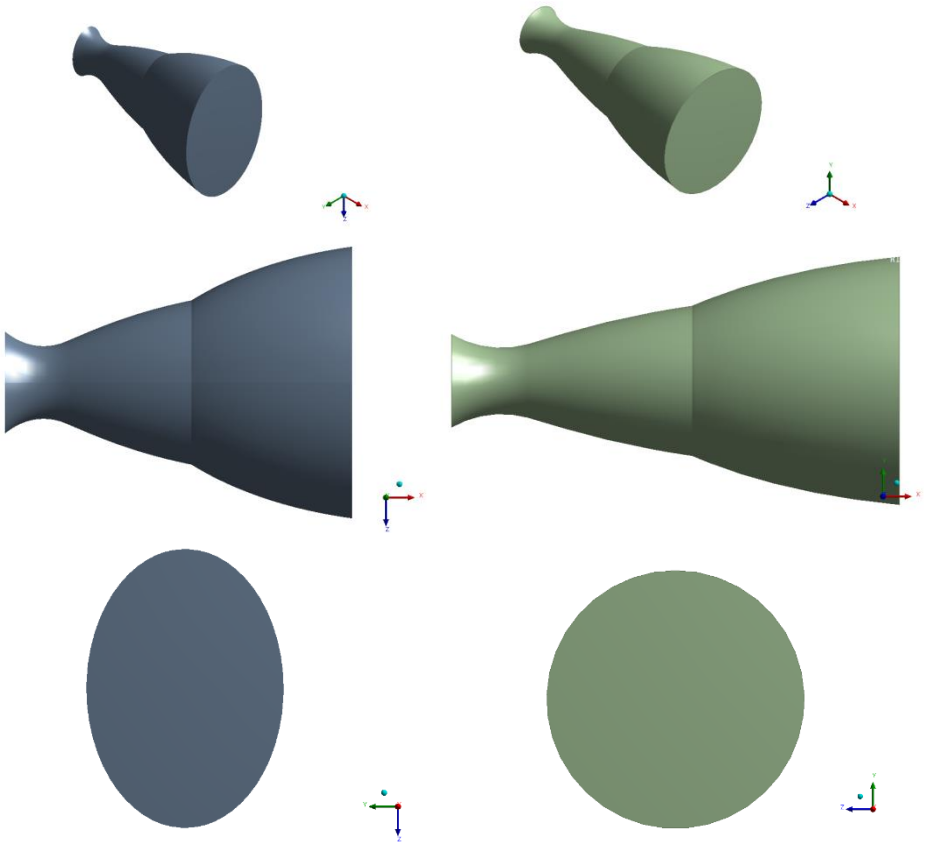

A : elliptical section B : circular section

Figure II- 29: Various views of two nozzle

II.3.4.2 Evolution of the mach number

The Mach number is a measure of an object's speed relative to the speed of sound in the surrounding medium. It is named after the Austrian physicist Ernst Mach. The Mach number is crucial in aerodynamics and aerospace engineering to determine the effects of gas compression, shock waves, and other phenomena associated with high speeds.

Figure II.30 depict a comparison of the Mach number evolution along the wall and axis for two types of nozzles: one with an elliptical section and the other with a circular section.

Regarding the Mach number evolution along the wall, observations indicate a similar trend for both nozzles, without significant variation. Notably, the Mach number increases rapidly at the throat and in the initial expansion zone. However, in the divergent part of the first bell, this increase slows down to reach a maximum value of 3.0338. At junction point J, the Mach number shows two distinct values (3.0338 and 3.73), with this difference attributed to the presence of a expansion wave centered at this point. Throughout the second bell, the Mach number remains constant.

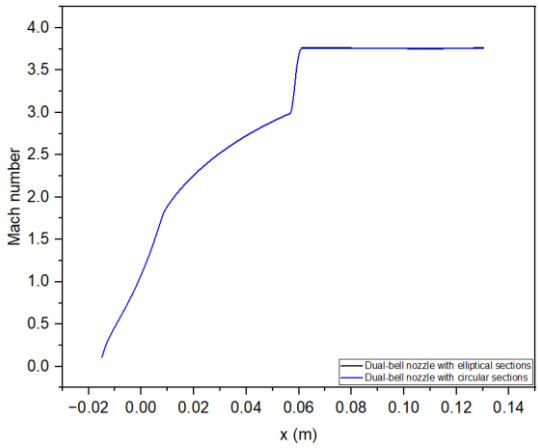

Figure II- 30: Mach evolution along the wall

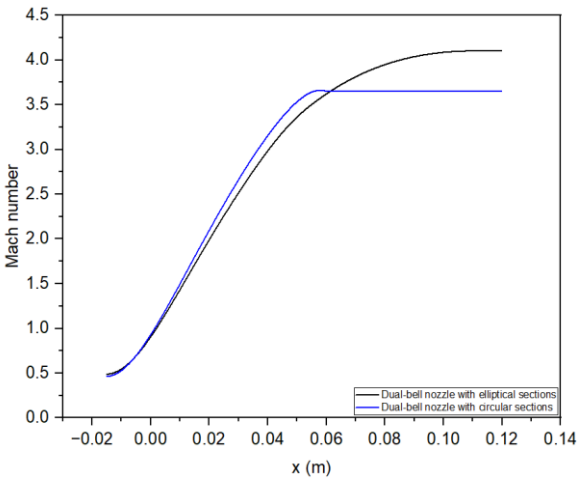

Figure II- 31: Mach number evolution along the axis.

To enhance this description, it is essential to specify that these figures allow for analysis of how the Mach number varies not only across the cross-sections of the nozzles but also along their axes. This analysis is crucial for evaluating velocity profiles and gas compression phenomena at different sections and positions along the studied nozzles. It provides a detailed view of velocity variations and flow characteristics at critical positions, thus offering valuable insights for optimizing and designing efficient nozzles in aerodynamic and aerospace applications.

Along the axis of both nozzles, significant variation in Mach number evolution was observed. Specifically, at the axial exit, the Mach number values are 5.123 and 5.28 respectively for the circular and elliptical section nozzles, marking an increase of 3%. This difference is consistent given the distinct geometries of the two sections.

This finding suggests an advantage for the elliptical section nozzle in this specific context. Indeed, the elliptical section appears to favor flow conditions that result in slightly higher Mach numbers at the axial exit compared to the circular section nozzle. This phenomenon can be further explored to assess its impact on aerodynamic performance and flow management in practical applications.

Since both nozzles were initially longer, they were truncated at the same point to reduce their weight, as shown in Figure II.31. In this case, the Mach numbers for the elliptical section nozzle and the circular section nozzle reached 4.103 and 3.66 respectively after truncation, representing an increase of 10.8%. This modification resulted in a notable difference in the performance of the two nozzle configurations. The elliptical section nozzle exhibits a higher Mach number after truncation, potentially indicating better efficiency in terms of flow dynamics and gas dynamics compared to the circular section nozzle. This observation underscores the importance of nozzle geometry in managing flow velocities and aerodynamic characteristics across diverse applications.

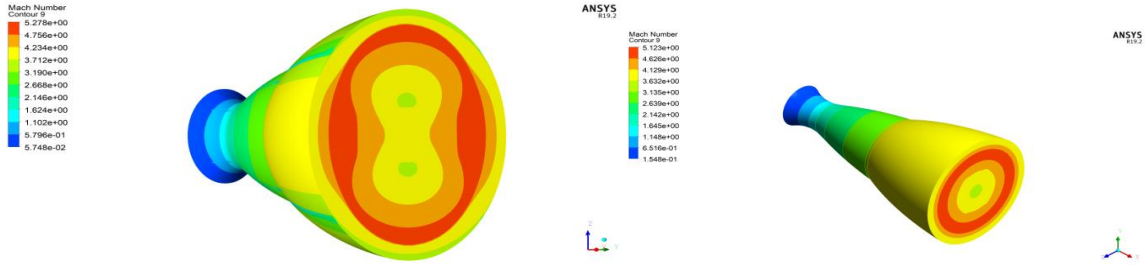

A : section elliptique B : section circulaire

Figure II- 32: Mach number contours (3D).

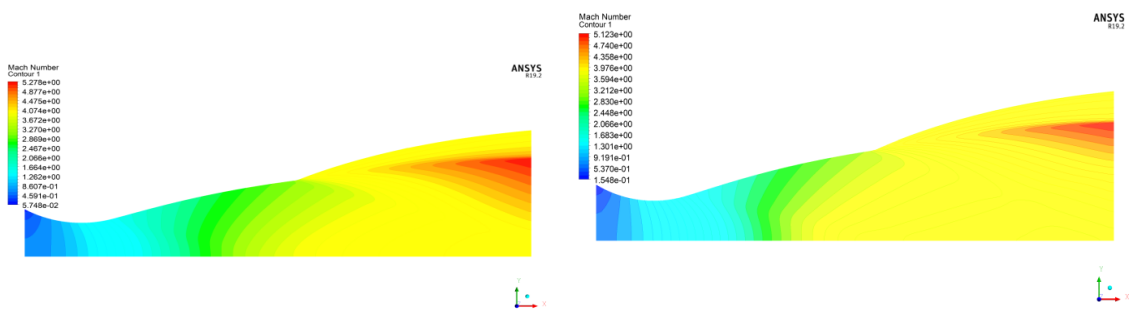

A : section elliptique B : section circulaire

Figure II- 33: Mach number contours (symmetry plane).

The results of the Mach field simulations are depicted using the fluent visualization software, renowned for its capability to display flow variables as contours. This software also facilitates the extraction of variables such as wall pressure, as well as visualization of velocity vectors and streamline patterns.

Figures II.32 and II.33 respectively show the Mach field for an elliptical section nozzle and a circular section nozzle, in both planar and 3D views, reproduced for the same nozzle pressure ratio (NPR).

In both simulations, the flow adheres closely to the nozzle walls, indicating absence of separation. This observation is crucial as it confirms favorable flow conditions and well-defined Mach profiles along the internal surfaces of the studied nozzles. This detailed visualization enables an in-depth analysis of flow characteristics and aerodynamic performance of the nozzles, thereby providing valuable insights for optimization and design in aerospace and propulsion applications.

II.3.4.3 Evolution of static pressure

In the domain of pressure, a notable observation is the rapid decrease at the throat and initial expansion zone, followed by a slower decrease along the divergent part formed by the first bell (see Figure II.34). At junction point J, the expansion wave is particularly pronounced, while along the second bell, the pressure remains constant at a value of 22,504.85 Pascals, a value imposed for both elliptical and circular nozzles of equal length. This suggests that the pressure evolution along the wall is not influenced by the section change at the exit.

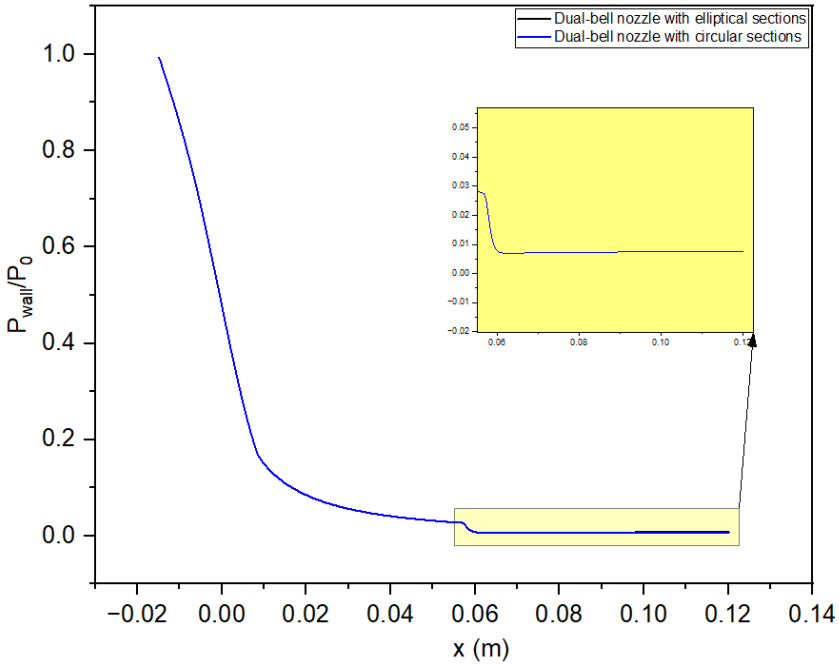

Figure II- 34: Static pressure evolution along the wall.

However, in figure II.35, along the axis, a significant evolution of pressure was observed, decreasing from the throat to the exit. However, the values reached are markedly different: 17203.1 Pascals for the elliptical section nozzle and 31229.7 Pascals for the circular section nozzle, representing a difference of 45% between the two.

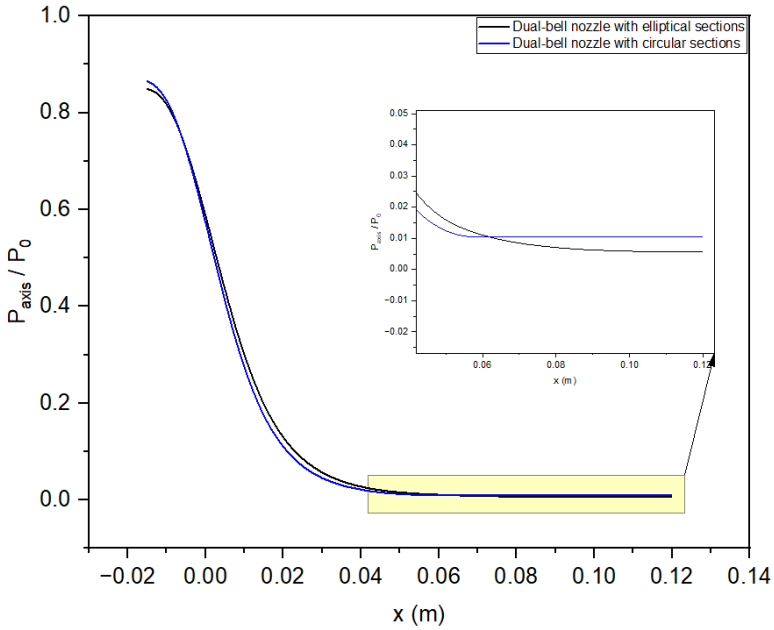

Figure II- 35: Pressure static evolution along the axis.

Figure II.36 and II.37 illustrate the static pressure contours for two types of 3D dual-bell nozzles: (A) with elliptical cross-sections and (B) with circular cross-sections, in three dimensions and in the symmetry plane of the nozzles, respectively. The static pressure at the exit of the dual-bell nozzle with an elliptical cross-section is lower than that at the exit of the dual-bell nozzle with a circular cross-section. This implies a higher operational (mode/altitude) efficiency for the dual-bell nozzle with an elliptical cross-section.

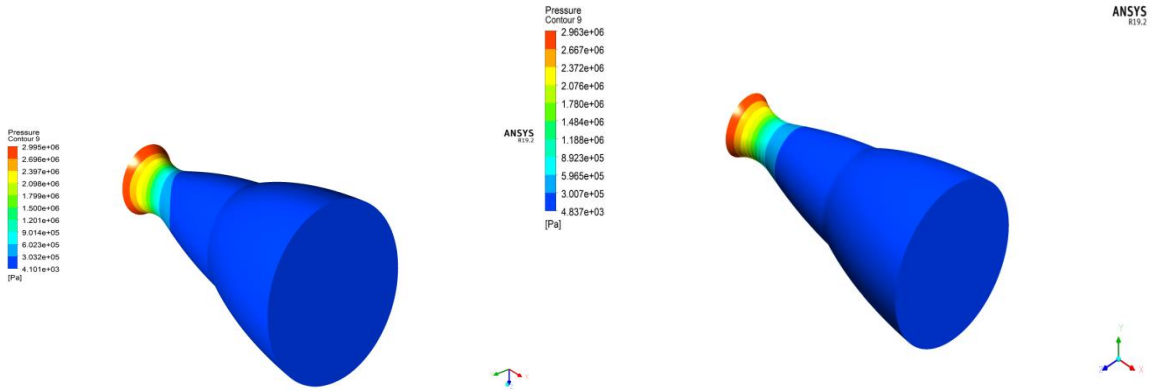

A : section elliptique **B : section circulaire**

Figure II- 36: Static pressure contours (3D).

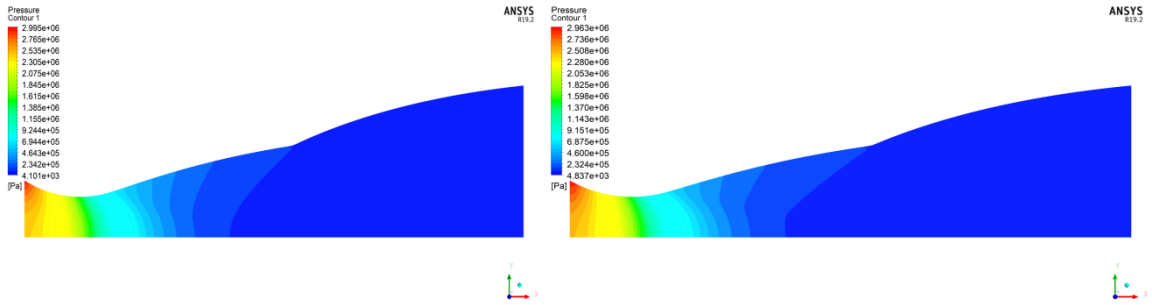

A : section elliptique **B : section circulaire**

Figure II- 37: Pressure static contours (symmetry plane).

II.3.4.4 Meshing a nozzle with an external domain

Meshing a nozzle including an external domain provides significant advantages for numerical simulations in fluid mechanics. This external domain allows for precise modeling of interactions between the internal flow of the nozzle and the surrounding flow, capturing confinement effects and variations in pressure and velocity at the interface. By reducing artificial boundary conditions, meshing with an external domain ensures more realistic and accurate results. It also enables faithful modeling of complex physical phenomena associated with viscous flow, leading to more consistent distributions of pressure, velocity, and temperature. Furthermore, studying edge effects becomes more thorough, facilitating understanding of the impact of external conditions on overall nozzle performance. In summary, incorporating an external domain in nozzle meshing enhances the reliability and accuracy of fluid mechanics simulations, while enabling a comprehensive analysis of fluid-environment interactions.

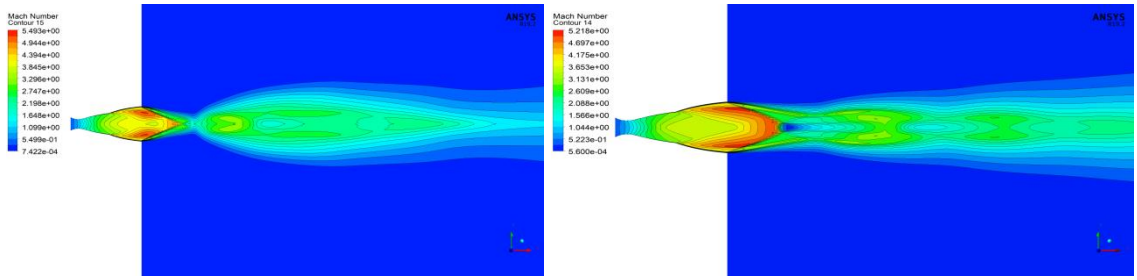

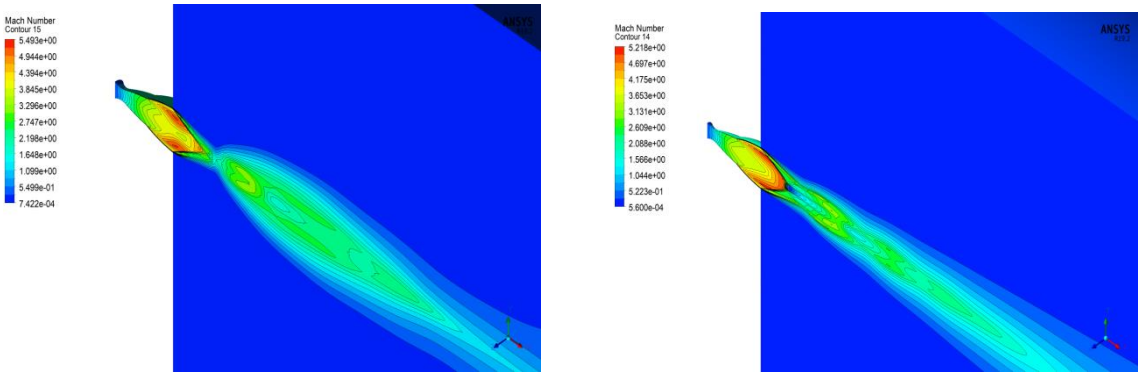

A : elliptical section ***B : circular section***

Figure II- 38: Simulation with external domaine.

Analysis of the Mach number contours reveals that the cross-sectional shape of the dual-bell nozzle (whether circular or elliptical) exerts a notable influence on the structure of the nozzle jet. This influence is primarily attributed to viscous effects and the substantial velocity gradient present at the nozzle wall.

For the same total nozzle length and under identical operating conditions (nozzle pressure ratio, NPR = 43), there is a significant increase in Mach number at the exit of the dual-bell nozzle with elliptical cross-sections. This increase primarily arises from the geometric shape of the nozzle, which enables an expansion of the exit area and consequently enhances the nozzle's performance.

II.3.4.5 Performances

The table below summarizes the performance of two nozzles of equal length but with varying exit sections: the first has a circular section, while the second is elliptical with a larger section by 29.3%.

Table II- 14: Performances comparison.

	Dual-bell nozzle with elliptical cross sections	**Dual-bell nozzle with circular cross sections**
Mass flow rate (kg/s)	3.408734	2.418662
Thrust Force (N)	2093.188334	1487.565895
Thrust Coefficient C_f	2.220941801	1.578356436
Specific Impulse I_{sp} (s)	614.0661999	615.0367

It has been observed that simultaneously with the increase in section, the performance of elliptical section nozzles has significantly improved. The mass flow rate obtained for the elliptical nozzle rose to 3.408734 kg/s, which represents a 29% increase compared to its circular section counterpart. Similarly, an increase of 28.93% was observed for the generated thrust as well as for the thrust coefficient.

This finding highlights the significant advantages offered by the elliptical geometry in terms of propulsion performance. The increases observed in mass flow rate, thrust, and thrust coefficient underscore the enhanced efficiency of the elliptical nozzle compared to the circular section one. These results are crucial for optimizing propulsion systems in various aerodynamic and aerospace contexts.

CONCLUSION

Nozzles play a crucial role in aerospace propulsion by converting the thermal energy of exhaust gases into propulsive thrust. Their design and optimization continue to be the focus of extensive research aimed at enhancing propulsion system performance. Recent efforts have concentrated on key aspects such as nozzle geometry to maximize gas expansion efficiency, minimizing pressure losses, and optimizing flow distribution at various altitudes and flight speeds. These endeavors aim not only to increase specific thrust and energy efficiency but also to reduce emissions and enhance operational reliability of propulsion systems. Advances in numerical modeling, advanced simulations, and cutting-edge manufacturing techniques further push the boundaries in this critical field of aerospace engineering.

Our contribution includes proposing the design of a double-bend nozzle with an elliptical exit section, a concept that has not been studied until now. We started from a conventional double-bend nozzle with a circular section and compared the results obtained for each configuration.

The study was structured into two distinct parts. The first part focused on a comprehensive literature review, analyzing nearly a hundred articles on nozzles from the perspectives of operation, manufacturing, technology, and development. This phase resulted in creating an essential reference document intended to serve as a foundation for students and anyone interested in the field of propulsion nozzles. This part of the study immersed us in a complex domain, teaching us methods to initiate research in a new field and how to effectively conduct a literature review.

The second part of our study represents our team's contribution under the guidance of our thesis advisor, aiming to design a double-bend nozzle with an elliptical exit section, a novel and promising concept. After developing this design using our methodology, we conducted a detailed study of flow through this nozzle, analyzing the evolution of flow parameters such as Mach number and static pressure. The results obtained were then compared with those obtained for a conventional double-bend nozzle with a circular section.

In conclusion of this comparative study between two types of double-bend nozzles, one elliptical and the other circular, several significant observations have been highlighted. The simulations and calculations revealed that the elliptical section nozzle exhibits superior performance in specific characteristics such as Mach number and static pressure.

It has been observed that along with an increase in nozzle section, the performance of elliptical section nozzles has significantly improved. Here are the detailed observations:

1. The Mach number for elliptical and circular nozzles is 5.123 and 5.28 respectively, showing an increase of 3%.
2. The mass flow rate for the elliptical nozzle has increased to 3.41 kg/s from 2.42 kg/s, representing a 29% increase.
3. Similarly, there has been an increase of 28.93% observed in generated thrust as well as thrust coefficient.

However, this design encountered a major drawback: it has a higher weight by 13.56% compared to the circular section nozzle. Weight is a critical decisive factor in aerospace. Nevertheless, solutions can be considered to address this issue:

1. For material selection, one potential solution could be the use of ceramic matrix composites (CMCs), which offer both lightweight and high thermal resistance.
2. Another critical aspect is nozzle thickness, which directly affects structural strength and weight.
3. Additionally, truncating the nozzle was a method explored in our study. Recognizing that an ideal nozzle would be very long and thus heavy, we opted to truncate the nozzle at coordinates (1.2, 3.74), significantly reducing its weight.

These technical adaptations and choices are crucial for optimizing nozzle performance while meeting specific aerospace constraints.

In conclusion, we hope this work will serve as a fundamental reference for students and researchers interested in the aerospace field, providing a solid foundation for those embarking on research in this exciting and evolving domain.

PERSPECTIVES

Overall, the study is comprehensive, but it could be enhanced by offering perspectives and directions for future research in this field. Here are some suggestions to further explore:

1. The first step will be manufacturing the innovative dual-bell nozzle with an elliptical cross-section and conducting an experimental campaign.
2. Conducting studies on the influence of geometrical parameters such as the base nozzle type(TOC, TOP),
3. The influence of the extension nozzle type (PP, NP),
4. The influence of the cross-sectional radius, etc., can further improve the performance of the nozzle.

BIBLIOGRAPHY

[1] Migdal D and Landis F 1962 Characteristics of conical supersonic nozzles; ARS J. 32 1898–1901

[2] Darwell H M and Badham H 1963 Shock formation in conical nozzles; AIAA J. 1 1932–1934

[3] Sunley H L G and Ferriman V N 1964 Jet separation inconical nozzles; Aeron. J. 68 808–817

[4] Migdal D and Kosson R 1965 Shock predictions in conical nozzles; AIAA J. 3 1554–1556

[5] Hoffman J D and Lorenc S A 1965 A parametric study ofgas-particle flows in conical nozzles; AIAA J. 3 103–106

[6] Wehofer S and Moger W C 1970 Transonic flow in conical convergent and convergent-divergent nozzles with non-uniform inlet conditions. In: 6th Propulsion Joint Specialist Conference, San Diego, California. 635

[7] Khan A A and Shembharkar T R 2008 Viscous flow analysis in a convergent–divergent nozzle. In: Proceedings of the International Conference on Aerospace Science and Technology, Bangalore, India

[8] Balabel A, Hegab A M, Nasr M and El-Behery S M 2011 Assessment of turbulence modeling for gas flow in twodimensional convergent-divergent rocket nozzle; Appl.Math. Modell. 35 3408–3422

[9] Zmijanovic V, Lago V, Sellam M and Chpoun A 2014 Thrust shock vector control of an axisymmetric conical supersonic nozzle via secondary transverse gas injection; Shock Waves 24 97–111

[10] Zhang Y, Chen H, Zhang M, Zhang M, Li Z and Fu S 2014 Performance prediction of conical nozzle using Navier- Stokes computation; J. Propuls. Power 31 192–203

[11] Jia R, Jiang Z and Zhang W 2015 Numerical analysis of flow separation and side loads of a conical nozzle during staging. In: Proceedings of the Institution of Mechanical Engineers, Part G: Journal of Aerospace Engineering. 845–855

[12] Jia R, Jiang Z, Xiang M and Zhang W 2016 Threedimensional numerical study of the conical nozzle side loads during staging; J. Aerosp. Eng. 29 04016038

[13] Dillaway R B 1957 A philosophy for improved rocket nozzle design; J. Jet Propuls. 27 1088–1093

[14] Rao G V R 1958 Exhaust nozzle contour for optimum thrust; J. Jet Propuls. 28 377–382

[15] Landsbaum E M 1960 Contour nozzles; ARS J. 30 244–250

[16] Farley J M and Campbell C E 1960 Performance of several method-of-characteristics exhaust nozzles. NASA TN D-293

[17] Ahlberg J H, Hamilton S, Migdal D and Nilson E N 1961 Trucated perfect nozzles in optimum nozzle design; Am. Rocket Soc. J. 31 614–620

[18] Lawrence R A and Weynand E E 1968 Factors affecting flow separation in contoured supersonic nozzles; AIAA J. 6 1159–1160

[19] Terhardt M, Hagemann G and Frey M 2001 Flow separation and side-load behavior of truncated ideal rocket nozzles. In: 37th Joint Propulsion Conference and Exhibit.3686

[20] Verma S B 2002 Study of flow separation in truncated ideal contour nozzle; J. Propuls. Power 18 1112–1121

[21] Hagemann G, Frey M and Koschel W 2002 Appearance of restricted shock separation in rocket nozzles; J. Propuls. Power 18 577–584

[22] Verma S B, Stark R and Haidn O 2006 Relation between shock unsteadiness and the origin of side-loads inside a thrust optimized parabolic rocket nozzle; Aerosp. Sci. Technol. 10 474–483

[23] Verma S B, Hadjadj A and Haidn O 2017 Origin of sideloads in a subscale truncated ideal contour nozzle; Aerosp.Sci. Technol. 71 725–732

[24] Stark R H and Wagner B H 2006 Experimental Flow investigation of a truncated ideal contour nozzle. In: 42nd AIAA/ASME/SAE/ASEE Joint Propulsion Conference & Exhibit. 5208

[25] Stark R and Wagner B 2009 Experimental study of boundary layer separation in truncated ideal contour nozzles; Shock Waves 19(3) 185–191

[26] Frey M, Makowka K and Aichner T 2017 The TICTOP nozzle: a new nozzle contouring concept; CEAS Space J. 9 175–181

[27] Baloni B D, Kumar S P and Channiwala S A 2017 Computational analysis of bell nozzles. In: 4th International Conference of Fluid Flow, Heat and Mass Transfer, Toronto, Canada , August 21 – 23, 2017. 110

[28] Zhang J A, Shotorban B and Zhang S 2017 Numerical experiment of aeroelastic stability for a rocket nozzle; J. Aerosp. Eng. 30 04017041

[29] Krase W H 1959 Performance analysis of plug nozzles for turbojet and rocket exhausts. In: ASME 1959 Gas Turbine Power Conference and Exhibit, American Society of Mechanical Engineers, Ohio, USA. V001T01A009

[30] Berman K and Crimp F W 1961 Performance of plug-type rocket exhaust nozzles; ARS J. 31 18–23

[31] Rao G V R 1961 Spike nozzle contour for optimum thrust. Planetary and Space Science 4, Jan.:92-101

[32] Johnson G R, Thompson H D and Hoffman J D 1974 Design of maximum thrust plug nozzles with variable inlet geometry; Comput. Fluids 2 173–19

[33] Rommel T, Hagemann G, Schley C A, Krulle G and Manski D 1997 Plug nozzle flowfield analysis; J. Propuls. Power 13 629–634

[34] Ruf J H and McConnaughey P K 1997 A numerical analysis of a three dimensional aerospike. In: 33rd Joint Propulsion Conference and Exhibit. 3217

[35] Ito T, Fujii K and Hayashi A K 2002 Computations of axisymmetric plug-nozzle flowfields: flow structures and thrust performance; J. Propuls. Power 18 254–260

[36] Besnard E, Chen H H, Mueller T and Garvey J 2002 Design, manufacturing and test of a plug nozzle rocket engine. In: 38th AIAA/ASME/SAE/ASEE Joint Propulsion Conference Exhibit. 4038

[37] Naghib-lahouti A and Tolouei E 2006 Investigation of the effect of base bleed on thrust performance of a truncated aerospike nozzle in off-design conditions. In: European Conference on Computational Fluid Dynamics

[38] Shahrokhi A and Noori S 2010 Survey of the central plug shape of the aerospike nozzle.

In: 17th Australasian Fluid Mechanics Conference, Auckland, New Zealand 5-9 December, 2010

[39] Chutkey K, Vasudevan B and Balakrishnan N 2014 Analysis of annular plug nozzle flowfield; J. Spacecr. Rockets 51 478–490

[40] Shanmuganathan V K, Gayathri N, Kabilan S and Umanath K 2015 Comparative study on performance of linear and annular aero-spike nozzles; Aust. J. Basic Appl. Sci. 9883–892

[41] Naveen Kumar K, Gopalsamy M, Antony D, Krishnaraj R and Viswanadh C B 2017 Design and optimization of aerospike nozzle using CFD. In: IOP Conference Series: Materials Science and Engineering. 012008

[42] Ge Wang; Bocheng Zhou; Ben Guan and Haiwei Yang (Numerical investigation on expansion–deflection nozzle flow during an ascending–descending trajectory).

[43] Chasman D, Birch M, Haight S and Graffam R 2005 A multi-disciplinary optimization method for multi nozzle grid (MNG) design - Final Report. In: 43rd AIAA Aerospace Sciences Meeting and Exhibit. 706

[44] Chasman D, Haight S and Facciano A 2005 Excessive nozzle erosion in a multi nozzle grid (MNG) test. In: 41st AIAA/ASME/SAE/ASEE Joint Propulsion Conference & Exhibit. 4495

[45] Chasman D, Haight S and Loehr R 2012 Viscous losses of MNG in hybrid motor tests. In: 48th AIAA/ASME/SAE/ASEE Joint Propulsion Conference & Exhibit. 4266

[46] Östlund, J., and Muhammad-Klingmann, B., "Supersonic flow separation with application to rocket engine nozzles," Transactions of the ASME, AMR, Vol. 58, pp. 143-177, 2005.

[47] Sauer, R. General characteristics of the flow through nozzles at near critical speeds. Natioanl advisory committee for aeronautics technical memorandum 1174.1947

[48] Hall,I.M. Transonic flow in two-dimensional and axially-symetrics nozzles. Quarterly Journal of Mecanics and applied mathematics 15: 487-508.1962

[49] Kliegel,J.R and Levine,J.N. transonic flow in small throat radius of curvature nozzles. American Institute of Aeronautics and Astronautics journal7:1373-1378.1969.

[50] Cline, M.C., "VNAP2: A computer program for computation of two-dimensional, time-dependent, compressible, turbulent flow," Kept. LA-8872, Los Alamos National Laboratory, Los Alamos, NM, Aug. 1981.

[51] Zucrow, M. J. and Hoffman, J. D., "Gas Dynamics," Vol. 1, John Wiley and Sons, New York, 1977.

[52] Zucrow, M.J. and Hoffman, J.D., "Gas Dynamics," Vol. 2, John Wiley and Sons, New York, 1977.

[53] Malina, F. J., "Characteristics of the rocket motor based on the theory of perfect gases", J. Frankling Inst., Vol. 230, pp. 433-454, 1940.

[54] Beneche, T. and Quick, W.W., "History of German guided missile development," AGARDograph 20, Verlag E. Appelhos & Co, Brunswick, Germany, 1957.

[55] Shapiro, A.H., "The dynamics and thermodynamics of compressible fluid flow," Volume I, The Ronald Press Co., New York, 1953.

[56] Anderson, J.D., "Modern compressible flow with historical perspective," McGraw-Hill Book Co.-Singapore, Jr-2nd ed, 1990.

[57] Östlund, J., "Flow processes in rocket engine nozzles with focus on flow separation and side-loads," Licentiate thesis TRITA-MEK-2002, RIT, Stockholm, Sweden.

[58] Ahlberg, J.H. et al., "Truncated perfect nozzles in optimum nozzle design," ARS Journal, Vol. 31, No. 5, pp. 614-620, 1961.

[59] Frey, H.M., and Nickerson, G.R., "TDK –Two Dimensional Kinetic reference program," SEA Inc. NAS8-36863, 1989.

[60] Guderley, K.G. et al., "Continuous and discontinuous solutions for optimum thrust nozzles of given length," Journal of Optimization Theory and Applications, Vol. 12, No. 6, pp. 588-628, 1973.

[61] Rao, G.V.R., "Exhaust nozzle contour for optimum thrust," Jet Propulsion, Vol. 28, No. 6, pp. 377-382, 1958.

[62] Shmyglevsky, Yu D., "Supersonic profiles with minimum drag," In Russian, Prikladnaya Matematika i Mekhanika, Vol. 22, No. 2, pp. 269-273, 1958.

[63] Shmyglevsky, Yu D., "Variational problems for supersonic bodies of revolution and nozzles," Prikladnaya Matematika i Mekhanika, Vol. 26, No. 1, pp. 110-125, 1962.

[64] Borisov, V.M. et Shmyglevsky Yu D. "The formulation of variational problems of gas dynamics," Prikladnaya Matematika i Mekhanika, Vol. 27, No. 1, pp. 183-184, 1963.

[65] Shmyglevsky, Yu D., "Some variational problems of gas dynamics," Fluid Dynamics Transactions, pp. 635-647, 1965.

[66] Shmyglevsky, Yu D., "Variational problems of gas dynamics," U.S.S.R. Compt. Maths. Math. Phys. Vol. 20, No. 5, pp. 113-127, 1980.

[67] Rao, G.V.R., "Recent developments in rocket nozzle configurations," ARS Journal, Vol. 31, No. 11, pp. 1488-1494, 1961.

[68] Rao, G.V.R., ''Approximation of optimum thrust nozzle contour,'' ARS Journal, Vol. 30, No. 6, pp. 561, 1960.

[69] Wade, M., Encyclopedia Astronautica, 25687 pages-9423 images, http://www.astronautix.com/, 2011.

[70] Gogish, L.V., "A study of short supersonic nozzles," Mekhanika Zhidkosti i Gaza, Vol. 1, No. 2, pp. 175-180, 1966.

[71] Hoffman, J.D., "Design of compressed truncated perfect nozzles," J. of Propulsion and Power, Vol.3, No. 2, pp. 150-156, 1987.

[72] H.W lipmann and A roshko (elements of gasdynamics).

[73] Jan Östlund May 2002 (flow processes in rocket engine nozzles with focus on flow separation and side-loads),

[74] Thèse de Anne-Sophie Mouronval, mars 2004 (études numerique des phénomenes aeroelastiques en aerodynamique supersonique. Application aux tuyere supersonique).

[75] Alexandre georges-picot, decembre 2014 (Développement de modèles physiques et numériques pour la simulation aux grandes échelles des écoulements dans les tuyères supersoniques).

[76] Ralf Stark (Flow Separation in Rocket Nozzles – An Overview).

[77] Joseph H. Ruf, David M. McDaniels Andrew M. Brown, (Nozzle Side Load Testing and Analysis at Marshall Space Flight Center).

[78] S. L. Tolentino, J. Mírez, and O. González, avril 2022 (Numerical analysis of the flow field in a planar nozzle for different divergent angles).

[78] Gerald Hagemann, Hans Immich, Thong Van Nguyen and Gennady E. Dumnov (Advanced Rocket Nozzles).

[79] Stark, R., "Flow Separation in Rocket Nozzles, a Simple Criteria," 41st AIAA/ASME/SAE/SEE Joint Propulsion Conference & Exhibit, Tucson, AZ, AIAA paper 2005-3940, 2005.

[80] Boman, A., "Apparatus for controlling the flow separation line of rocket nozzles," U.S. Patent No. 6.574.952 B2, 2003.

[81] Sato, M., et al., "Experimental study on transitional phenomena of extendible nozzle," 43rd AIAA/ASME/SAE/ASEE Joint Propulsion Conference and Exhibit, Cincinnati, OH, AIAA paper 2007-5471, 2007.

[82] Kusaka, K, et al., "Experimental study on extendible and dual-bell nozzles under high altitude conditions," 36th Joint Propulsion Conference and Exhibit, AIAA Paper 2000-3303, 2000.

[83] Schmucker, R., "Flow processes in over-expanded chemical rocket nozzles. Part 1: Flow separation," NASA TM-77396, 1984.

[84] Chiou, J., and Hung, R., "A study of forced flow separation in rocket nozzles," Final Report, Alabama University, Huntsville, 1974.

[85] Sutton, G.P., "Stepped Nozzle," U.S. Patent No. 5,779,151, 1998.

[86] Brown, J.L., et al., "Altitude compensating ablative stiffening band for rocket motor nozzles," U.S. Patent No. 08,034,452, 1993.

[87] Goncharov, N., et al., "Reusable launch vehicle propulsion based on the RD-0120 engine," 31st Joint Propulsion Conference and Exhibit, AIAA 1995-3003, 1995.

[88] Sutton, G.P. and Biblarz, O., "Rocket propulsion elements," 7th ed. John Wiley & Sons, 2001.

[89] Clayton. R. and Back, L., "Thrust improvement with ablative insert nozzle extensions," Journal of Propulsion and Power, Vol. 2, No. 1, pp. 91-93, 1986.

[90] Parsley, R.C. and Van Stelle, K.J., "Altitude compensating nozzle evaluation," 28th Joint Propulsion Conference and Exhibit, AIAA 92-3456, 1992.

[91] Semenov, V.V., et al., "Liquid propulsion with altitude compensation concept trade study," 57th International Astronautical Congress of the International Astronautical Federation, Valencia, Spain, IAC paper 06-C4.1.09, 2006.

[92] Musial, N.T. and Ward, J.J, "Overexpanded performance of conical nozzles with area ratios of 6 and 9 with and without supersonic external flow," NASA TM X-83, 1959.

[93] Bonniot, C.E., "Rocket engine expansion nozzle with complementary annular nozzle," U.S. Patent No. 05,067,316, 1991.

[94] Boccaletto, L. and Dussauge J.P., "High-performance rocket nozzle concept," J. of Propulsion and Power, Vol. 26, No. 5, 2010.

[95] Häggander, J. and Pekkari, L., "Rocket engine nozzle," U.S. Patent No. 06,308,514, 2001.

[96] Östlund, J. and BIgert, M., "A subscale investigation on side loads in sea level rocket nozzle," 35th AIAA/ASME/SAE/ASEE Joint Propulsion Conference and Exhibit, Fort

Lauderdale, Florida, AIAA 99-2759, 1999.

[97] Ewen, R.L. and O'Brian, C.J., ''Dual-Throat thruster test results,'' 22nd AIAA/ASME/SAE/ASEE Joint Propulsion Conference, Huntsville, Alabama, AIAA 86-1518, 1986.

[98] Beichel, R., "Dual expander rocket engine," U.S. Patent No. 04,220,001, 1980.

[99] Nguyen, T. V. et al., ''Aerodynamic performance analysis of dual-fuel/dual-expander nozzles,'' 24th AIAA/ASME/SAE/ASEE Joint Propulsion Conference, Boston, Massachusetts, AIAA 88-2818, 1988.

[100] Hagemann, G., et al., "Advanced rocket nozzles," J. of Propulsion and Power, Vol. 14, No. 5, pp. 620-634, 1998.

[101] Hagemann, G. et al., ''Dual-Expander engine flowfield simulations,'' 31st AIAA/ASME/SAE/ASEE Joint Propulsion Conference and Exhibit, San Diego, CA, AIAA 95-3135, 1995.

[102] Singer, V., "Method of making rocket motor extendible nozzle exit cone," U.S. Patent No. 04,707,899, 1987.

[103] Smith-Kent, R. and al., ''Analytical contouring of pintle nozzle exit cone using computational fluid dynamics,'' 31st AIAA/ASME/SAE/ASEE Joint Propulsion Conference and Exhibit, San Diego, CA, AIAA 95-2877, 1995.

[104] Singer, V., "Method of making rocket motor extendible nozzle exit cone," U.S. Patent No. 04,707,899, 1987.

[105] Smith-Kent, R. and al., ''Analytical contouring of pintle nozzle exit cone using computational fluid dynamics,'' 31st AIAA/ASME/SAE/ASEE Joint Propulsion Conference and Exhibit, San Diego, CA, AIAA 95-2877, 1995.

[106] Wasko, R. A., ''Performance of annular plug and expansion-deflection nozzles including external flow effects at transonic mach numbers,'' NASA TN D-4462, 1968.

[107] Dunn, S.S. and Coats, D.E., "Optimum nozzles contours for aerospike nozzles using the TDK 99TM computer code," 36th JANNAF Combustion Subcommittee, Cocoa Beach, FL, 1999.

[108] Calabro, M., et al., "ELV: pressure fed LOX/LH2 upper stage," Acta Astronautica, Vol. 64, No. 11-12, pp. 1015-1020, 2009.

[109] Le Bozec, A., et al., "Afterbody testing and comparison to CFD simulations," AIAA 8th International Space Planes and Hypersonic Systems and Technologies Conference. Norfolk, VA. 1998.

[110] Wisse, M.E.N., and Van Oudheusden, B., "Analytical optimisation of an inviscid flow linear plug nozzle boattail," 40th AIAA/SAE/ASME/ASEE Joint Propulsion Conference and Exhibit, Fort Lauderdale, FL. AIAA 2004-4017, 2004.

[111] Onofri, M., "Plug nozzles: summary of flow features and engine performance," OTAN Report RTO-TR-AVT-007-V1, 2002.

[112] Horn, M. and Fisher S., "Altitude compensating nozzles," Rocket dyne Division. NASA-CR-194719, 1994.

[113] Génin, C., et al., "Experimental and numerical study of dual-bell nozzle flow," Progress in Flight Physics Vol. 5, pp. 363-376, 2013.

[114] Martelli, E., et al., "Numerical parametric analysis of dual-bell nozzle flows," AIAA

Journal, Vol. 45, No. 3, pp. 640-650, 2007.

[115] Alziary de Roquefort, T., et al., "Charges latérales dans les tuyères axisymétriques," ATAC Technical Report.
[116] Foster, C. and Cowles, F., "Experimental study of gas-flow separation in over-expanded exhaust nozzles for rocket motors," Progress Report No. 4-103. JPL, 1949.
[117] Hagemann, G., et al., "Advanced rocket nozzles," J. of Propulsion and Power, Vol. 14, No. 5, pp. 620-634, 1998.
[118] Frey, M. and Hagemann, G. "Critical assessment of dual-bell nozzles," J. of Propulsion and Power, Vol. 15, No. 1, pp. 137-143, 1999.
[119] Immich, H. and Caporicci, M., "FESTIP technology developments in liquid rocket propulsion for reusable launch vehicles," 32nd AIAA Joint propulsion conference, Lake Buena Vista, Florida, AIAA-96-3113, 1996.
[120] Immich, H., Caporicci, M., "Status of the FESTIP rocket propulsion technology program," 33rd AIAA Joint propulsion conference, Seattle, WA, AIAA-97-3311, 1997.
[121] Miyazawa, M., et al., "Flight performance of dual-bell nozzles," 40th Aerospace science meeting, Reno, NV, AIAA-2002-0686, 2002.
[122] Hagemann, G., et al., "Experimental and analytical design verification of the dual-bell concept," J. of Propulsion and Power, Vol. 18, No. 1, pp. 116-122, 2002.
[123] Génin, C. and Stark, R., "Flow Transition in dual-bell nozzles," Shock Waves, Vol. 19, pp. 265-270, Springer-Verlag, 2009.
[124] Proshchanka, D., et al., "Control of operation mode transition in dual-bell nozzle," 46th AIAA/ASME/SAE/ASEE Joint propulsion conference, Nashville, TN, AIAA 2010-6815, 2010.
[125] Génin, C. and Stark, R., "Experimental study on flow transition in dual-bell nozzles," J. of Propulsion and Power, Vol. 26, No. 3, pp. 497-502, 2010.

[126] Stark, R. and Génin, C., "Side loads in dual-bell nozzles, Part I Phenomenology," 2010,
[127] Verma, S. B., et al., "Cold gas dual-bell tests in high-altitude simulation chamber," Shock Waves, Vol. 21, pp. 131-140, Springer-Verlag, 2011.
[128] Verma, S. B., et al., "Cold-gas experiments to study the flow separation characteristics of a dual-bell nozzle during its transition modes," Shock Waves, Vol. 20, pp. 191-203, Springer-Verlag, 2010.
[129] Martelli, E., et al., "Thermo-fluid dynamics analysis of film Cooling in Over expanded Rocket Nozzles," 42nd AIAA Joint Propulsion Conference, Sacramento, CA, AIAA 2006-5207, 2006.
[130] Mubarak A.K. & Tide P.S Design of a double parabolic supersonic nozzle and performance evaluation by experimental and numerical methods.
[131] Nikolaus A. Adams · Wolfgang Schröder · Rolf Radespiel · Oskar J. Haidn · Thomas Sattelmayer · Christian Stemmer · Bernhard Weigand Editors, résume les principaux succès du Centre de Recherche Collaboratif Transregio 40 (TRR40).

[132] Chloé Génin, Dirk Schneider, and Ralf Stark, Dual-Bell Nozzle Design.

[133] L'article intitulé "Parametrical Investigation of Transverse Injection in a Dual-Bell Nozzle During Altitude-Varying Conditions".

[134] Laughrey, J. A., Drape, D. J., & Hiley, P. E. (1981). Performance evaluation of an air vehicle utilizing nonaxisymrnetric nozzles. *Journal of Aircraft, 18*(2), 89-95. Published Online: 22 May 2012. https://doi.org/10.2514/3.57470

[135] Yunpeng, W. A. N. G., & Zonglin, J. I. A. N. G. (2021). A review of theories and methods for hypersonic nozzle design. *Advances in Mechanics, 51*(2), 257-294. https://doi.org/10.6052/1000-0992-20-002

[136] Gu, J. & Li, J. (2020). Aerodynamic performance analysis of a hypersonic vehicle with asymmetric nozzle under different altitudes, *Aerospace Science and Technology*, 104, 105919.

[137] Zhu, M., Fu, L., Zhang, S., & Zheng, Y. (2018). Design and optimization of three-dimensional supersonic asymmetric truncated nozzle. *Proceedings of the Institution of Mechanical Engineers, Part G: Journal of Aerospace Engineering*, *232*(15), 2923-2935.

https://doi.org/10.1177/0954410017718567

[138] Rylov, A. I. (1976). Analysis of some supersonic nonsymmetric nozzles. *Fluid Dynamics*, *11*(3), 477-479. https://doi.org/10.1007/BF01014473

[139] Rylov, A. I. (1977). Design of supersonic asymmetric nozzles. *Fluid Dynamics*, *12*(3), 414-420. https://doi.org/10.1007/BF01050573

[141] Yang, L., Huang, Y. & Chen, X. (2021). Effects of asymmetric nozzle on aerodynamic heating of a hypersonic vehicle, *Aerospace Science and Technology*, *118*, 106162

[142] Thangaraj, T., & Kaushik, M. (2023). Effects of circular and non-circular nozzle exit geometries on subsonic and supersonic jet propagations. *Proceedings of the Institution of Mechanical Engineers, Part G: Journal of Aerospace Engineering*, *237*(1), 209-229.

https://doi.org/10.1177/09544100221097537

[143] Vianna Moizes, D. A., Kotler, A. R., Thornton, M. R., & Ahmed, K. A. (2023). Comparison and Analysis of Hypersonic Scramjet Nozzles. In *AIAA SCITECH 2023 Forum* (p. 0716). Published Online: 19 Jan 2023. https://doi.org/10.2514/6.2023-0716

[144] Casper, J. L. (2019). Asymmetric supersonic nozzle design for enhanced thrust vectoring, *Journal of Propulsion and Power*, *35*(1), 94-101.

[145] Matveev, K. I. & Semenov, V. V. (2021). Numerical study of asymmetric nozzles for scramjet propulsion, *Aerospace Science and Technology*, *116*, 106229.

[146] Pal, S. & Chattopadhyay, H. (2018). Design optimization of asymmetric supersonic nozzle for supersonic combustion ramjet engine, Aerospace Science and Technology, 78, 29-41.

[147] Zhu, M., Fu, L., Zhang, S., & Zheng, Y. (2018). Design and optimization of three-dimensional supersonic asymmetric truncated nozzle. *Proceedings of the Institution of Mechanical Engineers, Part G: Journal of Aerospace Engineering*, *232*(15), 2923-2935.

https://doi.org/10.1177/0954410017718567

[148] Bajpai, A., & Rathakrishnan, E. (2018). Control of a supersonic elliptical jet. *The Aeronautical Journal*, *122*(1247), 131-147. https://doi.org/10.1017/aer.2017.114

[149] Kumar, S. A., & Rathakrishnan, E. (2016). Characteristics of a supersonic elliptic jet. *The Aeronautical Journal*, *120*(1225), 495-519. https://doi.org/10.1017/aer.2016.7